


For Reference

NOT TO BE TAKEN FROM THIS ROOM

Ex LIBRIS
UNIVERSITATIS
ALBERTAENSIS





Digitized by the Internet Archive
in 2023 with funding from
University of Alberta Library

<https://archive.org/details/Lin1974>

THE UNIVERSITY OF ALBERTA

FULLY DEVELOPED LAMINAR FLOW AND
GRAETZ PROBLEM IN CURVED RECTANGULAR
CHANNELS

by



RAN CHAU LIN

A THESIS

SUBMITTED TO THE FACULTY OF GRADUATE
STUDIES AND RESEARCH IN PARTIAL FULFILMENT OF THE
REQUIREMENTS FOR THE DEGREE OF MASTER OF SCIENCE

DEPARTMENT OF MECHANICAL ENGINEERING

EDMONTON, ALBERTA

SPRING, 1974

ABSTRACT

The Navier-Stokes equations are solved by numerical method for steady, fully developed, incompressible, laminar flow in curved rectangular channels considering the curvature ratio effect in the formulation. Solutions are obtained for aspect ratios 1, 2, 5 and 0.5 and Dean number ranges from 5 to 715, for example, for the case of curved square channel. It is found that an additional counter-rotating pair of vortices appears near the central outer region of the curved channel in addition to the familiar secondary flow at a certain higher Dean number. The correlation equations for the friction factor are developed. The friction factor results are compared with the available theoretical and experimental results and the agreement is found to be good. The curvature ratio effect is studied and it is confirmed that when $r \geq 10$, Dean's original formulation neglecting curvature ratio effect is applicable.

The Graetz problem in curved square channels considering the curvature ratio effect in the formulation is studied for the two basic thermal boundary conditions of constant wall temperature and uniform wall heat flux using the accurate velocity fields. The roles of Prandtl and Dean numbers on heat transfer results are found to be similar. When Prandtl or Dean number is large,

the local Nusselt number fluctuates before the asymptotic value is reached. The asymptotic Nusselt numbers are of practical importance and a simple correlation equation valid for the cases of constant wall temperature and uniform wall heat flux for curved square channels is developed.

The Graetz problem in curved rectangular channels with uniform convective boundary condition is also studied. The cases of Biot numbers 1 and 10 are studied in detail. The secondary flow effect on liquid solidification-free zone in curved rectangular channels is investigated for $Pr = 0.03$ (liquid metal) and $Pr = 10.05$ (water).

ACKNOWLEDGEMENTS

The author wishes to express his sincere appreciation
to:

- Dr. K.C. Cheng for his patient supervision and assistance during the course of this thesis investigation,
- Dr. J.W. Ou for his valuable suggestions and discussions,
- the Department of Mechanical Engineering, University of Alberta, and the Petroleum Education Aid Fund of Alberta for their financial support,
- Mrs. Barbara Galliaford for her patience in typing this thesis,
- his parents for their constant encouragement.

TABLE OF CONTENTS

	Page
CHAPTER I INTRODUCTION	1
CHAPTER II FULLY DEVELOPED LAMINAR FLOW IN	
CURVED RECTANGULAR CHANNELS	6
2.1 Governing Equations	6
2.2 Finite Difference Solution	14
2.3 Results and Discussion	22
2.4 Concluding Remarks	28
CHAPTER III GRAETZ PROBLEM IN CURVED SQUARE	
CHANNELS	30
3.1 Formulation of the Problem	30
3.2 Finite Difference Solution	37
3.3 Convergence of the Numerical	
Solution	43
CHAPTER IV RESULTS FOR CONSTANT WALL TEMPER-	
ATURE AND UNIFORM WALL HEAT FLUX	
BOUNDARY CONDITIONS	46
4.1 Results for Constant Wall Temper-	
ature Case	46
4.2 Results for Uniform Wall Heat Flux	
Case	49

	Page
4.3 Asymptotic Nusselt Number Results	50
4.4 Concluding Remarks	51
CHAPTER V RESULTS FOR UNIFORM CONVECTIVE BOUNDARY CONDITION	53
5.1 Temperature Field Development	53
5.2 Local Nusselt Number Result	54
5.3 The Effect of Secondary Flow on Liquid Solidification-Free Zone	55
5.4 Aspect Ratio Effect	57
5.5 Concluding Remarks	57
CHAPTER VI CONCLUSIONS	60
REFERENCES	63
APPENDIX A DERIVATION OF THE BASIC EQUATIONS FOR FLOW AND HEAT TRANSFER IN A CURVED RECTANGULAR CHANNEL	113
APPENDIX B COMPUTER PROGRAM	121
APPENDIX C.1 NUMERICAL RESULTS FOR CONSTANT WALL TEMPERATURE	147
APPENDIX C.2 NUMERICAL RESULTS FOR UNIFORM WALL HEAT FLUX	150

	Page
APPENDIX C.3	
NUMERICAL RESULTS FOR UNIFORM CONVECTIVE BOUNDARY CONDITION	154

LIST OF FIGURES

Figure		Page
1	Coordinate system and numerical grid for curved rectangular channel.	68
2	Stream-function contours for square channels.	69
3	Stream-function contours for $\gamma = 2$.	74
4	Stream-function contours for $\gamma = 5$.	75
5	Stream-function contours for $\gamma = 0.5$.	77
6	Distributions of secondary velocity components u, v at selected locations for $\gamma = 1$ and $K = 100$.	78
7	Distributions of secondary velocity components u, v at selected locations for $\gamma = 1$ and $K = 488$.	79
8	Axial velocity distributions in square channel with Dean number as parameter and comparison with experimental data.	80
9	Axial velocity distributions in square channel and comparison with experimental data.	82
10	Axial velocity distributions for $\gamma = 2$ with Dean number as parameter.	83
11	Axial velocity distributions for $\gamma = 5$ with Dean number as parameter.	84
12	Axial velocity distributions for $\gamma = 0.5$ with Dean number as parameter.	85

Figure		Page
13	Friction factor results and comparison with available theoretical and experimental results.	86
14	Typical temperature profile developments at $x = 0$ and $y = 0$ for constant wall temperature case.	87
15	Development of isothermals with $Pr = 5$ and $K = 100$ for constant wall temperature case.	91
16	Axial bulk temperature distribution for $Pr = 0.7$ and 10.05 with K as parameter for constant wall temperature case.	92
17	Local Nusselt number variations for $Pr = 0.1$ and 0.7 with K as parameter for constant wall temperature case.	93
18	Local Nusselt number variations for $Pr = 5$ and 500 with K as parameter for constant wall temperature case.	94
19	Typical temperature profile development at $x = 0$ and $y = 0$ for uniform wall heat flux case.	95
20	Development of isothermals with $Pr = 5$, and $K = 100$ for uniform wall heat flux case.	97
21	Axial distributions for $\bar{\theta}_w$ and θ_b for uniform wall heat flux case.	98
22	Local Nusselt number variations for $Pr = 0.1$ and 0.7 with K as parameter for uniform wall heat flux case.	99

Figure		Page
23	Local Nusselt number variations for $Pr=5$ and 500 with K as parameter for uniform wall heat flux case.	100
24	Heat transfer results for thermally fully developed region and comparison with experimental results.	101
25	Correlation equation for the asymptotic heat transfer results and comparison with experimental data.	102
26	Temperature profile development at $x = 0$ and $y = 0$ with Biot numbers 1 and 10 for uniform convective condition at wall.	103
27	Development of peripheral wall temperature distribution for Biot numbers 1 and 10 .	104
28	Axial bulk temperature distribution for $Pr=0.03$ with K as parameter for $Bi=1$ and 10 .	105
29	Axial bulk temperature distribution for $Pr=0.7$ with K as parameter for $Bi=1$ and 10 .	106
30	Axial bulk temperature distribution for $Pr=10.05$ with K as parameter for $Bi=1$ and 10 .	107
31	Local Nusselt number variation for $Pr=.03$ and 0.7 with Biot number 1 and 10 for uniform convective condition at wall.	108
32	Local Nusselt number variation with $Pr=10.05$ and Biot number 10 for uniform convective condition at wall.	109

Figure		Page
33	Length of liquid solidification-free zone with K as parameter for $Pr=0.03, 10.05$ and $Bi=1,10$.	110
34	Local Nusselt number variation for $Pr=0.03, 10.05$ and $Bi=10$ for aspect ratios $\gamma = 1, 2, 5, 0.5$.	111
35	Length of liquid solidification-free zone for $Pr=0.03,$ 10.05 and $Bi=1,10$ for aspect ratios $\gamma = 1, 2, 5, 0.5$.	112

LIST OF TABLES

TABLE		PAGE
1	Numerical Results for Friction Factor, $\gamma = 1.$	158
2	Numerical Results for Friction Factor, $\gamma = 2.$	159
3	Numerical Results for Friction Factor, $\gamma = 5.$	159
4	Numerical Results for Friction Factor, $\gamma = 0.5.$	160
5	Asymptotic Nusselt Numbers for Constant Wall Temperature and Uniform Wall Heat Flux Boundary Conditions.	161
6	Asymptotic Nusselt Numbers for Uniform Convective Boundary Condition.	162

LIST OF SYMBOLS

A	=	cross-sectional area of a channel
a	=	dimensional width of the rectangular channel or radius of tube
Bi	=	Biot number $\tilde{h} De/k$
b	=	dimensional height of the rectangular channel
$\vec{c}_1, \vec{c}_2, \vec{c}_3$	=	unit basic vectors
C_p	=	specific heat at constant pressure
De	=	hydraulic diameter
f	=	friction factors
\tilde{h}	=	external heat transfer coefficient
g	=	gravitational acceleration
h	=	heat transfer coefficient
K	=	Dean number, $Re(De/R)^{1/2}$
k	=	thermal conductivity
M	=	number of divisions in x-direction
N	=	number of divisions in y-direction or dimensional outward normal line
n	=	dimensionless outward normal line
Nu	=	average Nusselt number $\bar{h} De/k$
P	=	dimensional pressure
p	=	non-dimensional pressure
Pe	=	Peclet number, $Pr \cdot Re$

Pr	=	Prandtl number
q_w	=	uniform heat flux at wall
R	=	radius of curvature of a curved channel or tube
Re	=	Reynold's number, $\bar{W} De/\nu$
r	=	dimensionless radius of curvature of curved channel, R/De
S	=	circumference of cross-section
T	=	temperature
T_w	=	wall temperature
T_o	=	uniform fluid temperature at thermal entrance
T_∞	=	ambient temperature
U,V,W	=	velocity components in X,Y,Z directions
u,v,w	=	dimensionless velocity components in x,y,z directions
\bar{W}	=	mean axial velocity
\bar{w}	=	dimensionless mean axial velocity
X,Y,Z	=	rectangular torous coordinates
x,y,z	=	dimensionless torus coordinates

Greek Letters

α	=	thermal diffusivity
γ	=	aspect ratio b/a
ξ	=	dimensionless vorticity
θ	=	dimensionless temperature defined by specified formula
ϕ	=	angle (axial direction)
μ	=	viscosity
ν	=	kinematic viscosity

ρ	=	density
ψ	=	dimensionless stream function
ω	=	relaxation factor

Subscripts and Superscripts

b	=	bulk temperature
c	=	value for curved channel
i,j	=	space subscripts of a grid points in x and y direction respectively
K	=	Kth iteration for superscript
S	=	value for straight channel
w	=	value at wall
0	=	value at inlet
$-$	=	average value
\rightarrow	=	vector quantity

CHAPTER I

INTRODUCTION

Curved channels for fluid flow are used in various engineering applications, notably in heat exchanger and air conditioning apparatus. In contrast to fluid flow in the straight channels, curved channel flows are characterized by secondary flow in the cross section normal to the mainflow as a result of centrifugal forces acting on the fluid.

The phenomenon of steady fully developed laminar flow of a viscous fluid in a curved tube is now well understood and accurate friction factor correlation equations are available in the literature. For the analytical solution of the problem, Dean's perturbation analysis [1,2] is valid for small Dean number flow regime and the asymptotic boundary-layer analysis [3,4] is applicable only for large Dean numbers. Recently, numerical solution [5,6] has been carried out for Dean number, $Re(a/R)^{1/2}$, ranging from 1 to 1200 with curvature ratio parameter (R/a) varying from 10 to 100.

It is expected that the method of the solution for the equally important case of fully developed laminar flow in curved rectangular channels is similar to that for curved tubes. Indeed, the perturbation solutions [7,8] valid for small Dean

numbers and asymptotic solutions [9,10] for curved square channels based on boundary-layer approximation and applicable to large Dean numbers are available. The flow results from numerical solutions [11] are reported for curved rectangular channels with aspect ratios $\gamma = 0.2, 0.5, 1, 2$ and 5 up to Dean number, $K = \text{Re}(De/R)^{1/2}$, of order 100.

Heretofore, the theoretical analysis for flow in curved rectangular channels is limited to Dean's original formulation where the curvature ratio R/De is assumed to be large and the curvature ratio parameter does not appear independently in the governing equations. In view of the approximate nature of the boundary-layer method and the limited applicability of the perturbation solution, it is desirable to obtain numerical solution for Navier-Stokes equations including the curvature-ratio effect which govern the steady fully developed laminar flow in curved rectangular channels.

The superposition of the secondary flow on the axial flow has the effect of orderly mixing, which is expected to increase the heat and mass transfer rates. An effort will be made to bring out the heat transfer mechanism in the thermal entrance region. Actually, laminar forced convection heat transfer in the thermal entrance of curved pipes or channels is an extension of the classical Graetz problem and is one of the basic problems

in the convective heat transfer.

It is only recently that the Graetz problem has been studied for the case of curved circular pipes [16,19,20,21]. Heat transfer results in curved rectangular channels are reported so far only for the limiting conditions corresponding to the hydrodynamically and thermally fully developed flow fields [11,14]. With the assumption of constant physical properties, the momentum and energy equations are uncoupled and the Navier-Stokes equations governing a steady fully developed laminar flow can be solved independently.

It is desirable to study the Graetz problem in curved rectangular channels based on accurate flow field obtained from the numerical solution of Navier-Stokes equations considering the curvature ratio effect in the formulation. In order to limit the scope of present study, the Graetz problem in curved square channels is studied for the two basic thermal boundary conditions of constant wall temperature and uniform wall heat flux and uniform convective boundary condition.

In contrast to the first two boundary conditions, the available solutions [25, 26, 27, 28, 29, 30] to Graetz problem with convective boundary condition are fairly limited and are so far confined to straight tubes and parallel-plate channel only. No investigation has been reported for Graetz problem in

curved pipes or channels with convective boundary condition in spite of its practical and theoretical importance.

It should be pointed out that with convective boundary condition the solidification of liquids flowing in the curved tubes or channels may occur under extreme ambient conditions. In practice, the external heat transfer coefficient may vary circumferentially or axially. However, for simplicity, the external convection will be assumed to be uniform cooling. The present study based on uniform convective cooling yields the length of solidification-free zone preceding the region where the solidification occurs. The cases of water and liquid metal are studied in detail because of their practical importance. The aspect ratio effect is studied in the solidification-free zone analysis also.

In summary, the objectives of this investigation are:

1. Presentation of numerical results for fully developed laminar flows in curved rectangular channels with aspect ratios $\gamma = 0.5, 1, 2$ and 5 up to higher Dean number flow regime.
2. The numerical solution of Graetz problem in curved square channels for the two basic thermal boundary conditions of constant wall temperature and uniform wall heat flux.
3. The numerical solution of Graetz problem in curved rectangular channels for uniform convective boundary condition and a study of

the effect of secondary flow on solidification-free zone for liquid metal and water.

An effort will be made to compare the numerical results from the present analysis with the theoretical and experimental results available in the literature.

CHAPTER II

FULLY DEVELOPED LAMINAR FLOW IN CURVED RECTANGULAR CHANNELS

2.1 Governing Equations

For the theoretical analysis of the flow in curved channels, a toroidal coordinate system as illustrated in Fig. 1 is introduced. One assumes that the flow is steady, fully developed, laminar and incompressible. The detailed derivation of the basic governing equations is given in Appendix A. The results are:

Continuity equation

$$\frac{\partial U}{\partial X} + \frac{\partial V}{\partial Y} + \frac{U}{R(1+X/R)} = 0 \quad (1)$$

Momentum equation in X direction

$$\rho \left(U \frac{\partial U}{\partial X} + V \frac{\partial U}{\partial Y} - \frac{W^2}{R(1+X/R)} \right) = - \frac{\partial P}{\partial X} + \mu \left[\frac{\partial^2 U}{\partial X^2} + \frac{\partial^2 U}{\partial Y^2} + \frac{1}{R(1+X/R)} \frac{\partial U}{\partial X} - \frac{U}{R^2(1+X/R)^2} \right] \quad (2)$$

Momentum equation in Y direction

$$\rho \left(U \frac{\partial V}{\partial X} + V \frac{\partial V}{\partial Y} \right) = - \frac{\partial P}{\partial Y} + \mu \left[\frac{\partial^2 V}{\partial X^2} + \frac{\partial^2 V}{\partial Y^2} + \frac{1}{R(1+X/R)} \frac{\partial V}{\partial X} \right] \quad (3)$$

Momentum equation in Z direction

$$\rho \left(U \frac{\partial W}{\partial X} + V \frac{\partial W}{\partial Y} + \frac{UW}{R(1+X/R)} \right) = - \frac{1}{1+X/R} \frac{\partial P}{\partial Z} + \mu \left[\frac{\partial^2 W}{\partial X^2} + \frac{\partial^2 W}{\partial Y^2} + \frac{1}{R(1+X/R)} \frac{\partial W}{\partial X} - \frac{W}{R^2(1+X/R)^2} \right] \quad (4)$$

The corresponding boundary conditions are

$U=V=W=0$ at walls

$$V = \frac{\partial U}{\partial Y} = \frac{\partial W}{\partial Y} = 0 \text{ along the line of symmetry } Y=0 \quad (5)$$

It is convenient to introduce the following dimensionless variables:

$$X=De \ x, \ Y=De \ y, \ Z=De \ z, \ R=De \ r, \ U= \frac{v}{De} u, \ V= \frac{v}{De} v,$$

$$W= \frac{v}{De} w, \ P= \frac{\rho v^2}{De} p, \text{ where } De= 2ab/(a+b)$$

The governing equations then become;

$$u \frac{\partial u}{\partial x} + v \frac{\partial v}{\partial y} + \frac{u}{r(1+x/r)} = 0 \quad (6)$$

$$u \frac{\partial u}{\partial x} + v \frac{\partial u}{\partial y} - \frac{w^2}{r(1+x/r)} = - \frac{\partial P}{\partial x} + \frac{\partial^2 u}{\partial x^2} + \frac{\partial^2 u}{\partial y^2} + \frac{1}{r(1+x/r)} \frac{\partial u}{\partial x} - \frac{u}{r^2(1+x/r)^2} \quad (7)$$

$$u \frac{\partial v}{\partial x} + v \frac{\partial v}{\partial y} = - \frac{\partial P}{\partial y} + \frac{\partial^2 v}{\partial x^2} + \frac{\partial^2 v}{\partial y^2} + \frac{1}{r(1+x/r)} \frac{\partial v}{\partial x} \quad (8)$$

$$u \frac{\partial w}{\partial x} + v \frac{\partial w}{\partial y} + \frac{u w}{r(1+x/r)} = - \frac{1}{1+x/r} \frac{\partial P}{\partial z} + \frac{\partial^2 w}{\partial y^2} + \frac{1}{r(1+x/r)} \frac{\partial w}{\partial x} - \frac{w^2}{r^2(1+x/r)^2} + \frac{\partial^2 w}{\partial x^2} \quad (9)$$

One can eliminate the pressure terms from the secondary flow equations and obtain the following vorticity transport equation for secondary flow.

$$u \frac{\partial \xi}{\partial x} + v \frac{\partial \xi}{\partial y} - \frac{3}{r(1+x/r)} \frac{\partial \xi}{\partial x} + \frac{2}{(1+x/r)^2} w \frac{\partial w}{\partial y} = \frac{\partial^2 \xi}{\partial x^2} + \frac{\partial^2 \xi}{\partial y^2} \quad (10)$$

where

$$\xi = \left(\frac{\partial v}{\partial x} - \frac{\partial u}{\partial y} \right) / (1+x/r)$$

The dimensionless stream function is defined as

$$u = \frac{1}{1+x/r} \frac{\partial \psi}{\partial y} \quad , \quad v = - \frac{1}{1+x/r} \frac{\partial \psi}{\partial x} \quad (11)$$

Then one obtains the following stream function-vorticity equation.

$$(1+x/r)^2 \xi = - \left(\frac{\partial^2 \psi}{\partial x^2} + \frac{\partial^2 \psi}{\partial y^2} \right) + \frac{1}{r(1+x/r)} \frac{\partial \psi}{\partial x} \quad (12)$$

The axial flow equation remains the same. It is restated as;

$$u \frac{\partial w}{\partial y} + v \frac{\partial w}{\partial x} + \frac{uw}{r(1+x/r)} = - \frac{1}{1+x/r} \frac{\partial P}{\partial z} + \frac{\partial^2 w}{\partial x^2} + \frac{\partial^2 w}{\partial y^2} + \frac{1}{r(1+x/r)} \frac{\partial w}{\partial x} - \frac{w^2}{r^2(1+x/r)^2} \quad (13)$$

The boundary conditions for the above three variables are;

(a) the axial velocity w

$$\begin{aligned} w &= 0 && \text{at walls} \\ \frac{\partial w}{\partial y} &= 0 && \text{along the line of symmetry } y=0 \end{aligned} \quad (14)$$

(b) the stream function ψ

$$\psi = 0 \text{ at walls and along the line of symmetry } y=0 \quad (15)$$

(c) the vorticity ξ (16)

ξ is not known in advance at the walls. This will be discussed in detail in the next section, However, $\xi = 0$ along the line of symmetry $y=0$.

At this point, it is noted that a numerical solution is the only practical approach for the solution of the above set of simultaneous quasilinear, second-order partial differential equations of elliptic type.

Before the numerical solution technique is introduced, two alternative expressions for the product of friction factor and Reynolds number, fRe , are presented here:

1. The expression based on the velocity gradient along the channel walls.

The surface area of the upper half of a rectangular channel along the axial length $\Delta Z = R\Delta\phi$ is

$$A = A_1 + A_2 + A_3$$

where

$$A_1 = \int_0^{\frac{b}{2}} \int_{\phi_1}^{\phi_2} \left(R - \frac{a}{2}\right) d\phi dY = \left(R - \frac{a}{2}\right) \Delta\phi \frac{b}{2}$$

$$A_2 = \int_0^{\frac{b}{2}} \int_{\phi_1}^{\phi_2} \left(R + \frac{a}{2}\right) d\phi dY = \left(R + \frac{a}{2}\right) \Delta\phi \frac{b}{2}$$

$$A_3 = \int_{-\frac{a}{2}}^{\frac{a}{2}} \int_{\phi_1}^{\phi_2} (R+x) d\phi dX = R \Delta\phi a$$

$$\text{Or } A = A_1 + A_2 + A_3 = R\Delta\phi(a+b) \quad (17)$$

The average shear stress $\overline{\tau}_w$ is

$$\begin{aligned} \overline{\tau}_w &= \frac{1}{A} \int_A \tau_w dA \\ &= \frac{1}{A} \left[\left(R - \frac{a}{2}\right) \Delta\phi \int_0^{\frac{b}{2}} \tau_w dY + \left(R + \frac{a}{2}\right) \Delta\phi \int_0^{\frac{b}{2}} \tau_w dY \right. \\ &\quad \left. + \Delta\phi \int_{-\frac{a}{2}}^{\frac{a}{2}} (R+x) \tau_w dX \right] \\ &= \frac{1}{R(a+b)} \left[\left(R - \frac{a}{2}\right) \int_0^{\frac{b}{2}} \tau_w dY + \left(R + \frac{a}{2}\right) \int_0^{\frac{b}{2}} \tau_w dY + \right. \\ &\quad \left. \int_{-\frac{a}{2}}^{\frac{a}{2}} (R+x) \tau_w dX \right] \end{aligned} \quad (18)$$

Using the non-dimensional quantities, one has

$$\begin{aligned} \overline{\tau}_w = \frac{\mu v}{De^2} \frac{2\gamma}{(1+\gamma)^2} \left[(1 - (1+1/\gamma)/4r) \int_0^{(\frac{1}{4})(1+\gamma)} \left(\frac{\partial w}{\partial n} \right) dy + \right. \\ \left. (1 + (1+1/\gamma)/4r) \int_0^{(\frac{1}{4})(1+\gamma)} \left(\frac{\partial w}{\partial n} \right) dy \right. \\ \left. + \int_{-(\frac{1}{4})(1+1/\gamma)}^{(\frac{1}{4})(1+1/\gamma)} (1+x/r) \left(\frac{\partial w}{\partial n} \right) dx \right] \quad (19) \end{aligned}$$

The product of friction factor and Reynold's number is defined as;

$$f \cdot Re = \frac{\tau_w}{\frac{1}{2} \rho \overline{w}^2} \cdot \frac{\overline{w} De}{\nu} = \frac{2 \overline{\tau}_w De}{\mu \overline{w}}$$

Substituting equation (19) into the above equation, one has

$$\begin{aligned} (f \cdot Re)_1 = \frac{4\gamma}{\overline{w}(1+\gamma)^2} \left[(1 - (1+1/\gamma)/4r) \int_0^{(\frac{1}{4})(1+\gamma)} \left(\frac{\partial w}{\partial n} \right) dy + \right. \\ \left. (1 + (1+1/\gamma)/4r) \int_0^{(\frac{1}{4})(1+\gamma)} \left(\frac{\partial w}{\partial n} \right) dy \right. \\ \left. + \int_{-(\frac{1}{4})(1+1/\gamma)}^{\frac{1}{4}(1+1/\gamma)} (1+x/r) \left(\frac{\partial w}{\partial n} \right) dx \right] \quad (20) \end{aligned}$$

when $1/r \ll 1$, a simplified expression for $(fRe)_1$ becomes

$$(fRe)_1 = 2 \left(\frac{\partial \bar{w}}{\partial n} \right)_w / \bar{w} \quad (20a)$$

II. The expression based on the overall force balance for the differential axial length dZ .

A force balance on a flow element with axial length dZ gives;

$$- dp A = f \cdot dZ \cdot S \cdot \frac{1}{2} \rho \bar{w}^2$$

So

$$f = \frac{De}{2\bar{w}^2} \left(- \frac{1}{\rho} \frac{dp}{dZ} \right)$$

$$= \frac{De}{2 \frac{v^2}{De^2} \bar{w}^2} \left(- \frac{1}{\rho} \frac{\frac{\rho v^2}{De^2}}{De} \frac{dp}{dz} \right) = \frac{1}{2\bar{w}^2} \left(- \frac{dp}{dz} \right)$$

One then obtains:

$$(f \cdot Re)_2 = \frac{1}{2\bar{w}} \left(- \frac{dp}{dz} \right) \quad (21)$$

These two alternative methods of calculation for (fRe) provide a means of assessing the accuracy of the numerical solution. This will be discussed in the finite difference solution section.

2.2 Finite Difference Solution

Using the three-point central difference approximation for all the derivatives in equations (10), (12) and (13), each equation can be transformed into a set of linear algebraic equations in the following form:

$$A F_{i-1,j} + B F_{i,j} + C F_{i+1,j} = D, \quad i = 1, 2, \dots, M \quad (22)$$

where F is a dummy variable which stands for ξ , ψ and w , and A , B , C and D are the coefficients with $j=2, \dots, N$. For the vorticity transport equation (10), $F = \xi$ and the coefficients A , B , C and D are given as:

$$\begin{aligned} A &= \frac{1}{\Delta x^2} - \frac{1.5}{\Delta x(1+x_i/r)} + \frac{u_{i,j}}{2\Delta x} \\ B &= -\frac{2}{\Delta x^2} - \frac{2}{\Delta y^2} \\ C &= \frac{1}{\Delta x^2} + \frac{1.5}{\Delta x(1+x_i/r)} - \frac{u_{i,j}}{2\Delta x} \\ D &= \frac{w_{i,j}(w_{i,j+1} - w_{i,j-1})}{\Delta y(1+x_i/r)^2} - \left(\frac{1}{\Delta y^2} - \frac{v_{i,j}}{2\Delta y} \right) \xi_{i,j-1} \\ &\quad - \left(\frac{1}{\Delta y^2} + \frac{v_{i,j}}{2\Delta y} \right) \xi_{i,j+1} \end{aligned} \quad (23)$$

For the stream function vorticity equation (12), one has $F=\psi$ and the coefficients are

$$\begin{aligned}
 A &= \frac{1}{\Delta x^2} + \frac{1}{2\Delta x r(1+x_i/r)} \\
 B &= -\frac{2}{\Delta x^2} - \frac{2}{\Delta y^2} \\
 C &= \frac{1}{\Delta x^2} - \frac{1}{2\Delta x r(1+x_i/r)} \\
 D &= -(1+x_i/r)^2 \xi_{i,j} - \frac{\psi_{i,j+1} + \psi_{i,j-1}}{\Delta y^2}
 \end{aligned} \tag{24}$$

Similarly, with $F=w$ for axial velocity equation (13), the coefficients become

$$\begin{aligned}
 A &= \frac{1}{\Delta x^2} + \frac{u_{i,j}}{2\Delta x} - \frac{1}{2\Delta x r(1+x_i/r)} \\
 B &= -\frac{2}{\Delta x^2} - \frac{2}{\Delta y^2} - \frac{u_{i,j}}{r(1+x_i/r)} \\
 C &= \frac{1}{\Delta x^2} - \frac{u_{i,j}}{2\Delta x} + \frac{1}{2\Delta x r(1+x_i/r)} \\
 D &= -\frac{1}{1+x_i/r} \frac{\partial p}{\partial z} - \left(\frac{1}{\Delta y^2} - \frac{v_{i,j}}{2\Delta y} \right) w_{i,j+1} - \left(\frac{1}{\Delta y^2} + \frac{v_{i,j}}{2\Delta y} \right) w_{i,j-1}
 \end{aligned} \tag{25}$$

The secondary velocity components u and v are computed from the following finite-difference equations.

$$\begin{aligned}
u_{i,j} &= \frac{1}{1+x_i/r} \frac{\psi_{i,j+1} - \psi_{i,j-1}}{2\Delta y} \\
v_{i,j} &= -\frac{1}{1+x_i/r} \frac{\psi_{i+1,j} - \psi_{i-1,j}}{2\Delta x}
\end{aligned} \tag{26}$$

The boundary conditions can be written in finite difference form as;

$$\begin{aligned}
\psi_{1,j} &= w_{1,j} = \psi_{M+1,j} = w_{M+1,j} = 0 & \text{for } j=1,2,\dots,N+1 \\
\psi_{i,N+1} &= w_{i,N+1} = 0 & \text{for } i=1,2,\dots,M+1 \\
\psi_{i,1} &= \xi_{i,1} = 0 & \text{for } i=1,2,\dots,M+1 \\
w_{i,1} &= (4w_{i,2} - w_{i,3})/3 & \text{for } i=1,2,\dots,M+1
\end{aligned} \tag{27}$$

As far as the vorticity at the boundaries is concerned, it is treated in the following way. One can represent the vorticity at the inner wall as $\xi_{1,j}$, $j=1,\dots,N+1$, referring to the grid point system as shown in Fig. 1. At the wall, $u=v=0$, and $\partial u/\partial y = 0$ but $\partial v/\partial x \neq 0$, so one can obtain

$$\xi_{1,j} = - \frac{1}{(1+x_1/r)^2} \left(\frac{\partial^2 \psi}{\partial x^2} \right)_{1,j} \quad j=1, \dots, N+1 \quad (28)$$

Similarly, at the outer wall

$$\xi_{M+1,j} = - \frac{1}{(1+x_{M+1}/r)^2} \left(\frac{\partial^2 \psi}{\partial x^2} \right)_{M+1,j} \quad j=1, \dots, N+1 \quad (29)$$

and at the upper wall

$$\xi_{i,N+1} = - \frac{1}{(1+x_i/r)^2} \left(\frac{\partial^2 \psi}{\partial y^2} \right)_{i,N+1} \quad i=1, \dots, M+1 \quad (30)$$

By using Taylor's series expansion, one has

$$\psi_2 = \psi_1 + \left(\frac{\partial \psi}{\partial x} \right)_1 \Delta x + \left(\frac{\partial^2 \psi}{\partial x^2} \right)_1 \frac{\Delta x^2}{2!} + \left(\frac{\partial^3 \psi}{\partial x^3} \right)_1 \frac{\Delta x^3}{3!} + O(\Delta x^4) \quad (31a)$$

$$\psi_3 = \psi_1 + \left(\frac{\partial \psi}{\partial x} \right)_1 (2\Delta x) + \left(\frac{\partial^2 \psi}{\partial x^2} \right)_1 \frac{(2\Delta x)^2}{2!} + \left(\frac{\partial^3 \psi}{\partial x^3} \right)_1 \frac{(2\Delta x)^3}{3!} + O(\Delta x^4) \quad (31b)$$

here 1 stands for the position at wall, 2 for the interior point next to the wall, and 3 for the interior point next to 2. From the boundary conditions, one knows that

$$\psi_1 = \left(\frac{\partial \psi}{\partial x} \right)_1 = 0, \text{ Then equation (31a and b) become}$$

$$\psi_2 = \left(\frac{\partial^2 \psi}{\partial x^2} \right)_1 \frac{\Delta x^2}{2!} + \left(\frac{\partial^3 \psi}{\partial x^3} \right)_1 \frac{\Delta x^3}{3!} + O(\Delta x^4) \quad (32a)$$

$$\psi_3 = \left(\frac{\partial^2 \psi}{\partial x^2}\right)_1 \frac{(2\Delta x)^2}{2!} + \left(\frac{\partial^3 \psi}{\partial x^3}\right)_1 \frac{(2\Delta x)^3}{3!} + O(\Delta x^4) \quad (32b)$$

Neglecting the second term of equation (32a) one obtains

$$\left(\frac{\partial^2 \psi}{\partial x^2}\right)_1 = \frac{2\psi_2}{\Delta x^2} + O(\Delta x^3) \quad (33a)$$

and from (32a) and (32b), eliminating the third order term, one has

$$\left(\frac{\partial^2 \psi}{\partial x^2}\right)_1 = \frac{8\psi_2 - \psi_3}{2\Delta x^2} + O(\Delta x^4) \quad (33b)$$

Equation (33a) has larger truncation error than equation (33b), but it is a stable representation. Equation (33a) is employed in this study. The vorticity at walls is expressed in the following way:

For the inner wall

$$\xi_{1,j} = - \frac{1}{(1+x_1/r)^2} \frac{2\psi_{2,j}}{\Delta x^2}, \quad j = 1, \dots, N+1 \quad (34)$$

For the outer wall

$$\xi_{M+1,j} = - \frac{1}{(1+x_{M+1}/r)^2} \frac{2\psi_{M,j}}{\Delta x^2}, \quad j = 1, \dots, N+1 \quad (35)$$

For the upper wall

$$\xi_{i,N+1} = - \frac{1}{(1+x_i/r)^2} \frac{2\psi_{i,N}}{\Delta y^2}, \quad i = 1, \dots, M+1 \quad (36)$$

Using the boundary conditions stated, the set of finite difference equations can be written in the following matrix form after applying equation (22) to the grid points along the line $j=2, \dots, N$

$$\tilde{A} \tilde{E} = \tilde{D} \quad (37)$$

where

$$\tilde{A} = \begin{pmatrix} B_1 & C_1 & & & \\ A_2 & B_2 & C_2 & & \\ & A_3 & B_3 & C_3 & \\ & & & & A_{M-1} & B_{M-1} & C_{M-1} \\ & & & & A_M & B_M & \end{pmatrix} \quad \tilde{E} = \begin{pmatrix} F_{1,j} \\ F_{2,j} \\ \cdot \\ \cdot \\ \cdot \\ \cdot \\ F_{M,j} \end{pmatrix} \quad \tilde{D} = \begin{pmatrix} D_{1,j} \\ D_{2,j} \\ \cdot \\ \cdot \\ \cdot \\ \cdot \\ D_{M,j} \end{pmatrix}$$

It is noted that a tridiagonal matrix results for the system of algebraic equations for each line $j=2, \dots, N$. The finite difference solution of the coupled equations together with the associated boundary conditions are carried out in the

following manner:

1. For given curvature ratio r and axial pressure gradient, the initial values for dependent variables ξ , ψ and w are provided.
2. Using the initial values for stream function ψ , the boundary vorticity is computed using equation (34, 35, and 36). After obtaining the boundary vorticities, the vorticity transport equation (23) is solved by the Gaussian elimination method [12] along the lines $j=2, \dots, N$.
3. The elliptic equation for stream function, ψ , is solved by a line iterative method [12] using a relaxation factor ω as

$$\psi_{i,j}^{(n+1)} = \psi_{i,j}^{(n)} + \omega (\psi_{i,j}^{(n+1)} - \psi_{i,j}^{(n)}) \quad (38)$$

The iteration is terminated when the following relative error criterion is satisfied

$$\max |\psi_{i,j}^{(n+1)} - \psi_{i,j}^{(n)}| / \max |\psi_{i,j}^{(n+1)}| < 10^{-4}$$

4. The secondary velocity components are computed by equation (26). Using the updated secondary velocity components, the axial momentum equation can be solved following exactly the method described in step (3). Thus one completes one cycle of outer iteration.

5. Steps 2 to 4 are repeated until the following convergence criterion is satisfied for ψ and w .

$$\max |F_{i,j}^{(k+1)} - F_{i,j}^{(k)}| / \max |F_{i,j}^{(k+1)}| < 10^{-3} \quad (39)$$

where k stands for k th outer iteration.

Numerical experiments are conducted to establish the mesh size and the values of the relaxation factor ω , ranging from 1 to 0.1, are used as Dean number increases from lower values to higher values. Convergence study of the numerical solution can be made by comparison with the known exact solution for the limiting case of straight rectangular channels $K=0$. By using the mesh size of $M \times N = 20 \times 10$ for curved square channels, the values for $(fRe)_1$ and $(fRe)_2$ are found to agree with each other to within one per cent up to $K=202$. For higher Dean numbers the mesh size of 20×10 is found to be inadequate and the mesh size of 40×20 is used. The numerical results are listed in Tables 1 to 4 for the aspect ratios $\gamma = 1, 2, 5$ and 0.5 , respectively. The difference in values based on two alternative methods of computing fRe can be traced back to the difficulty in calculating the accurate velocity gradient at wall, $(\partial w / \partial n)_w$, using the three-point finite difference approximation, because of rather steep velocity gradient near the wall. After

considerable numerical experiments, it is established that the values for $(fRe)_2$ based on overall force balance are reliable and believed to be accurate within two per cent for higher Dean number range. It is also found that the curvature effect in the definition for $(fRe)_1$ in equation (20) is rather small and can be neglected practically. However, the value for $(fRe)_1$ in equation (20) is found to be closer to $(fRe)_2$ than that using equation (20a). Based on the above discussion, the numerical values from $(fRe)_2$ are taken to be the solution in the present analysis. The computing time required is less than two minutes on IBM 360/67 for each Dean number investigated.

2.3 Results and Discussion

2.3.1 The effect of Dean number on secondary flow patterns

The effect of Dean number on secondary flow pattern in the form of stream function contours is shown in Fig. 2 for fully developed flow in a curved square channel. The occurrence of two vortices for curved pipes or rectangular channels is well understood. However, Fig. 2(b) shows that at $K=202$, an additional counter-rotating pair of vortices appears near the central part of the outer wall. This situation was also pointed out in earlier work [11]. In interpreting the graphical results, it is well to note that the values of stream function at the eye of the vortice represents the strength of the secondary flow. The

intensity of the secondary vortices shown in Fig. 2(b), (c) and (d) is seen to be comparable to that of primary vortices. It is of particular interest to note that at $K=520$, the additional secondary vortices disappear completely as shown in Fig. 2(e) and the secondary flow pattern also changes appreciably. The appearance of the secondary vortices near the central outer wall can be understood since the flow field is known to be unstable there due to centrifugal instability [13]. Apparently, the centrifugal instability problem in curved rectangular channels needs further investigation. The shift of the location of vortex center with the increase of the Dean number is also of interest.

2.3.2 The effect of aspect ratio on secondary flow patterns

The secondary flow patterns for the aspect ratios $\gamma = 2, 5$ and 0.5 are shown in Fig. 3, 4, and 5 respectively, for various Dean numbers. In presenting the graphical results, an attempt was made to illustrate the new aspects of the secondary flow patterns and the circumstances under which the counter-rotating secondary vortices appear in addition to the primary vortices. With aspect ratio $\gamma = 5$, a pair of secondary vortices with weak intensity appear at a rather low Dean number $K = 76$. With $\gamma = 5$, one clearly sees that the eye of the primary vortices moves toward the upper or lower wall with the increase of Dean number.

In order to gain further insight into secondary flow patterns, the distributions of the secondary flow velocity components u, v , along $x = -0.35, 0, 0.25$ and $y = 0.1, 0.25$ in a square channel are shown in Figs. 6 and 7 for Dean numbers $K = 100$ and 488, respectively. It is useful to note that the solid line represents the distribution for u -component and the dashed line for v -component.

The direction of the secondary velocity component is self-evident and is not indicated in the figure. Based on the results shown in Figs. 6 and 7 and the existence of the additional counter-rotating vortex rolls, the validity of boundary-layer approximation for high Dean numbers flow regime needs re-examination. For example, at $K = 488$ the reverse flow appears for u and v near the central outer wall due to the additional counter-rotating vortices.

2.3.3 Axial velocity distributions and comparison with experimental data

The axial velocity profiles along the horizontal and vertical center-line are shown in Figs. 8 to 12 for the aspect ratios $\gamma = 1, 2, 5$ and 0.5 with Dean number as parameter. Experimental data [10, 14] are available for the case of curved square channel and some representative comparisons are shown in Figs. 8 and 9. Some discrepancy is observed between theoretical and experimental

results but it would be rather difficult to explain the exact reasons. For the case of $K = 368$ shown in Fig. 9, an additional pair of counter-rotating vortices already appears and the probe for velocity measurement may disturb the flow pattern there. No attempt was made to compare the present numerical results with other experimental velocity distributions shown in Figs. 7 and 8 of [14] since the Dean number reported there can be obtained only by trial and error method. However, a qualitative comparison is possible for some Dean numbers. For example, the vertical velocity profile for $K = 488$ shown in Fig. 8(b) agrees well with the profiles for $K \geq 251$ shown in Fig. 7 of [14]. The behavior of horizontal central velocity profiles for $K = 202$ and 488 is consistent with that of stream-function contours shown in Fig. 2(b) and (d), respectively.

In Fig. 10, the effect of Dean number on axial velocity profiles is seen to be rather regular indicating rather stable flow field up to $K = 278$ for $\gamma = 2$. At $\gamma = 5$, the effect of Dean number on axial velocity profile is seen to be rather weak up to $K = 123$ investigated. For $\gamma = 0.5$, the behavior of axial velocity profile is qualitatively similar to that of square channel. For $K \geq 176$, the location of the maximum axial velocity moves progressively toward $x = 0$ and its magnitude decreases as Dean number increases. Although not presented here, it is noted that the horizontal central velocity profiles for $K = 520$ and 618 become quite irregular for $\gamma = 1$ and it is tempting to consider

this phenomenon as the transition from laminar to turbulent flow.

2.3.4 Friction factor results

The friction factor results are summarized in Fig. 13 together with the available theoretical and experimental results [9, 10, 11 15], for square channels only, plotted for comparison. In Fig. 13, the aspect ratio effect on friction factor results is evident. The difference in the results for $\gamma = 0.5$ and 2 is of some interest. The reason can be explained from the axial velocity distributions. For $\gamma = 1$ and $K < 200$, the present numerical result agrees very well with earlier results [11]. The effect of curvature ratio on friction in square channels is also shown in the inset of Fig. 13 using somewhat magnified scale. The trend of the curvature ratio effect on friction factor result is similar to that observed in curved pipes [5, 16]. The difference between friction factor results for $r = 10$ and 100 is rather small. In view of the curvature ratio effect noted in [17] for curved tubes, one may conclude that when $r \geq 10$, Dean's original formulation [1,2], neglecting curvature ratio effect, is practically applicable also for curved rectangular channels.

2.3.5 Correlation equation for friction factor

It is expected that the friction factor results for curved rectangular channels can be correlated as a power series

in K as demonstrated for the case of fully developed laminar flow in curved pipes [18]. The correlation equation is useful for design purposes and the results for aspect ratios $\gamma = 1, 2, 5$ and 0.5 based on the present numerical results and using the least square method are given as,

$$f_c/f_s = C_0 K^{1/2} (1 + C_1 K^{-1/2} + C_2 K^{-1} + C_3 K^{-3/2} + C_4 K^{-2})$$

(40)

where

γ	C_0	C_1	C_2	C_3	C_4
1	0.1278	-0.257	0.669	187.7	-512.2
2	0.2736	-24.79	325.2	-1591	2728
5	0.0805	-5.218	104.4	-202.8	0
0.5	0.0974	4.366	-13.56	131.8	-182.6

The maximum deviation is less than two per cent for all cases in the available Dean number ranges as shown in Fig. 13.

For the case of curved circular pipes, the friction factor ratio for the same Reynold's number in curved and straight pipes, f_c/f_s , is known to depend on curvature ratio [5, 16]. However, the curvature ratio effect on friction factor results is not expected to be detected readily by experimental investigation [15]. In interpreting the predictions based on correlation equation (40), it is well to note that the correlation at higher Dean numbers, for example, for $\gamma = 1$, is based on numerical results for $r = 10$ and 4 listed in Table 1. The deviation of

correlated equation from Ludwig's experimental data [9] shown in Fig. 13 may be attributed to the curvature ratio effect. The experimental data shown in Fig. 13 for the range $K = 10^2 \sim 10^3$ are taken from [15] for $r = 17.5$ only and the agreement there is seen to be reasonable. In this study, no attempt was made to develop correlation equation considering curvature ratio effect. In high Dean number range, the slope of the curve from the present correlation seems to agree well with that of the experimental correlation equation $f_c/f_s = 0.107K^{1/2}$ proposed by Baylis [15] for square channel.

2.4 Concluding Remarks

1. Fully developed laminar flow in curved rectangular channels is approached by numerical method considering curvature ratio effect in the formulation. It is found that when $r \geq 10$, the curvature ratio effect can be neglected practically and Dean's original formulation is applicable.
2. The present analysis based on the complete Navier-Stokes equations reveals that an additional pair of secondary vortices appears near the central outer region of the channel at a certain higher Dean number depending on the aspect ratio. This phenomenon is consistent with Dean's instability problem for curved parallel-plate channel flow. The existence of two pairs of primary and secondary vortices poses some questions regarding the adequacy of

the boundary layer approximation for the high Dean number flow regime. Within the scope of present investigation, the secondary vortices disappear at $K = 520$, for example, for the curved square channel.

3. The numerical results are tabulated for future reference and the correlation equations for the friction factor are developed. The graphical results are designed to illustrate new aspects of flow fields in curved rectangular channels. For square channels, the numerical solution covers the Dean number range $5 \sim 715$. It is noted that a convergent solution can be obtained by the present numerical method for higher Dean numbers using finer mesh sizes but at the expense of considerable computing time.

4. The solution of the flow problem in curved rectangular channels is basic to various heat and mass transfer problems. Some related thermal entrance region problems will be studied in the next three chapters.

CHAPTER III

GRAETZ PROBLEM IN CURVED SQUARE CHANNELS

3.1 Formulation of the Problem

The classical Graetz problem is the theoretical analysis of laminar heat transfer in the thermal entrance region of straight tubes or channels. This analysis has been extended by several authors to different wall conditions and various real effects which were not considered originally by Graetz. The Graetz problem in curved square channels is characterized by the inclusion of the secondary flow effect, induced by the centrifugal force, in addition to the axial main flow effect.

The following assumptions are made in order to limit the scope of the present analysis:

1. The physical properties are constant and free convection effect is negligible.
2. Viscous dissipation effect is negligible.
3. Heat sources do not exist.
4. The axial conduction term is negligible for large Peclet number, ($Pe > 50$).

With assumption 1, the energy equation is seen to be uncoupled with the momentum equations. The flow problem solved in Chapter II can be applied to the present problem as well. One

can just concentrate on the discussion of energy equation.

The governing equation for the energy transport in curved square channels is given below using the same coordinate system as that used in Chapter II for flow problem. The derivation of the energy equation is given in Appendix A.

$$U \frac{\partial T}{\partial X} + V \frac{\partial T}{\partial Y} + \frac{W}{1+X/R} \frac{\partial T}{\partial Z} = \alpha \left[\frac{\partial^2 T}{\partial X^2} + \frac{\partial^2 T}{\partial Y^2} + \frac{1}{R(1+X/R)} \frac{\partial T}{\partial X} \right] \quad (41)$$

The thermal boundary conditions to be considered in this study are:

(1) Constant wall temperature

$$T = T_o \quad \text{at entrance } (z \leq 0)$$

$$T = T_w \quad \text{at wall}$$

$$\frac{\partial T}{\partial Y} = 0 \quad \text{along the line of symmetry } y = 0$$

(2) Uniform wall heat flux

$$T = T_o \quad \text{at entrance } (z \leq 0) \quad (42)$$

$$q_w = -k \left(\frac{\partial T}{\partial N} \right)_w = \text{const. at walls}$$

$$\frac{\partial T}{\partial Y} = 0 \quad \text{along the line of symmetry } y = 0$$

(3) Uniform convective boundary condition

$$T = T_o \quad \text{at entrance } (z \leq 0)$$

$$-k \left(\frac{\partial T}{\partial N} \right)_w = h(T_w - T_\infty) \text{ at walls}$$

$$\frac{\partial T}{\partial Y} = 0 \quad \text{along the line of symmetry } y = 0$$

Introducing the following non-dimensional quantities:

$$X = De x, Y = De y, Z = De Pr Re z, R = De r$$

$$U = \frac{v}{De} u, V = \frac{v}{De} v, W = \bar{W}_W$$

$$T - T_W = (T_O - T_W)\theta \text{ for constant wall temperature case,}$$

$$T - T_O = (q_w De / K)\theta \text{ for uniform wall heat flux,}$$

and

$$T - T_\infty = (T_O - T_\infty)\theta \text{ for wall convection,}$$

where

$$De = 2ab/(a+b), Re = \bar{W} De / v$$

equation (41) becomes

$$u \frac{\partial \theta}{\partial x} + v \frac{\partial \theta}{\partial y} + \frac{w}{1+x/r} \frac{1}{Pr} \frac{\partial \theta}{\partial z} = \frac{1}{Pr} \left[\frac{\partial^2 \theta}{\partial x^2} + \frac{\partial^2 \theta}{\partial y^2} + \frac{1}{r(1+x/r)} \frac{\partial \theta}{\partial x} \right] \quad (43)$$

and the corresponding boundary condition becomes

(I) Constant wall temperature case

$$\theta = 1 \quad \text{at entrance } (z \leq 0)$$

$$\theta = 0 \quad \text{at walls}$$

$$\frac{\partial \theta}{\partial y} = 0 \quad \text{along the line of symmetry } y=0$$

(II) Uniform wall heat flux case

$$\theta = 0 \quad \text{at entrance } (z \leq 0)$$

$$\frac{\partial \theta}{\partial n} = 1 \quad \text{at walls} \quad (44)$$

$$\frac{\partial \theta}{\partial y} = 0 \quad \text{along the line of symmetry } y=0$$

(III) Uniform convective boundary condition

$$\theta = 1 \quad \text{at entrance } (z \leq 0)$$

$$\frac{\partial \theta}{\partial n} = -Bi \theta_w \quad \text{at walls, where } Bi = \tilde{h} De/k$$

$$\frac{\partial \theta}{\partial y} = 0 \quad \text{along the line of symmetry } y=0$$

The Nusselt number variation in the thermal entrance region is of considerable importance in the present study. The Nusselt number $Nu = \bar{h} De/k$ can be obtained in two ways for each boundary condition as:

(a) Constant wall temperature case

Considering the wall temperature gradient, one obtains

$$-k \left(\frac{\partial T}{\partial n} \right)_w = h (T_b - T_w)$$

$$h = - \frac{k \left(\frac{\partial T}{\partial n} \right)_w}{T_b - T_w} \quad (45)$$

Using the dimensionless quantities introduced above, one obtains

$$h = - \frac{k \frac{T_o - T_w}{De} \left(\frac{\partial \theta}{\partial n} \right)_w}{t_b - T_w} = - \frac{k}{De} \frac{\left(\frac{\partial \theta}{\partial n} \right)_w}{\theta_b} \quad (46)$$

The average value becomes

$$\bar{h} = - \frac{k}{De} \frac{1}{\theta_b} \frac{\int \left(\frac{\partial \theta}{\partial n} \right)_w dS}{S} = - \frac{k}{De} \frac{\left(\frac{\partial \theta}{\partial n} \right)_w}{\theta_b} \quad (47)$$

Following the usual definition for the Nusselt number, one has

$$Nu_1 = \frac{\bar{h}De}{k} = - \frac{\overline{\left(\frac{\partial \theta}{\partial n}\right)_w}}{\theta_b} \quad (48)$$

where θ_b is the bulk temperature which is defined as:

$$\theta_b = \frac{\iint_A w \theta dA}{\iint_A w dA} \quad (49)$$

On the other hand, an energy balance of bulk flow with axial length dZ yields,

$$\begin{aligned} \rho C_p \overline{\frac{W}{1+X/R} \frac{\partial T}{\partial Z}} A dZ &= \bar{h} (T_w - T_b) dZ \cdot S \\ \bar{h} &= \frac{A}{S} \frac{\rho C_p \overline{\left(\frac{W}{1+X/R} \frac{\partial T}{\partial Z}\right)}}{T_w - T_b} \end{aligned} \quad (50)$$

where

$$\overline{\left(\frac{W}{1+X/R} \frac{\partial T}{\partial Z}\right)} = \frac{1}{A} \iint_A \frac{W}{1+X/R} \frac{\partial T}{\partial Z} dA$$

Using the same dimensionless quantities, one obtains

$$\begin{aligned} \bar{h} &= \frac{A}{S} \frac{\rho C_p \frac{\bar{W}(T_o - T_w)}{RePrDe} \overline{\left(\frac{w}{1+x/r} \frac{\partial \theta}{\partial z}\right)}}{T_w - T_b} \\ &= - \frac{1}{4} \frac{k}{De} \frac{\overline{\left(\frac{w}{1+x/r} \frac{\partial \theta}{\partial z}\right)}}{\theta_b} \end{aligned} \quad (51)$$

Hence, one has

$$Nu_2 = \frac{\bar{h}De}{k} = - \frac{1}{4} \frac{1}{\theta_b} \overline{\left(\frac{w}{1+x/r} \frac{\partial \theta}{\partial z} \right)} \quad (52)$$

(b) Uniform wall heat flux case

Performing the same procedures as for case (a), one obtains

$$Nu_1 = \frac{1}{\bar{\theta}_w - \theta_b} \quad (53)$$

$$Nu_2 = \frac{1}{4} \frac{1}{\bar{\theta}_w - \theta_b} \overline{\left(\frac{w}{1+x/r} \frac{\partial \theta}{\partial z} \right)} \quad (54)$$

where

$$\bar{\theta}_w = \frac{1}{S} \int_S \theta_w dS$$

(c) Uniform convective boundary condition

Following a similar procedure as noted in case (a), one obtains

$$Nu_1 = - \frac{Bi \bar{\theta}_w}{\bar{\theta}_w - \theta_b} \quad (55)$$

$$Nu_2 = - \frac{1}{4} \frac{1}{\bar{\theta}_b - \bar{\theta}_w} \overline{\left(\frac{w}{1+x/r} \frac{\partial \theta}{\partial z} \right)} \quad (56)$$

where

$$\bar{\theta}_w = \frac{1}{S} \int_S \theta_w dS$$

Simpson's integration formula is employed to carry out the calculations of the average quantities appearing in equations (48) to (56). Simple backward difference approximation is used to calculate the temperature gradient, $\partial\theta/\partial z$. As to the wall temperature gradient calculation in equation (48), three-point finite-difference approximation is used.

The bulk temperature development relationship in the uniform wall heat flux case is of special interest. Considering the energy balance for the axial length dZ , of the channel, one has

$$\rho \text{ Cp } \overline{\frac{W}{1+X/R} \frac{\partial T}{\partial Z}} A dZ = q_w \cdot S \cdot dZ \quad (57)$$

$$\overline{\frac{W}{1+X/R} \frac{\partial T}{\partial Z}} = \frac{q_w \cdot S}{\rho \text{ Cp } A}$$

After using dimensionless variables, the above equation reduces to

$$\overline{\frac{w}{1+x/r} \frac{\partial \theta}{\partial z}} = 4 \quad (58)$$

If the quantity $x/r \ll 1$, the equation yields

$$w \frac{\partial \theta}{\partial z} = 4 \quad (59)$$

Equation (59) can be written in the following way:

$$\frac{\iint_A w \frac{\partial \theta}{\partial z} dA}{A} = 4$$

or

$$\frac{\partial}{\partial z} \left(\frac{\iint_A w \theta dA}{A} \right) = 4 \quad (60)$$

From the non-dimensional quantities, one has the following relationship:

$$\iint w dA / A = 1 \quad (61)$$

Equation (60) is divided by the left hand side of equation (61), then one obtains

$$\frac{\partial}{\partial z} \left(\frac{\iint w \theta dA}{\iint w dA} \right) = 4 \quad (62)$$

$$\frac{\partial \theta_b}{\partial z} = 4$$

Two separate methods of calculating Nu and equation (62) provide a means of assessing the accuracy of the numerical solution.

3.2 Finite Difference Solution

The velocity components, u, v , and w are available from

the numerical solution of the fully developed flow problem in Chapter II. Consequently, the finite-difference grid-size $M \times N$ used for the energy equation is the same as that used in flow problem. With $u=v=0$ and $1/r=0$, the present Graetz problem is seen to be analogous to the unsteady state two dimensional heat conduction problem. However, the convective terms due to secondary flow becomes increasingly important in equation (43) as Dean or Prandtl number increases. The alternating direction implicit (ADI) method due to Peaceman and Rachford [22] is employed to transform equation (43) into a set of algebraic equations.

The numerical procedure consists of two steps for a given axial step distance Δz . The entire temperature field is known at the previous axial step z (n th step). The half axial step computes the temperature values for all grid points at axial distance $z + 0.5 \Delta z$, just considering the variation in the x direction. The full axial step computes the final temperature at the fully advanced axial distance $z + \Delta z$, proceeding another $0.5 \Delta z$ after half axial step, by using the half axial step values and considering only the variation in the y direction. Using second-order central difference approximation for all derivatives, one has the following finite difference linear algebraic equations:

(1) Half axial step (implicit in x)

Indicating the known temperature at the nth axial distance (z) by θ^n and the unknown temperature at half axial distance (z + 0.5 Δz) by a single asterisk, the finite difference analog of equation (43) can be written as:

$$\begin{aligned}
 & u_{i,j} \frac{\theta_{i+1,j}^* - \theta_{i-1,j}^*}{2\Delta x} + v_{i,j} \frac{\theta_{i,j+1}^n - \theta_{i,j-1}^n}{2\Delta y} + \\
 & \frac{1}{Pr} \frac{w_{i,j}}{1+x_i/r} \frac{\theta_{i,j}^* - \theta_{i,j}^n}{0.5\Delta z} \\
 & = \frac{1}{Pr} \left[\frac{\theta_{i+1,j}^* - 2\theta_{i,j}^* + \theta_{i-1,j}^*}{\Delta x^2} + \frac{\theta_{i,j+1}^n - 2\theta_{i,j}^n + \theta_{i,j-1}^n}{\Delta y^2} + \right. \\
 & \quad \left. \frac{1}{r(1+x_i/r)} \frac{\theta_{i+1,j}^* - \theta_{i-1,j}^*}{2\Delta x} \right] \quad (63)
 \end{aligned}$$

The above equation can be rearranged in the following form:

$$A \theta_{i+1,j}^* + B \theta_{i,j}^* + C \theta_{i-1,j}^* = D \theta_{i,j+1}^n + E \theta_{i,j}^n + F \theta_{i,j-1}^n \quad (64)$$

with

$$\begin{aligned}
 A &= \frac{u_{i,j}}{2\Delta x} - \frac{1}{Pr\Delta x^2} - \frac{1}{2Pr\Delta x r(1+x_i/r)} \\
 B &= \frac{1}{Pr} \left(\frac{2w_{i,j}}{\Delta z(1+x_i/r)} + \frac{2}{\Delta x^2} \right)
 \end{aligned}$$

$$C = -\frac{u_{i,j}}{2\Delta x} - \frac{1}{Pr\Delta x^2} + \frac{1}{2Pr\Delta x r(1+x_i/r)}$$

$$D = -\frac{v_{i,j}}{2\Delta y} + \frac{1}{Pr\Delta y^2}$$

$$E = \frac{1}{Pr} \left(\frac{2w_{i,j}}{\Delta z(1+x_i/r)} - \frac{2}{\Delta y^2} \right)$$

$$F = \frac{v_{i,j}}{2\Delta y} + \frac{1}{Pr\Delta y^2}$$

$\theta_{i,j}^*$ can be obtained by solving the above equation using Gaussian elimination method [12]. With $\theta_{i,j}^*$ available, then one proceeds to the next step.

(2) Full axial step (implicit in y)

With $\theta_{i,j}^*$ as the known values and $\theta_{i,j}^{**}$ as still unknown values, the finite difference analog equation becomes

$$\begin{aligned} u_{i,j} \frac{\theta_{i+1,j}^* - \theta_{i+1,j}^*}{2\Delta x} + v_{i,j} \frac{\theta_{i,j+1}^{**} - \theta_{i,j-1}^{**}}{2\Delta y} + \\ \frac{1}{Pr} \frac{w_{i,j}}{(1+x_i/r)} \frac{\theta_{i,j}^{**} - \theta_{i,j}^*}{0.5\Delta z} \\ = \frac{1}{Pr} \left[\frac{\theta_{i+1,j}^* - 2\theta_{i,j}^* + \theta_{i-1,j}^*}{\Delta x^2} + \frac{\theta_{i,j+1}^{**} - 2\theta_{i,j}^{**} + \theta_{i,j-1}^{**}}{\Delta y^2} + \right. \\ \left. \frac{1}{r(1+x_i/r)} \frac{\theta_{i+1,j}^* - \theta_{i-1,j}^*}{2\Delta x} \right] \end{aligned} \quad (65)$$

or in the form:

$$A \theta_{i,j+1}^{**} + B \theta_{i,j}^{**} + C \theta_{i,j-1}^{**} = D \theta_{i+1,j}^{*} + E \theta_{i,j}^{*} + F \theta_{i-1,j}^{*} \quad (66)$$

With

$$A = \frac{v_{i,j}}{2\Delta y} - \frac{1}{Pr\Delta y^2}$$

$$B = \frac{1}{Pr} \left(\frac{2w_{i,j}}{\Delta z(1+x_i/r)} + \frac{2}{\Delta y^2} \right)$$

$$C = -\frac{v_{i,j}}{2\Delta y} - \frac{1}{Pr\Delta y^2}$$

$$D = -\frac{u_{i,j}}{2\Delta x} + \frac{1}{Pr\Delta x^2} + \frac{1}{2Pr\Delta x r(1+x_i/r)}$$

$$E = \frac{1}{Pr} \left(\frac{2w_{i,j}}{\Delta z(1+x_i/r)} - \frac{2}{\Delta x^2} \right)$$

$$F = \frac{u_{i,j}}{2\Delta x} + \frac{1}{Pr\Delta x^2} - \frac{1}{2Pr\Delta x r(1+x_i/r)}$$

Again, using Gaussian elimination method, one finishes a complete axial step calculation. Therefore, the (n+1)th step temperature distribution is obtained. Repeating these two steps, the temperature values in the thermal entrance region can be obtained.

The corresponding boundary conditions in finite difference

form are:

(a) Constant wall temperature case

$$\begin{aligned}
 \theta_{1,j} &= \theta_{M+1,j} = 0 & \text{for } j=1, \dots, N+1 \\
 \theta_{i,N+1} &= 0 & \text{for } i=1, \dots, M+1 \\
 \theta_{i,j-1} &= \theta_{i,j+1} & \text{at } j=1 \text{ for } i=1, \dots, M+1
 \end{aligned} \tag{67}$$

(b) Uniform wall heat flux case

$$\begin{aligned}
 \theta_{i-1,j} &= 2\Delta x + \theta_{i+1,j} & \text{at } i=1, \text{ for } j=1, \dots, N+1 \\
 \theta_{i+1,j} &= 2\Delta x + \theta_{i-1,j} & \text{at } i=M+1, \text{ for } j=1, \dots, N+1 \\
 \theta_{i,j+1} &= 2\Delta y + \theta_{i,j-1} & \text{at } j=N+1, \text{ for } i=1, \dots, M+1 \\
 \theta_{i,j-1} &= \theta_{i,j+1} & \text{at } j=1, \text{ for } i=1, \dots, M+1
 \end{aligned} \tag{68}$$

(c) Uniform convective boundary condition

$$\begin{aligned}
 \theta_{i-1,j} &= -2\Delta x Bi \theta_{i,j} + \theta_{i+1,j} & \text{at } i=1, \text{ for } j=1, \dots, N+1 \\
 \theta_{i+1,j} &= -2\Delta x Bi \theta_{i,j} + \theta_{i-1,j} & \text{at } i=M+1, \text{ for } j=1, \dots, N+1 \\
 \theta_{i,j+1} &= -2\Delta y Bi \theta_{i,j} + \theta_{i,j-1} & \text{at } j=N+1, \text{ for } i=1, \dots, M+1 \\
 \theta_{i,j-1} &= \theta_{i,j+1} & \text{at } j=1, \text{ for } i=1, \dots, M+1
 \end{aligned} \tag{69}$$

It must be pointed out that in the calculation of wall temperature for both uniform wall heat flux and wall convection cases, the governing equation takes the following simple form:

$$\frac{\partial^2 \theta}{\partial x^2} + \frac{\partial^2 \theta}{\partial y^2} + \frac{1}{r(1+x/r)} \frac{\partial \theta}{\partial x} = 0 \quad (70)$$

In finite difference analog, it becomes

$$\begin{aligned} & \left(\frac{1}{\Delta x^2} + \frac{1}{2r(1+x_i/r)\Delta x} \right) \theta_{i+1,j} - \left(\frac{1}{\Delta x^2} + \frac{1}{2r(1+x_i/r)\Delta x} \right) \theta_{i,j} + \\ & \left(\frac{1}{\Delta x^2} - \frac{1}{2r(1+x_i/r)\Delta x} \right) \theta_{i-1,j} \\ & + \frac{1}{\Delta y^2} (\theta_{i,j+1} + \theta_{i,j-1}) = 0 \end{aligned} \quad (71)$$

By applying the boundary conditions at wall, the wall temperature can be computed after the temperatures in the interior region are found.

3.3 Convergence of the Numerical Solutions

The stability of the numerical solution depends on grid-size ($M \times N$) and the axial step size (Δz). For the flow problem in curved square channel, the grid-size of 20×10 and occasionally

40x20 was found to be satisfactory from the viewpoint of accuracy and computing time. For the present problem, the following scheme of axial step variation obtained by trial and error method leads to stable and convergent solution.

Axial step, n	Step size, Δz
1 ~ 100	5×10^{-5}
101 ~ 450	10^{-4}
451 ~ 650	2×10^{-4}
651 ~ 850	5×10^{-4}
n > 851	10^{-3}

The solution is terminated when the asymptotic solution which will be discussed later, is reached.

The accuracy of the numerical result can be assessed by noting the known asymptotic Nusslet number of 2.98 and 3.091 for the constant wall temperature and uniform wall heat flux cases, respectively. The present calculations agree very well with the foregoing values. For the case of constant wall temperature, the difference in the values for Nu_1 and Nu_2 from equations (48) and (52) is found to be relatively large when Prandtl or Dean number is large. For example, the asymptotic Nusselt number Nu_1 and Nu_2 deviates from the average value by 7 per cent with $Pr=0.7$, $K=368$ and $M \times N=40 \times 20$. Similar observations is also noted in [16] for the case of curved pipes.

By further reduction in mesh size and axial step, it is confirmed that the values from Nu_1 is a reasonably accurate one and consequently the numerical value from Nu_1 is used in presenting the result. It is suspected that the numerical evaluation of $\partial\theta/\partial z$ is a source of difficulty for Nu_2 in the constant wall temperature case. For the case of uniform wall heat flux, Nu_1 and Nu_2 are seen to be identical if the relationship represented by equation (62) is used. It is also clear that the numerical value from Nu_1 is more accurate than Nu_2 . In contrast to the case of constant wall temperature, the two values from Nu_1 and Nu_2 are found to agree with each other very well. At a higher Dean number $K=488$, the deviation from the average value is found to be 3 per cent with $Pr=0.1$ and $M \times N=20 \times 10$. The numerical result also checks well with equation (62). For the case of wall convection, Nu_1 and Nu_2 agree with each other just as good as in the case of uniform wall heat flux for all parameters investigated.

From the foregoing discussion, it is concluded that the numerical values from Nu_1 are sufficiently accurate for these thermal boundary conditions and the accuracy is considered to be within about 2 per cent. The computing time required in obtaining a complete result for each Dean number is approximately 3 minutes with $M \times N=20 \times 10$ and 9 minutes with $M \times N=40 \times 20$ on IBM 360/67 system.

CHAPTER IV

RESULTS FOR CONSTANT WALL TEMPERATURE AND UNIFORM WALL HEAT FLUX BOUNDARY CONDITIONS

4.1 Results for Constant Wall Temperature Case

4.1.1 Temperature field development

In this study, the effect of Dean number on the development of temperature field in the thermal entrance region is of special interest. The temperature profile developments along the central vertical and horizontal axes are shown in Fig. 14(a) to (d) for Dean numbers $K = 14, 100, 368$, and 488 , respectively, with $Pr = 0.7$. In examining the graphical results, one should note the gradual distortion of the profile and the shift of the location of maximum value for θ as the Dean number increases. It is pointed out that at $K = 368$ and 488 two pairs of counter-rotating vortex rolls already appear and the detailed secondary flow patterns are shown in Chapter II. The development of isothermals at several axial locations for $Pr = 5$ and $K = 100$ is illustrated in Fig. 15. The development of the plume-like behavior in the form of warm current penetrating into the cold fluid core region and the appearance of the two eyes for isothermals are noteworthy. The phenomenon is similar to that observed in curved circular pipes [19, 20, 21]. The effect of Dean number on bulk

temperature distribution along downstream direction is shown in Fig. 16 for $Pr = 0.7$ and 10.05.

4.1.2 Heat transfer result

The variation of local Nusselt number in the thermal entrance region is of practical importance and the results for $Pr = 0.1, 0.7, 5$ and 500 are shown in Figs. 17 and 18. At $Pr = 0.1$, the general feature of local Nusselt number variation is similar to that of the classical Graetz solution ($K=0$). The behavior for Nu can be explained from equation (43). At small Prandtl number the axial convective term dominates over the convective terms due to secondary flow. Consequently, the curves for different Dean numbers are nearly parallel and straight in the Leveque solution region near the thermal entrance ($z=0$) and the difference in Nusselt number values is caused by the different degree of axial velocity profile distortion for w due to Dean number effect. For small Prandtl numbers, the role of axial convective term in the energy equation is important.

At $Pr = 0.7$, one can already see the existence of minimum Nusselt number values at some downstream location depending on Dean number. At this particular location, apparently, the axial convective term and the convective terms due to secondary flow are equally important and one may conclude that the entrance effect and the secondary flow effect are in balance.

After passing the minimum Nusselt number point, the secondary flow effect dominates over the entrance effect and the local Nusselt number continues to increase until the local maximum values is reached. Eventually, the Nusselt number values remain constant further downstream and one may conclude that the limiting asymptotic value, corresponding to the fully developed temperature field is reached. It is clear that the thermal entrance length decreases with the increase of Dean number. For the case of $Pr = 0.7$, it is instructive to contrast the Nusselt number variation with temperature profile development shown in Fig. 14 and the bulk temperature distribution shown in Fig. 16.

A characteristically different kind of Nusselt number behavior appears when Prandtl number is large. For example, at $Pr = 500$ and a relatively low Dean number $K = 14$, the secondary flow is rather weak and the Nusselt number variation in the Leveque solution region is identical with the case with $K = 0$. However, at some downstream position the secondary effect appears and the deviation occurs. After reaching the local maximum value for Nu , a fluctuating phenomenon appears before a stationary value is reached further downstream. The present fluctuating Nusselt number phenomenon is similar to that reported in the earlier numerical studies [16, 19] for the case of curved pipes. It should be pointed out that numerical difficulty was encountered for $K > 14$ with $Pr = 500$. From the foregoing discussion, one can also understand the Nusselt number behavior for $Pr = 5$ as shown

in Fig. 18.

4.2 Results for Uniform Wall Heat Flux Case

Temperature field developments and heat transfer results similar to those presented earlier are shown in Fig. 19 to 23. The behavior of temperature profile development shown in Fig. 19(b) can be understood better if it is contrasted to the corresponding isothermal pattern shown in Fig. 20 and the distributions for $\bar{\theta}_w$ and θ_b shown in Fig. 21. For the case of uniform wall heat flux, apparently the left-hand corner is a hot spot and the wall temperature is highest there. When the temperature field becomes fully developed, the axial distributions for θ_b and θ_w become parallel to each other and correspondingly the local Nusselt number approaches a constant value depending on Prandtl and Dean numbers. The thermal entrance length is of practical interest and can be determined from Figs. 21 to 23 by noting the above fact. The local Nusselt number result shows that for a given Prandtl number, the thermal entrance length decrease with the increase of Dean number and the Prandtl number effect is also seen to be similar for a given Dean number. The roles of Dean and Prandtl numbers on heat transfer result are seen to be similar and this observation can also be seen from equation (43). The relative magnitude of the convective terms due to secondary flow, $Pr(u \frac{\partial \theta}{\partial x} + v \frac{\partial \theta}{\partial y})$, increase with the increase of Prandtl or Dean number.

The behavior of local Nusselt number in the Leveque solution region and the occurrence of minimum and subsequent local maximum Nusselt number can be explained. However, the fluctuating Nusselt number phenomenon before approaching the asymptotic value as shown in Fig. 23 cannot be explained readily. The reported numerical results [16, 19] and the present work show qualitative agreement regarding the fluctuating Nusselt number phenomenon. Apparently, the fluctuating phenomenon is caused by the convective terms due to secondary flow in the energy equation (43). Considering the fact that numerical difficulty also arises when Prandtl or Dean number is very large, one cannot rule out entirely the possibility that the phenomenon is caused by numerical instability [20, 21]. At present it is not clear why the Nusselt number decrease faster along the axial direction than the case of straight channel. Perhaps the question can only be answered by very precise and accurate experimental measurements. However, the fluctuating phenomenon is probably of theoretical interest only and in practical applications the asymptotic Nusselt number is important when Prandtl or Dean number is large.

4.3 Asymptotic Nusselt Number Results

The asymptotic Nusselt number is of practical importance and the numerical results for the two thermal boundary conditions are listed in Table 5 and plotted in Fig. 24. The

experimental data [14] for the case of uniform wall heat flux with $Pr = 0.71$ are also shown there for comparison. The agreement with the present analysis is seen to be reasonable. This confirms the good accuracy of the numerical analysis noted earlier. The difference between the two thermal boundary conditions is seen to be relatively small for $Pr = 0.7$ and 5 . In view of this fact, the numerical results for the two boundary conditions were correlated by the following equation within a maximum deviation of 12% using the least-square method.

$$Nu = 0.152 + 0.627(K^{1/2} Pr^{1/4}) \quad . \quad 0.7 \leq Pr \leq 5, \quad 14 \leq K \leq 500 \quad (72)$$

The parameter $(KPr^{1/2})$ is based on earlier study [23] for curved pipes.

4.4 Concluding Remarks

1. The present analysis includes the curvature ratio effect in the formulation. However, recent work [24] for fully developed laminar forced convection in curved tubes with the thermal boundary condition of axially uniform wall heat flux and peripherally uniform wall temperature concludes that the curvature ratio parameter has a negligible effect on the average Nusslet number in the range of $R/a = 10$ to 100 . For the present problem involving curved square channels, the curvature ratio effect is also expected

to be negligible for Nu with $r \geq 10$.

2. In examining the graphical results presented, it is well to note that two pairs of vortex rolls already appear at Dean number $K = 202$, for example. In the results of Chapter II, no attempt was made to determine exactly the Dean number corresponding to the onset of centrifugal instability.

3. The present numerical results reveal fluctuating Nusselt number behavior before reaching the asymptotic value when the Prandtl or Dean number is large. The phenomenon is similar to that observed in curved circular pipes [16,19]. An attempt was made to clarify the heat transfer mechanism particularly the Prandtl and Dean number effects in the thermal entrance region of curved square channels.

4. In order to limit the scope of the present investigation, the aspect ratio effect on the present convective heat transfer problem in curved rectangular channels was not studied here. However, the analysis can be made by using the flow fields reported in Chapter II.

5. Some local Nusselt number results in the thermal entrance region are tabulated in Appendix C.1 and C.2 for possible future reference.

CHAPTER V

RESULTS FOR UNIFORM WALL CONVECTIVE BOUNDARY CONDITION

5.1 Temperature Field Development

The development of the temperature field along the central and vertical planes of a curved square channel is shown in Fig. 26 for $Pr = 10.05$, $K = 368$ and $Bi = 1, 10$. The corresponding wall temperature distribution θ_w around the channel periphery is shown in Fig. 27. It is noted that at $K = 368$, an additional pair of vortex rolls already appears near the central outer region of the channel. It will be instructive to examine the temperature profile development with local Nusselt number variation which will be shown later. Because of the nature of present convective boundary condition, the developing wall temperature distribution for θ_w is of special interest. It is clearly seen that the value of θ_w is lowest at the inside corners. The temperature values are lower near the corners and the corners points may be regarded as cold spot. It should be pointed out that the secondary flow is rather weak near the corners. Noting the relationship $\partial\theta/\partial n = -Bi \theta_w$ from equation (44) and the fact that the Biot number is constant, it is seen that the distribution of the wall temperature gradient

$\partial\theta/\partial n$ is also similar to the distribution for θ_w .

The axial variation of bulk temperature θ_b for $Pr = 0.03, 0.7$ and 10.05 are shown in Figs. 28 to 30 with Dean number as parameter. At $Bi = 1$, the Dean number effect is relatively small. These figures also illustrate the Biot number effect. With perfect insulation ($Bi \rightarrow 0$), the bulk temperature θ_b remains to be one. For a given Dean number, the Prandtl number effect is seen to be rather small.

5.2 Local Nusselt Number Result

The local Nusselt number variation in the thermal entrance region of curved square channels are illustrated in Figs. 31 and 32 with Dean number as parameter for $Pr = 0.03, 0.7$, and 10 , respectively. As shown in Fig. 31, the Biot number effect on local Nusselt number is rather small and at $K = 368$, for example, the values with $Bi = 1$ is only slightly higher than those for $Bi = 10$. Although not shown in Fig. 31, the value for the limiting case ($Bi \rightarrow \infty$) is only slightly lower than the value for $Bi = 10$.

At low Prandtl number such as $Pr = 0.03$, the local Nusselt number behavior is similar to that of straight channel $K = 0$. This phenomenon has been discussed in Chapter IV for constant wall temperature and uniform wall heat flux boundary conditions. For Prandtl number 0.7 and 10.05 , the local Nusselt

number fluctuates before the fully developed stationary value is reached. This fluctuating behavior has already been pointed out in Chapter IV also. The asymptotic Nusselt number is of practical interest and the results are given in Table 6. It is noted that the Biot number effect is rather small and a maximum deviation from the uniform wall temperature case ($Bi \rightarrow \infty$) is only 4 per cent for a given Dean number.

5.3 The Effect of Secondary Flow on Liquid Solidification-Free Zone

In the case of uniform convective cooling at the outer surface with ambient temperature T_∞ lower than the liquid freezing temperature T_f and in view of the wall temperature distribution shown in Fig. 27, it is clear that liquid solidification will start at the inner corner point B when the freezing temperature is reached there at some downstream distance referred to as the length of solidification-free zone or the solid-phase entrance ($z = z_f$). When the solid-phase surrounds the channel inner wall completely, the thermal boundary condition becomes isothermal. The solidification of liquid metal or water in curved channels is of considerable practical importance. However, in this investigation only the prediction of solidification-free zone will be considered.

For a study of solidification-free zone, it is convenient to introduce the superheat ratio parameter [28] defined as, $\epsilon = (T_o - T_f)/(T_f - T_\infty) = -1 + \theta_f^{-1}$, where $\theta_f < 1$. It is noted that solidification begins when the wall temperature θ_w at inner corners (cold spot) equals θ_f . Consequently, the superheat ratio ϵ corresponding to the solidification-free zone length z_f can be computed readily. The results are plotted in Fig. 33 for $Pr = 0.03$ (liquid metal) and 10.05 (water) with Dean number as parameter for the cases $Bi = 1$ and 10. Since the present analysis is based on the constant physical property assumptions, with $Pr = 10.05$ for water, for example, the temperature difference $(T_o - T_f)$ is practically limited to about 20°C. Furthermore, with $T_\infty = -0.5^\circ\text{C}$ and -100°C , ϵ becomes 40 and 0.2, respectively. In interpreting the results shown in Fig. 33, it is well to note that as ϵ approaches zero and infinity, z_f also approaches zero and infinity, respectively. The trend for $K = 0$ is similar to that reported in [28, 30] for straight tubes. With $Pr = 0.03$ and $Bi = 1$, the secondary flow effect seems to be small. It is sufficient here to use the case of $Pr = 10.05$ and $Bi = 10$ to explain the secondary flow effect on solidification-free zone. Apparently, the character of Dean number effect changes at the threshold value of $\epsilon=37$. Noting that the value of ϵ decreases as the ambient temperature T_∞ decreases, with a given $\epsilon < 37$, the secondary flow tends to

mix the warmer liquid and correspondingly, the solidification-free length increases with the increase of Dean number. On the other hand, with $\varepsilon > 37$ (or relatively higher T_∞) the secondary flow tends to bring the cold spot temperature to the freezing temperature at shorter entrance distance z_f . Further physical insight can be gained by considering a given value of z_f and the corresponding different values for different Dean numbers.

5.4 Aspect Ratio Effect

The results for the typical local Nusselt number and solidification-free zone for $Pr = 10.05$ (water) and 0.03 (liquid metal) are also presented in Figs. 34 and 35, respectively, for aspect ratios $\gamma = 1, 2, 5$ and 0.5 with $Bi = 1$ and 10 . The Nusselt number behavior is characteristically different between $Pr = 0.03$ and 10.05 . The fluctuating Nusselt number phenomenon before approaching the asymptotic value for $Pr = 10.05$ and $K > 171$ is somewhat similar to the earlier investigation [16, 19, 31] but the number of fluctuating cycles before the complete damping is far fewer than that shown in Fig. 9 of [16] for the constant wall temperature case with $Pr = 10$ in helical coils. The aspect ratio effect can only be seen clearly with comparable Dean number.

5.5 Concluding Remarks

1. The Graetz problem in curved rectangular channels

without the assumption of large curvature ratio R/De is solved numerically for the uniform convective boundary condition. The solution also yields the length of liquid solidification-free zone. The numerical result reveals that solidification will start at the inner corners which represent a cold spot. One may also reason that solidification will start at inner wall for the practically important case of curved circular tubes.

2. The Nusselt number behavior in the thermal entrance region is characteristically different between large and small Prandtl numbers. For given values of Prandtl and Dean numbers, the Biot number effect on local Nusselt number is found to be rather small within the range of present investigation. The fluctuating Nusselt number behavior before the eventual damping of the cyclic behavior and the approach of the asymptotic value is similar to that reported in earlier investigations. Both the Prandtl and Dean numbers have the effect of decreasing the thermal entrance length.

3. For a given value of Biot number, the secondary flow effect on the length of liquid solidification-free zone is greater for larger Prandtl number. For given values of Prandtl number and superheat ratio, the Dean number effect on solidification-free length is completely opposite depending on whether the solidification occurs in thermally developing or fully developed zones. The present investigation on solidification-free zones also provides

some insight into the solidification problem in curved channels for liquid metal and water.

4. Typical local Nusselt number results in the thermal entrance region are tabulated in Appendix C.3 for possible future reference.

CHAPTER VI

CONCLUSION

1. It is found that when $r \geq 10$, the curvature ratio effect on laminar flow results can be neglected practically. In laminar forced convection heat transfer analysis, the curvature ratio effect is also included in the formulation. However, it is also concluded that the curvature ratio effect is expected to be negligible for Nusselt number with $r \geq 10$.
2. The appearance of the additional secondary vortex rolls at a certain higher Dean number for fully developed laminar flow in curved rectangular channels is a new physical phenomenon revealed by the present analysis. The intensity of the secondary vortices is seen to be comparable to that of the primary vortices. Although some experimental works on curved channel flows have been reported in the literature, the effort appears to have been directed toward obtaining experimental data for friction factor and heat transfer coefficient only. It is suggested that a flow visualization study be conducted to confirm the existence of the additional streamwise vortex rolls near the central outer wall of the curved rectangular channels.

3. The Prandtl and Dean number effects on the heat transfer results are found to be similar for the three different thermal boundary conditions investigated. When Prandtl number is small, the local Nusselt number variation in the thermal entrance region behaves in the same way as the Graetz problem in straight channels. When Prandtl or Dean number is large, some cyclic behavior of Nusselt number appears before the fully developed asymptotic value is reached. For large Prandtl or Dean number case, the fully developed region is of practical interest since the thermal entrance length decreases with the increase of Prandtl or Dean number. Within the scope of this investigation, the effects of different thermal boundary conditions on the asymptotic Nusselt number values appear to be small for given Prandtl number and Dean numbers. In the case of uniform convective boundary condition, the cases of Biot numbers 1 and 10 are studied. The difference between the Nusselt number results for $Bi=1$ and 10 is found to be small. The limiting cases ($Bi \rightarrow 0$) and ($Bi \rightarrow \infty$) correspond to the complete insulation and the constant wall temperature cases, respectively.
4. It is found that the secondary flow effect on the liquid solidification-free zone in the curved rectangular channels is significant. For given values of Prandtl number and superheat ratio, the secondary flow effect on

solidification-free zone is completely opposite depending on whether the solidification occurs in the thermally developing or fully developed region. Although the problem has not been studied for the case of practically important case of curved circular tubes, one may expect that the trend of the phenomenon would be the same. In view of the significance of the secondary flow effect on liquid solidification-free zone in curved channels, a study of the secondary flow effect due to buoyance forces in straight tubes or channels seems to be important.

5. Graetz problem in curved tubes has been studied by several investigators in recent years. It is worthwhile to point out that hydrodynamic entrance region problem in helically coiled pipes has been solved successfully by numerical method [31]. This fact immediately suggests that the hydrodynamic entrance region problem in curved rectangular channels can be approached by numerical method. Furthermore, a possibility exists that the entrance region problem for simultaneous development of velocity and temperature fields can also be solved by numerical method.

REFERENCES

1. Dean, W.R., "Note on the Motion of Fluid in a Curved Pipe", Philosophical Magazine, Vol. 4, 1927, pp. 208-223.
2. Dean, W.R., "The Stream-Line Motion of Fluid in a Curved Pipe", Philosophical Magazine, Vol. 5, 1928, pp. 673-695.
3. Barua, S.N., "On Secondary Flow in Stationary Curved Pipes", Quarterly Journal of Mechanics and Applied Mathematics, Vol. 16, 1962, pp. 61-77.
4. Mori, Y., and Nakayama, W., "Study on Forced Convective Heat Transfer in Curved Pipes"; (1st Report, Laminar Region), International Journal of Heat and Mass Transfer, Vol. 8, 1965, pp. 67-82.
5. Austin, L.R., and Seader, J.D., "Fully Developed Viscous Flow in Coiled Circular Pipes", AIChE Journal, Vol. 19, 1973, pp. 85-94.
6. Austin, L.R., "The Development of Viscous Flow Within Helical Coils", Ph.D. Thesis, University of Utah, 1971.
7. Ito, H., "Theory on Laminar Flows Through Curved Pipes of Elliptic and Rectangular Cross-Sections", The Reports of the Institute of High Speed Mechanics, Tohoku University, Sendai, Japan, Vol. 1, 1951, pp. 1-16.
8. Cuming, H.G., "The Secondary Flow in Curved Pipes", Aeronautical Research Council, Reports and Memoranda, No. 2880, 1952.

9. Ludwig, H., "Die Ausgebildete Kanalströmung in Einem Rotierenden System", Ingenieur-Archiv, Vol. 19, 1951, pp. 296-308.
10. Mori, Y., and Uchida, Y., "Study on Forced Convective Heat Transfer in Curved Square Channel", Trans. Japan Society of Mechanical Engineers, Vol. 33, 1967, pp. 1836-1846.
11. Cheng, K.C., and Akiyama, M., "Laminar Forced Convection Heat Transfer in Curved Rectangular Channels", International Journal of Heat and Mass Transfer, Vol. 13, 1970, pp. 471-490.
12. Young, D., "The Numerical Solution of Elliptic and Parabolic Partial Differential Equations", Survey of Numerical Analysis, Edited by J. Todd, McGraw-Hill, New York, 1962, pp. 380-438.
13. Stuart, J.T., "Hydrodynamic Stability", Laminar Boundary Layers, Edited by L. Rosenhead, Oxford University Press, 1963, p. 505.
14. Mori, Y., Uchida, Y., and Ukon, T., "Forced Convective Heat Transfer in a Curved Channel with a Square Cross Section", International Journal of Heat and Mass Transfer, Vol. 14, 1971, pp. 1787-1805.
15. Baylis, J.A., "Experiments on Laminar Flow in Curved Channels of Square Section", Journal of Fluid Mechanics, Vol. 48, 1971, pp. 417-422.

16. Tarbell, J.M., and M.R. Samuels, "Momentum and Heat Transfer in Helical Coils", Chemical Engineering Journal, Vol. 5, 1973, pp. 117-127.
17. Nunge, R.J., and Lin, T.S., "Laminar Flow in Strongly Curved Tubes", AIChE Journal, Vol. 19, 1973, pp. 1280-1281.
18. Ito, H., "Laminar Flow in Curved Pipes", ZAMM, Vol. 49, 1969, pp. 653-663.
19. Dravid, A.N., Smith, K.A., Merrill, E.W., and Brian, P.L.T., "Effect of Secondary Fluid Motion on Laminar Flow Heat Transfer in Helically Coiled Tubes", A.I.Ch.E. Journal Vol. 17, 1971, pp. 1114-1122.
20. Akiyama, M., and Cheng, K.C., "Laminar Forced Convection in the Thermal Entrance Region of Curved Pipes with Uniform Wall Temperature", The Canadian Journal of Chemical Engineering, Vol. 52, 1974.
21. Akiyama, M., and Cheng, K.C., "Graetz Problem in Curved Pipes with Uniform Wall Heat Flux", Applied Scientific Research (in press).
22. Peaceman, D.W., and Rachford, H.H., "The Numerical Solution of Parabolic and Elliptic Differential Equations", Journal of the Society of Industrial and Applied Mathematics, Vol. 3, 1955, pp. 28-41.
23. Akiyama, M., and Cheng, K.C., "Boundary Vorticity Method for Laminar Forced Convection Heat Transfer in Curved

- Pipes", International Journal of Heat and Mass Transfer, Vol. 14, 1971, pp. 1659-1675.
24. Kalb, C.E., and Seader, J.D., "Heat and Mass Transfer Phenomena for Viscous Flow in Curved Circular Tubes", International Journal of Heat and Mass Transfer, Vol. 15, 1972, pp. 801-817.
25. Schneider, P.J., "Effect of Axial Fluid Conduction on Heat Transfer in the Entrance Regions of Parallel Plates and Tubes", Trans. ASME, Vol. 79, 1957, pp. 765-773.
26. Hsu, C.J., and Huang, C.J., "Heat or Mass Transfer in Laminar Flow Through a Concentric Annulus with Convective Flux at Walls", Chem. Engrg., Sci. Vol. 21, 1966, pp. 209-221.
27. Hsu, C.J., "Exact Solution to Entry-Region Laminar Heat Transfer with Axial Conduction and the Boundary Condition of the Third Kind", Chem. Engrg., Sci, Vol. 23, 1968, pp. 457-468.
28. Lock, G.S.H., Freeborn, R.D.J., and Nyren, R.H., "Analysis of Ice Formation in a Convectively-Cooled Pipe", Heat Transfer 1970, Vol. 1, Cu 2.9, Elsevier, Amsterdam.
29. Zerkle, R.D., "The Effect of External Thermal Insulation on Liquid Solidification in a Tube", Proc. of the 6th South-eastern Seminar on Thermal Sciences, 1970, pp. 1-19.

30. Hwang, G.J., and Yih, I., "Correction on the Length of Ice-Free Zone in a Convectively-Cooled Pipe", Int. J. of Heat and Mass Transfer, Vol. 16, 1973, pp. 681-683.
31. Patankar, S.V., Pratap, V.S., and Spalding, D.B., "Prediction of Laminar Flow and Heat Transfer in Helically Coiled Pipes", J. Fluid Mech., Vol. 62, 1974, pp. 539-551.
32. Malvern, L.E., "Introduction to the Mechanics of a Continuous Medium", Prentice-Hall, Inc. Englewood Cliffs, New Jersey, 1969, pp. 641-672.

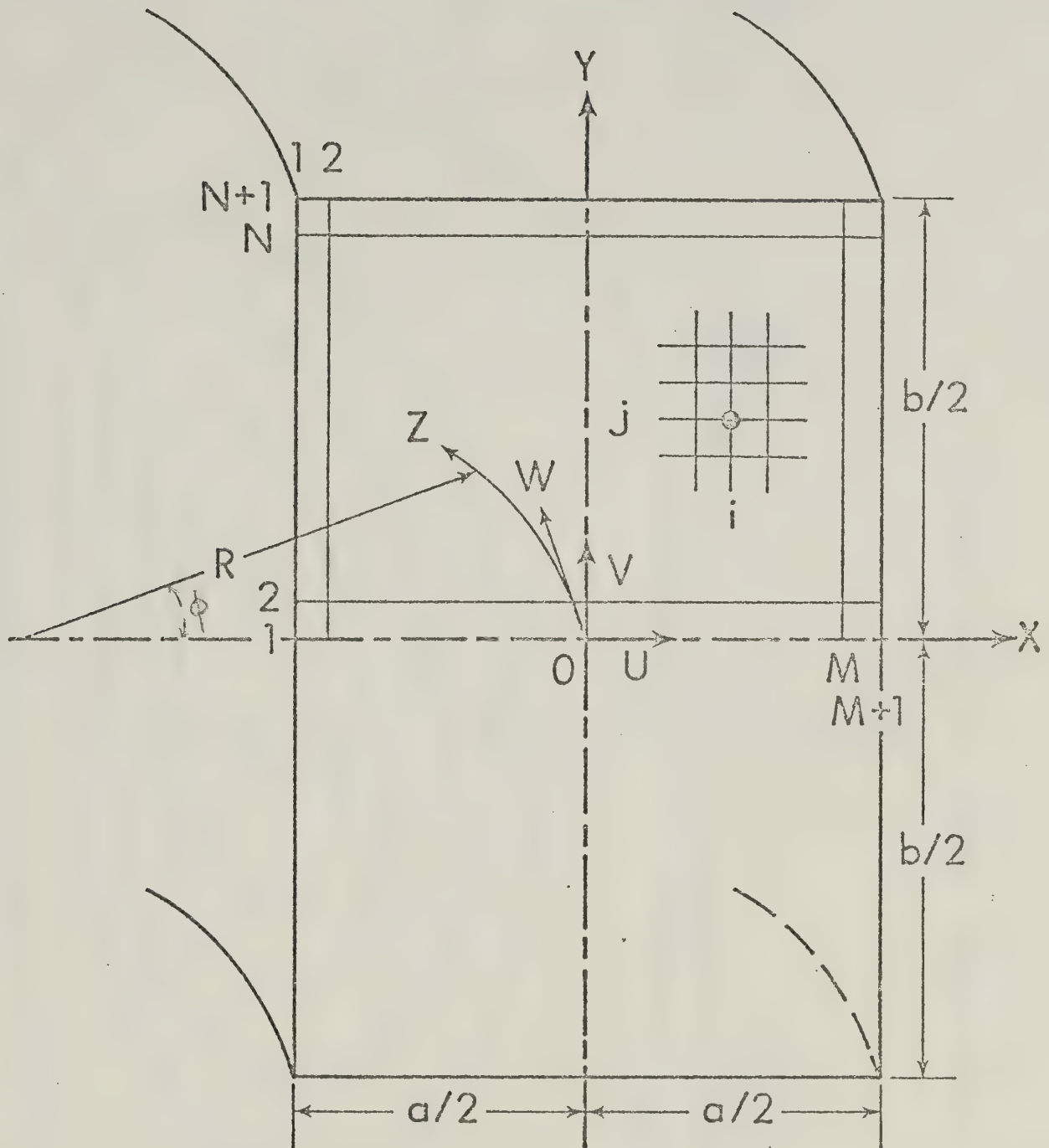


Fig. 1 Coordinate system and numerical grid for curved rectangular channel

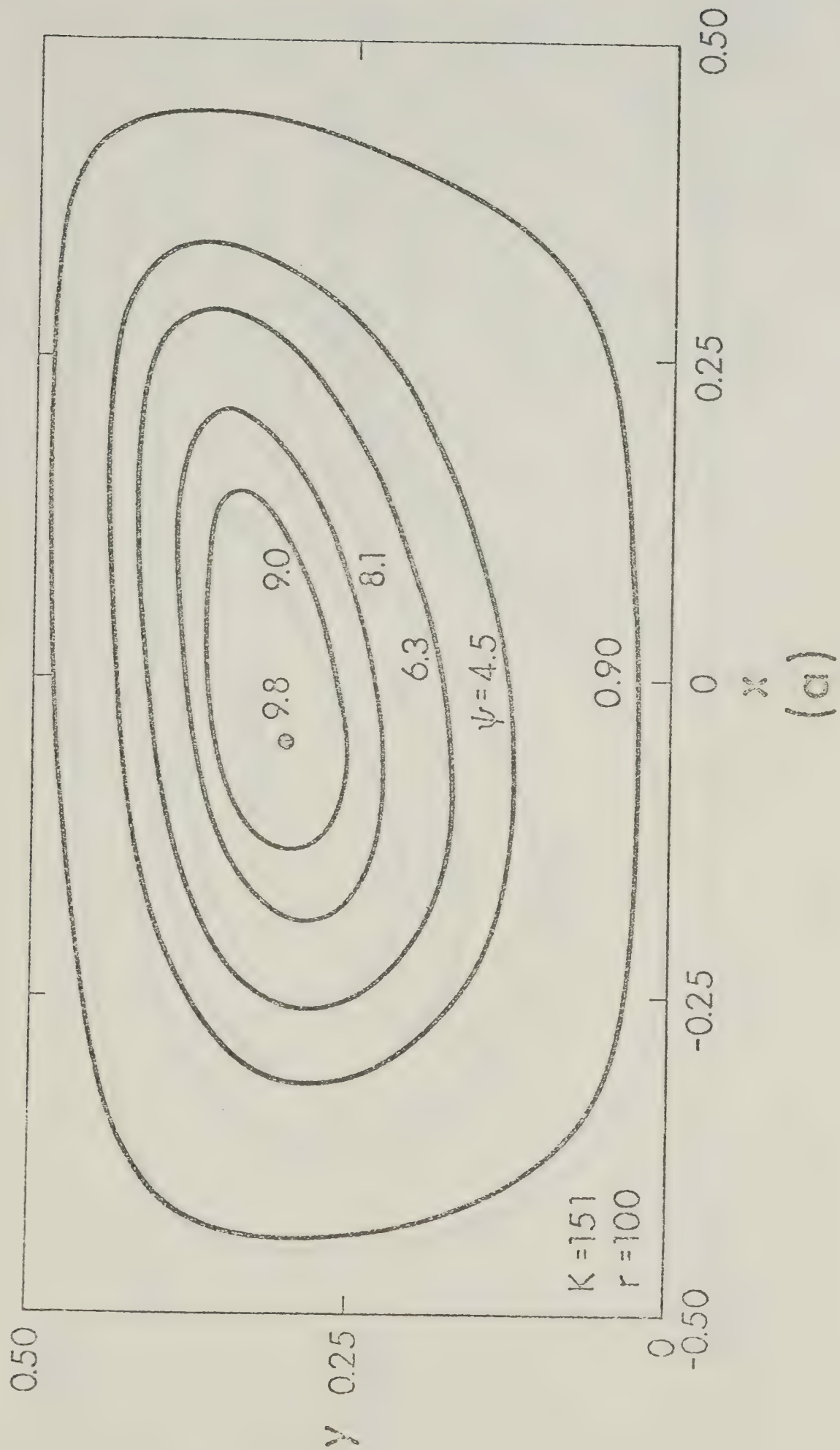
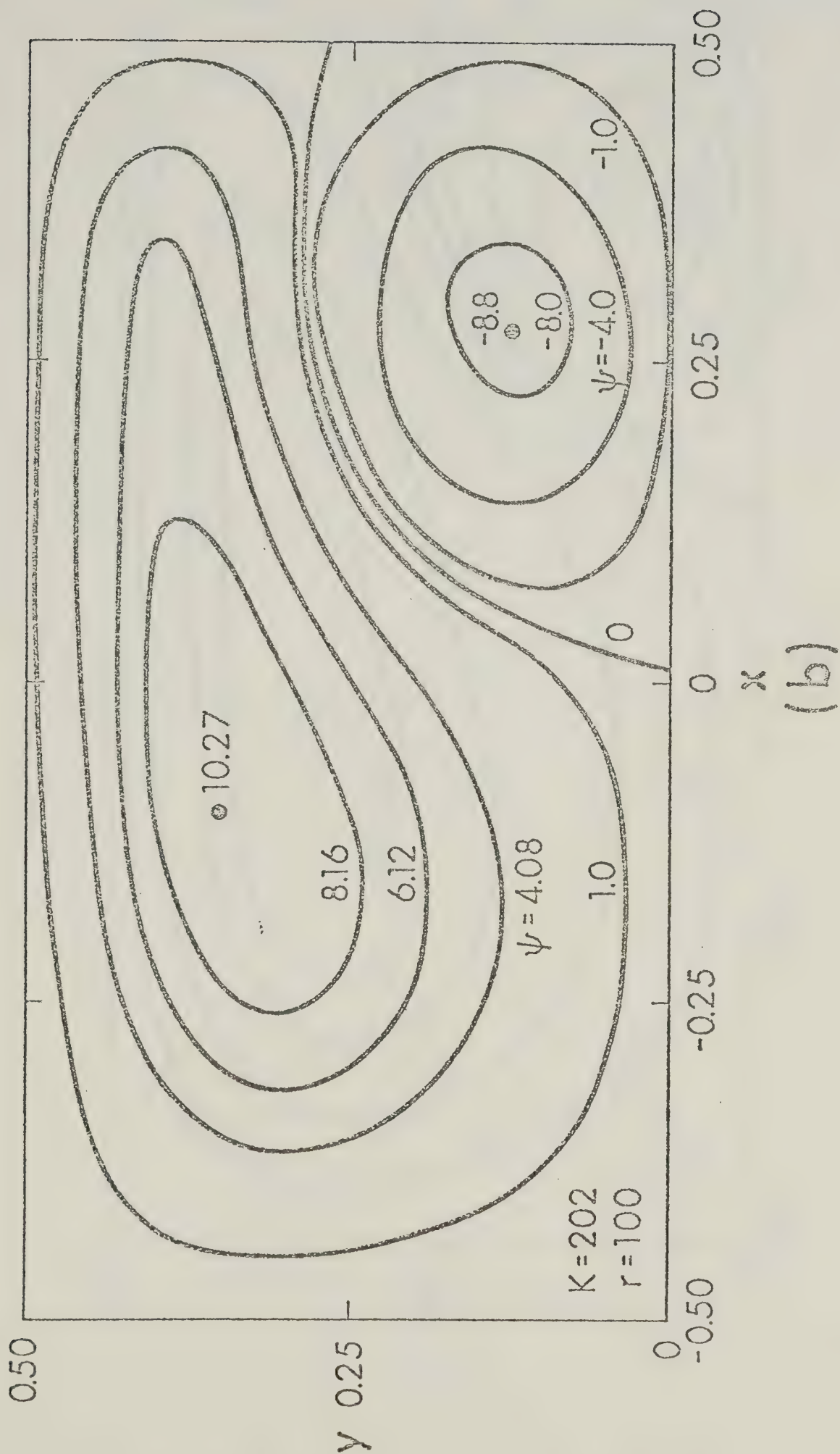
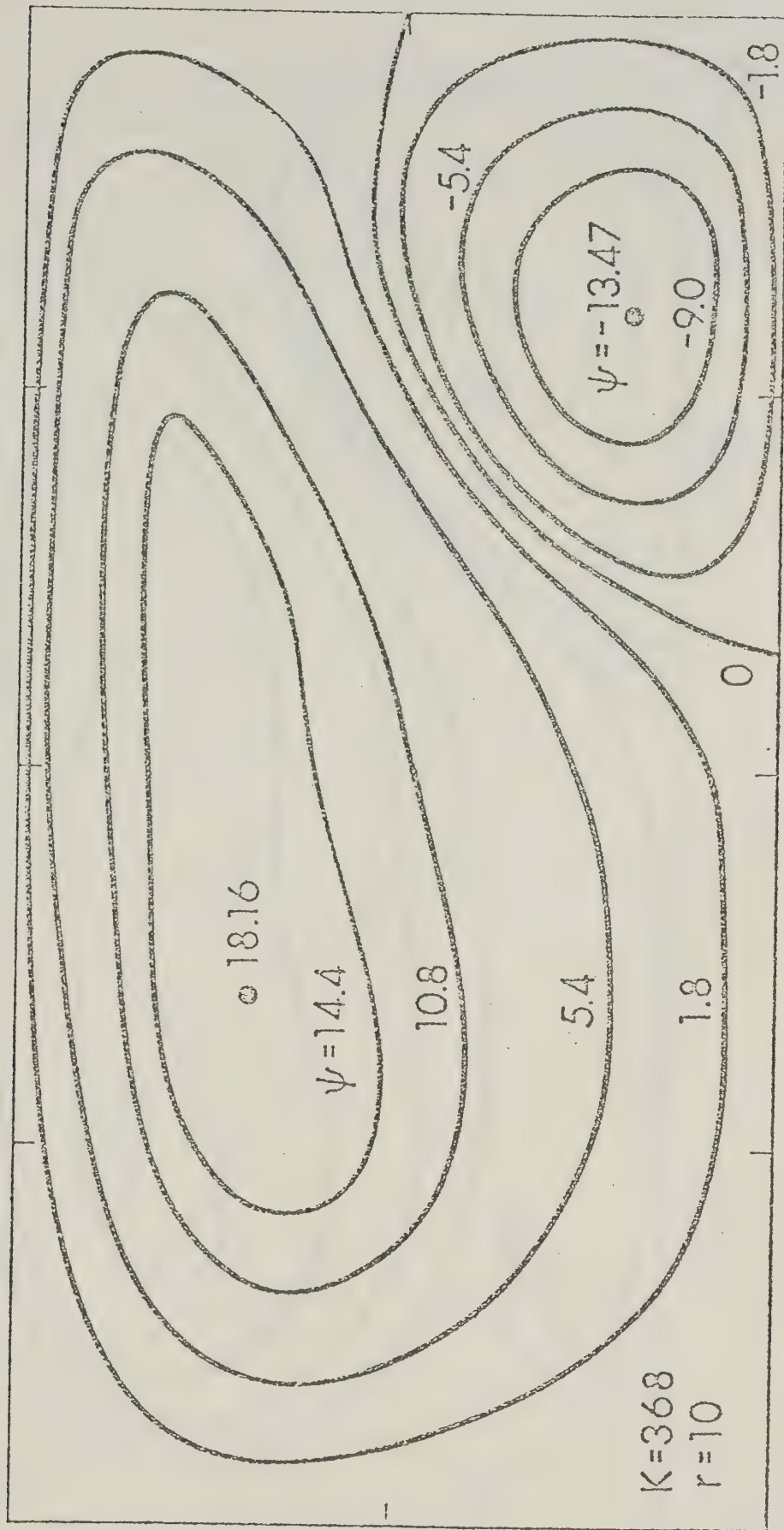


Fig. 2 Stream-function contours for square channels.



0.50

y 0.25



K=368
r=10

0 -0.50

-0.25

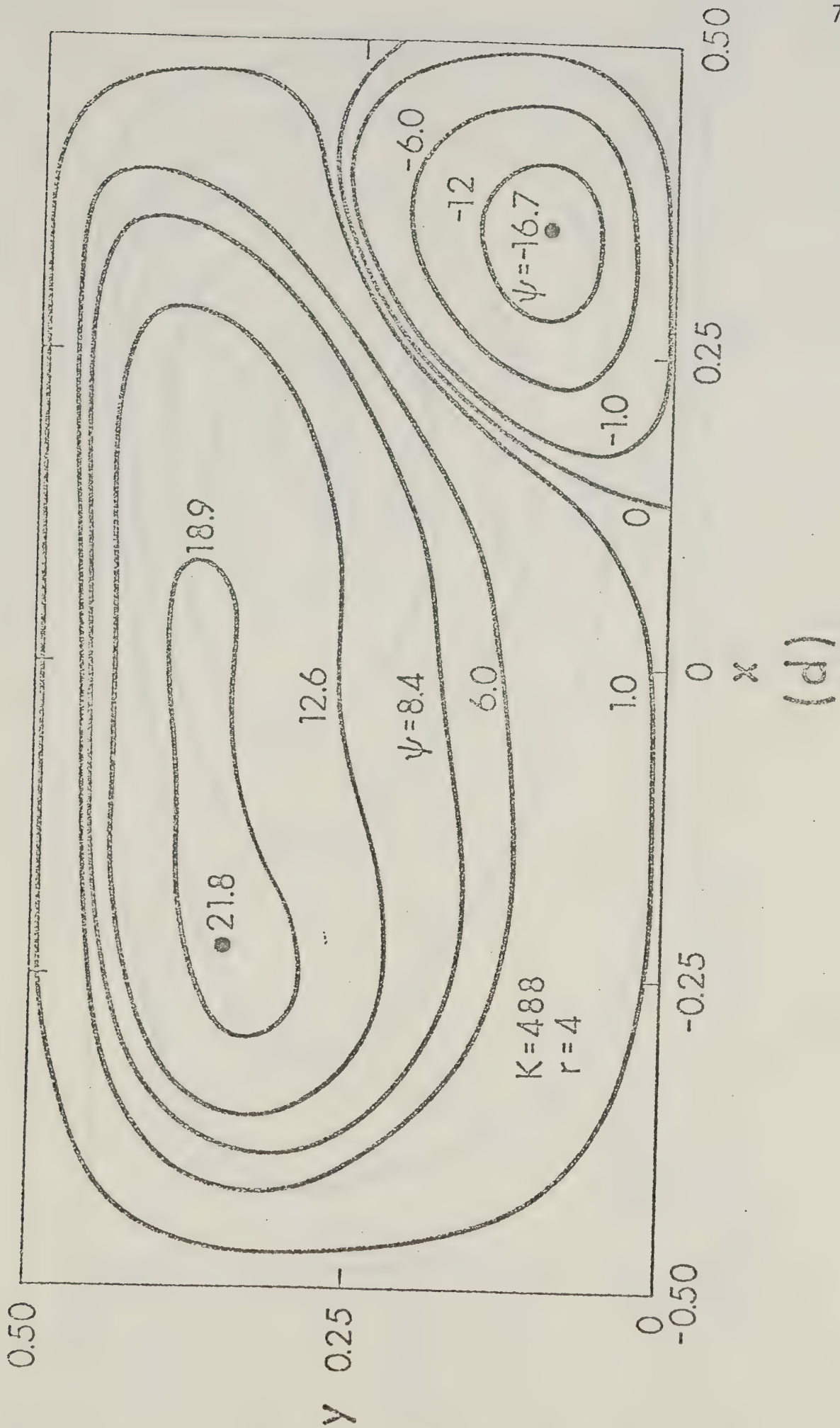
x

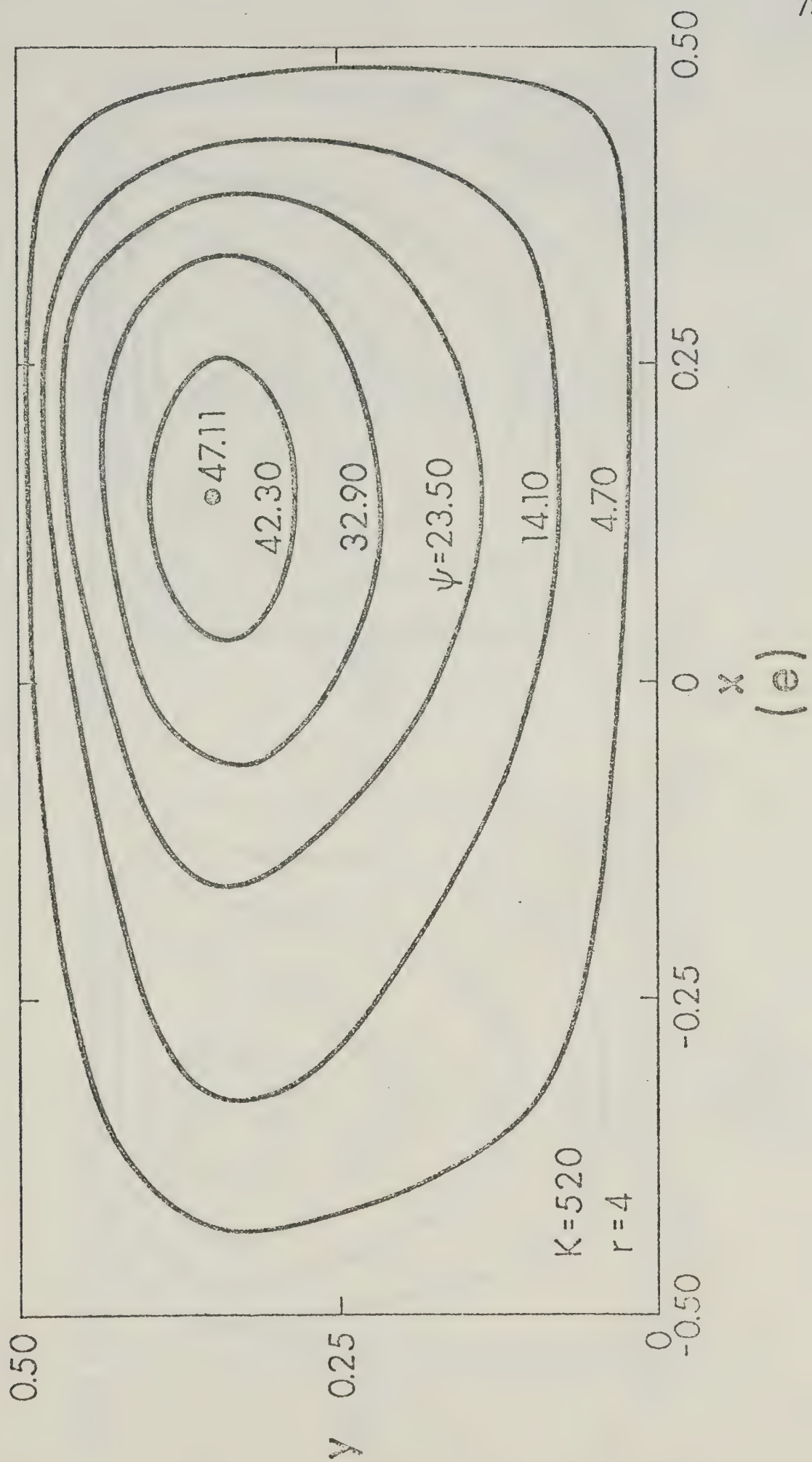
0

0.25

0.50

(c)





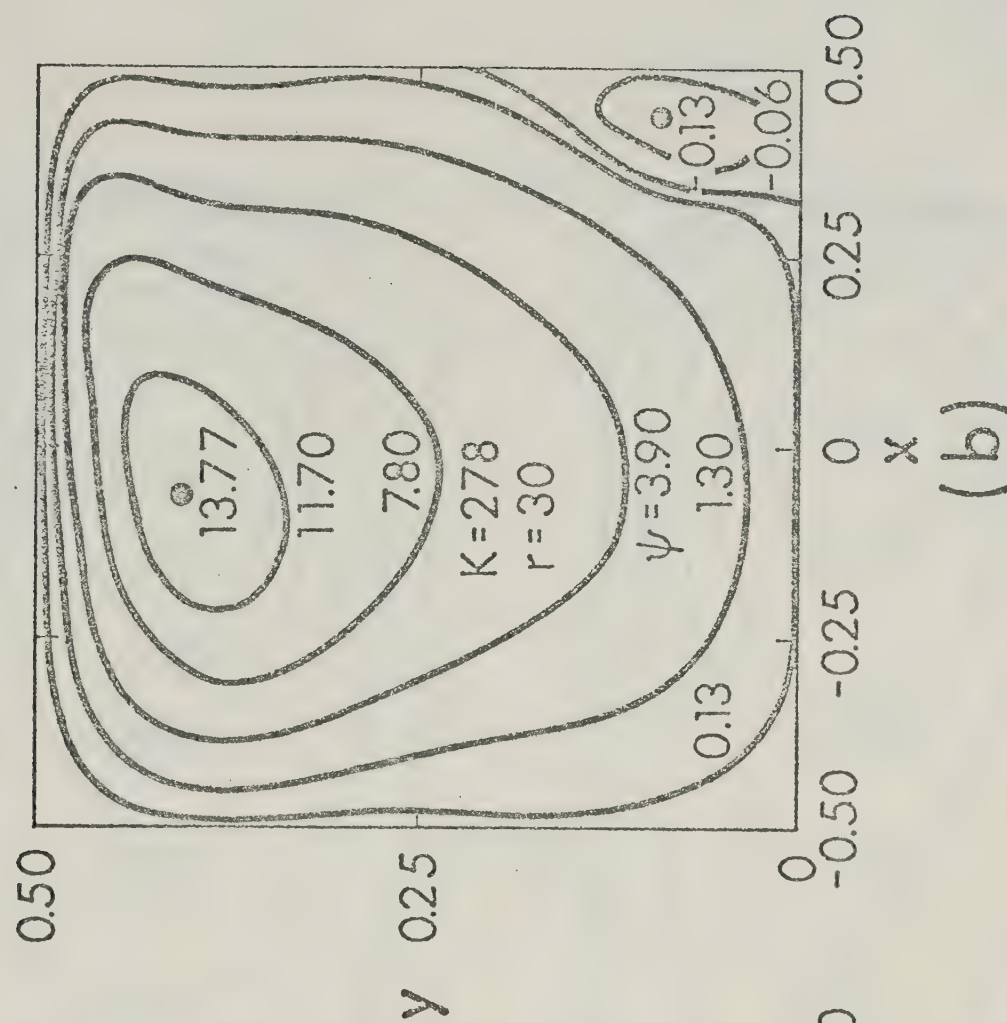
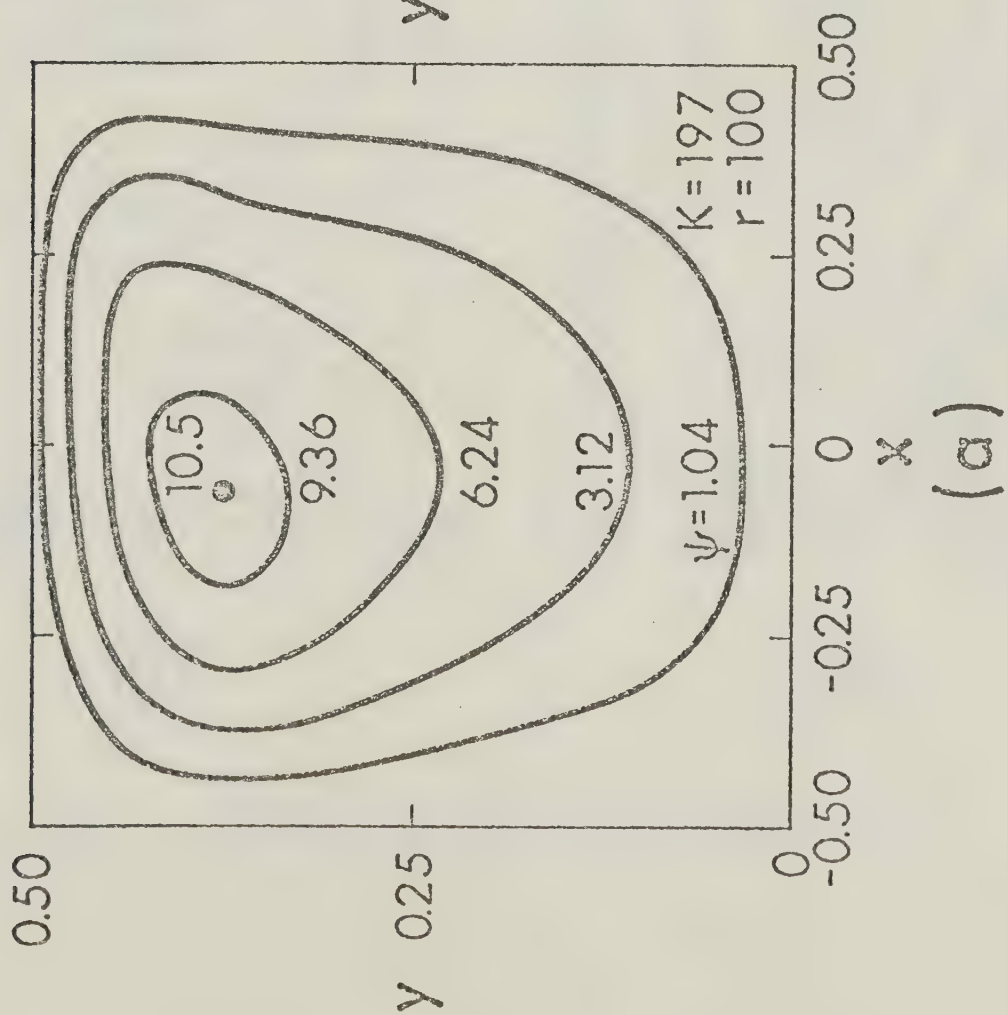


Fig. 3 Stream - function contours for $\gamma = 2$

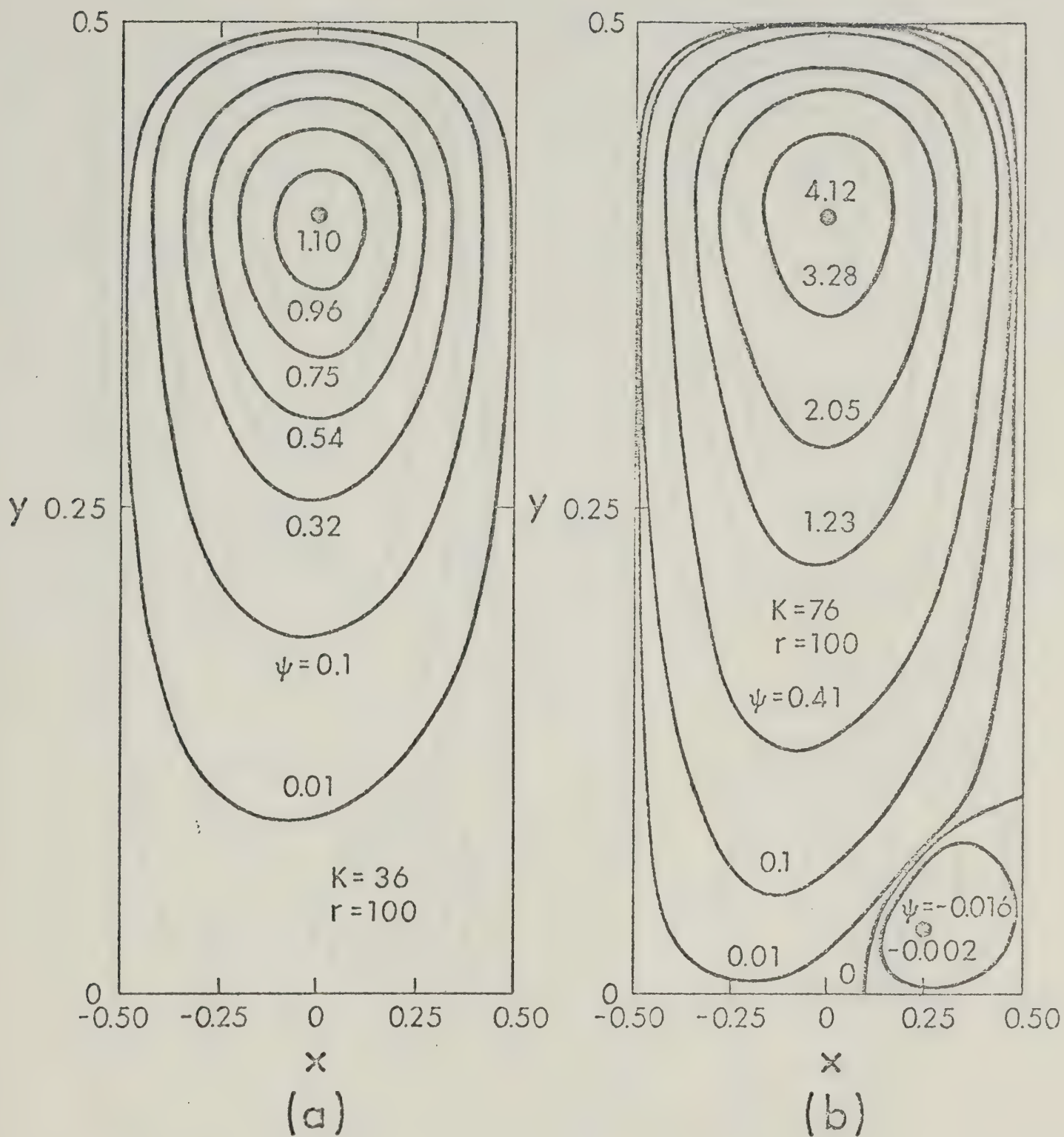
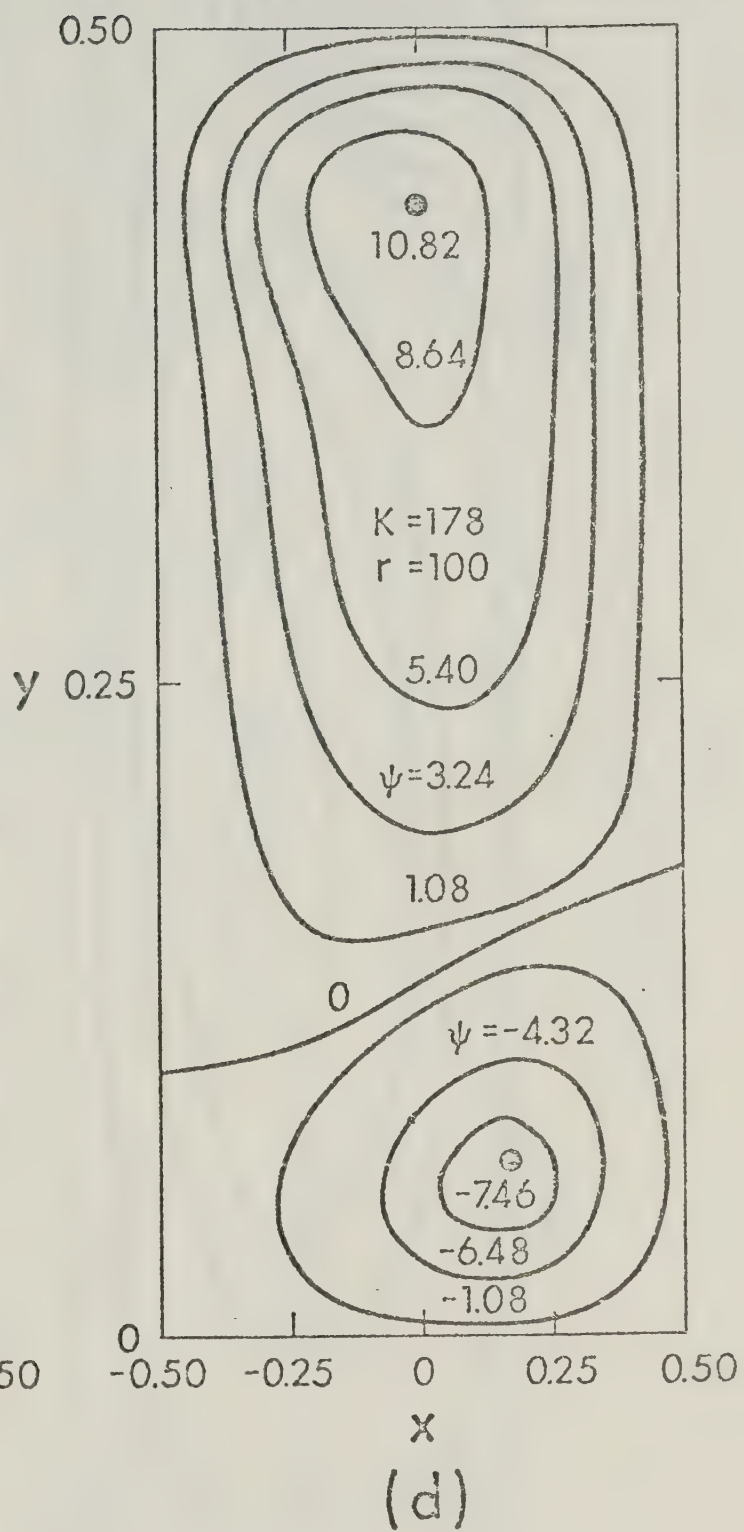
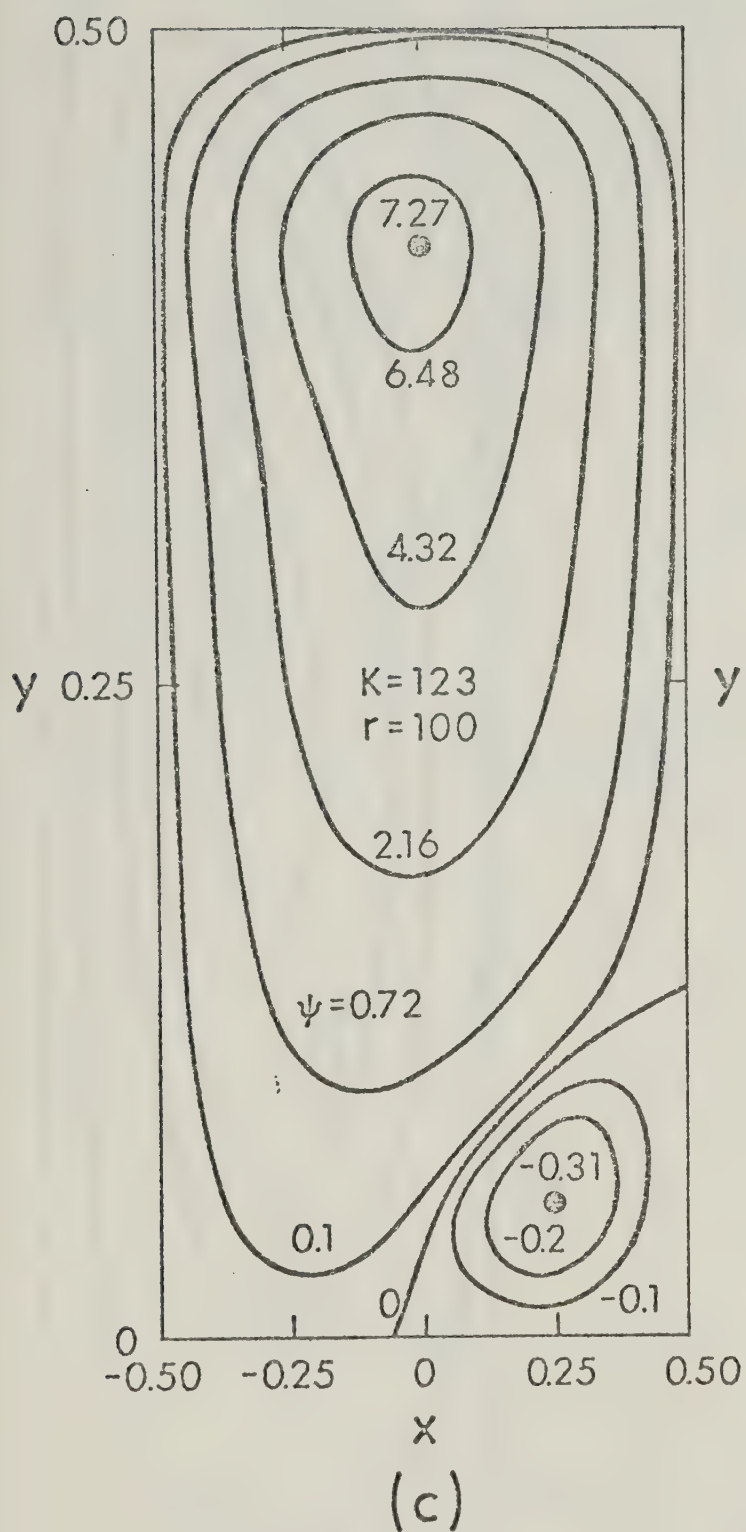


Fig. 4 Stream - function contours for $\gamma = 5$



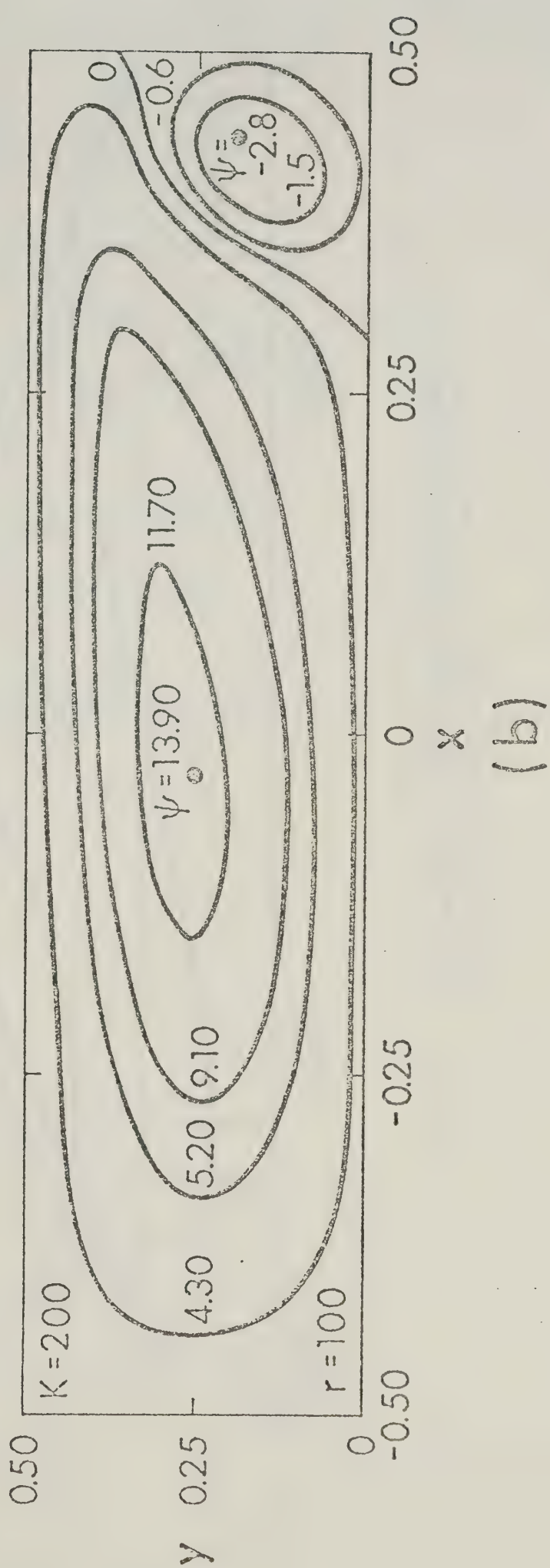
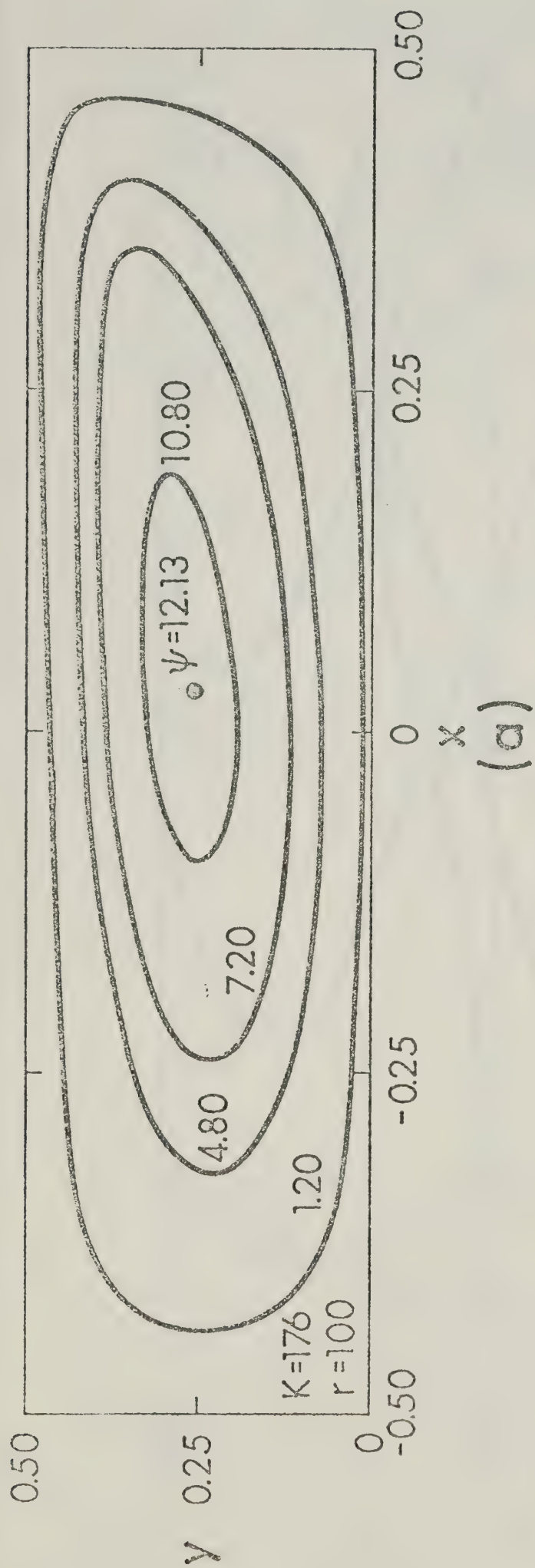


Fig. 5 Stream - function contours for $\gamma = 0.5$

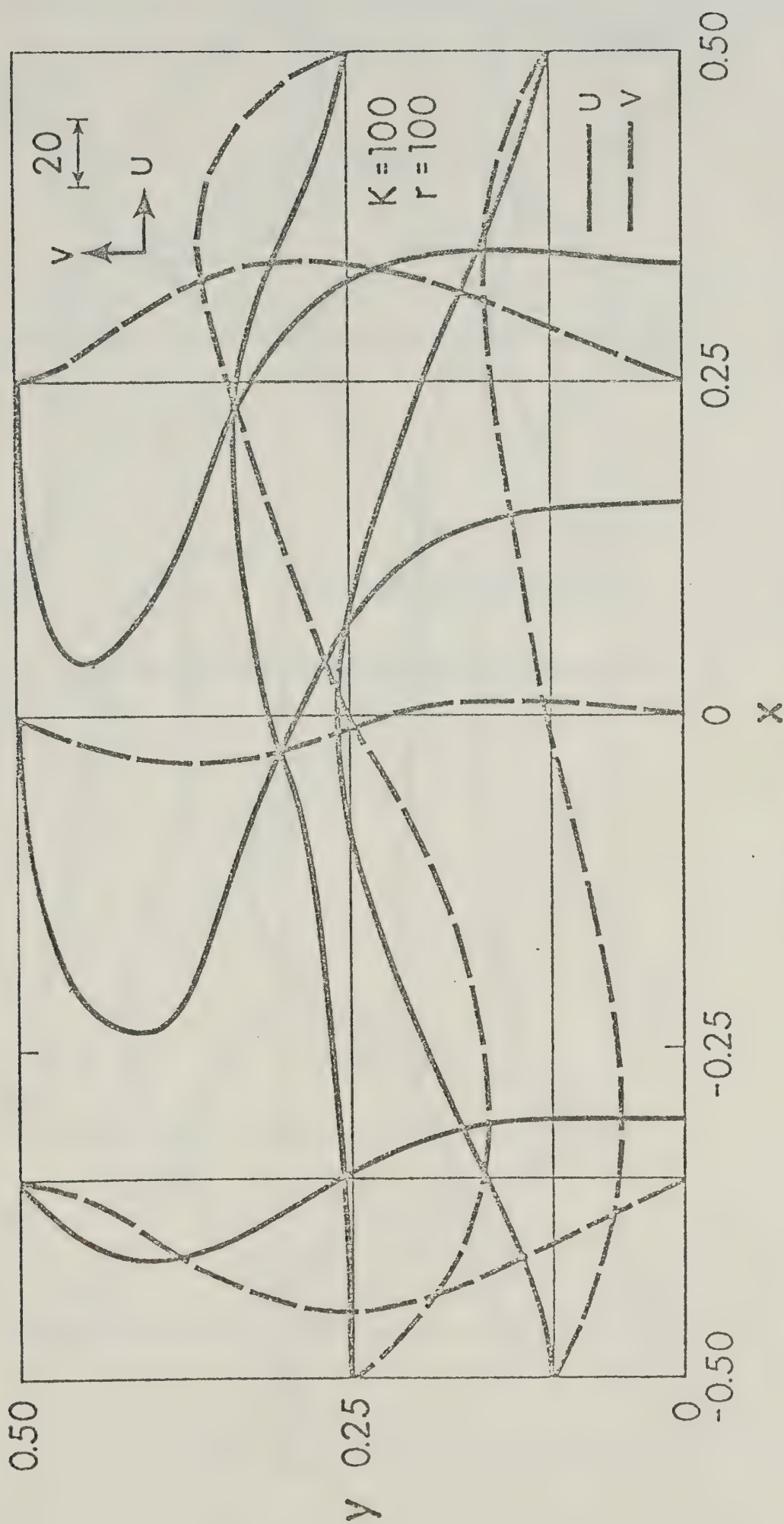


Fig. 6 Distributions of secondary velocity components u, v at selected locations for $\gamma = 1$ and $K = 100$

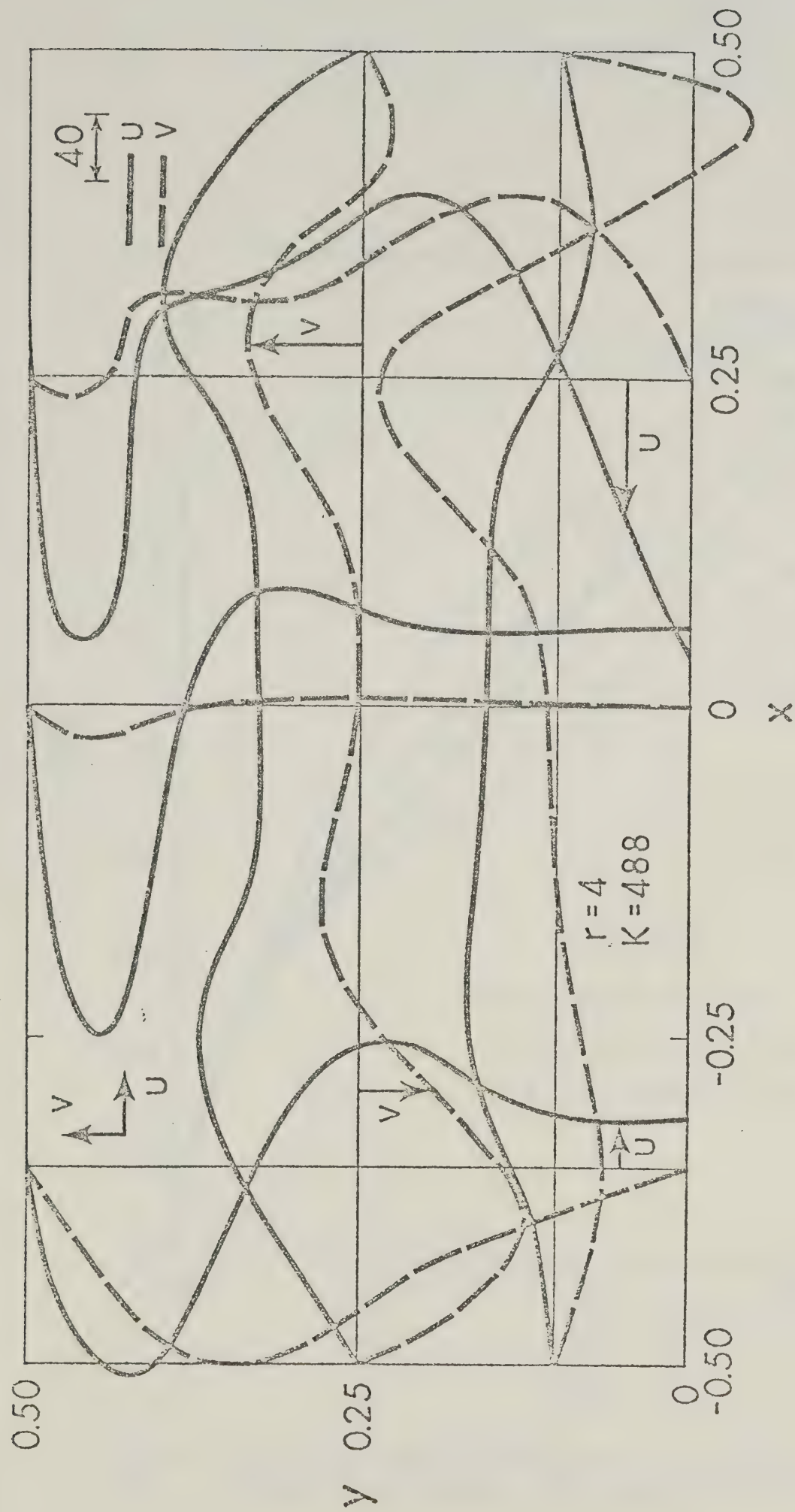


Fig. 7 Distributions of secondary velocity components u, v at selected locations for $\gamma = 1$ and $K = 488$

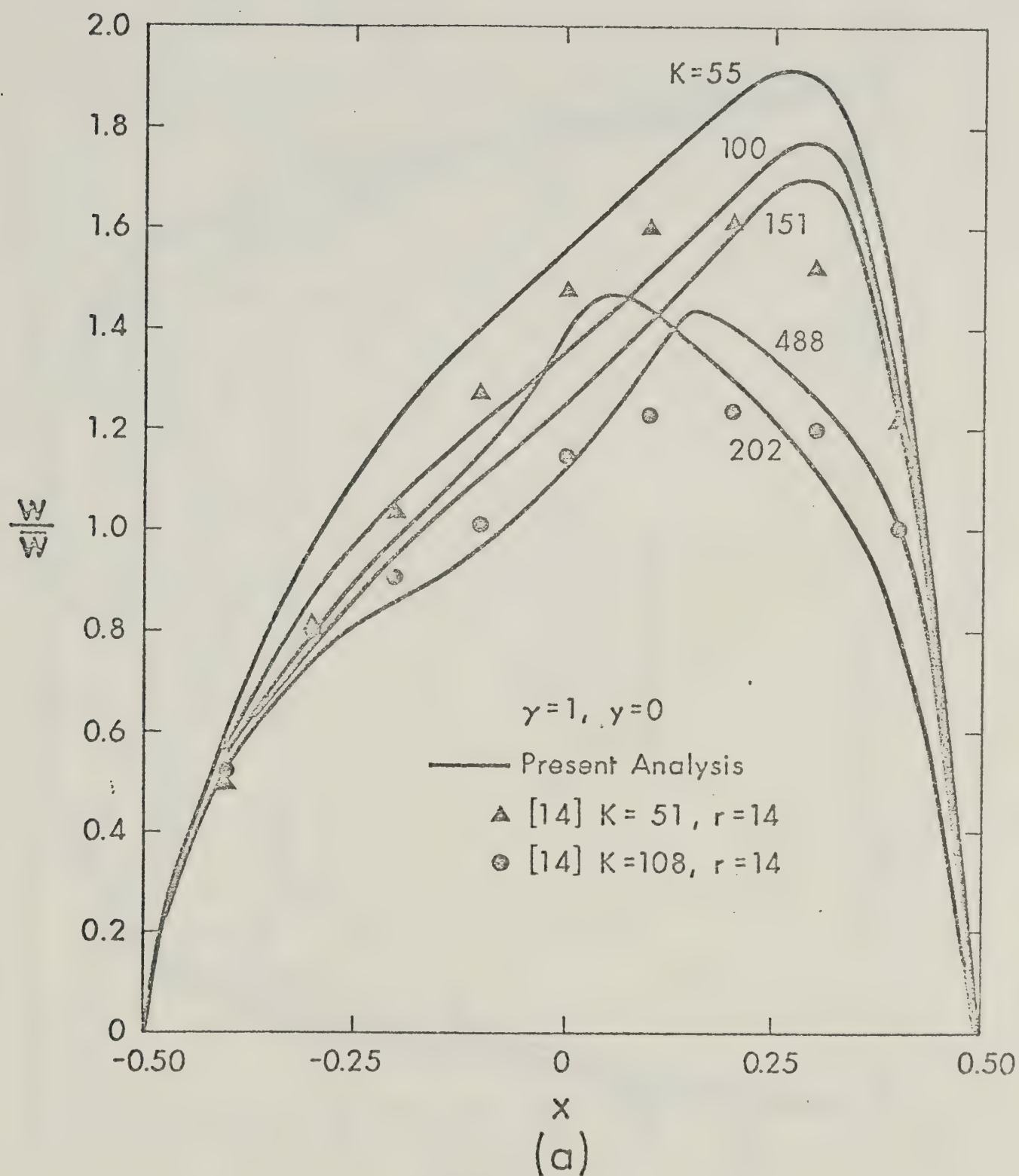
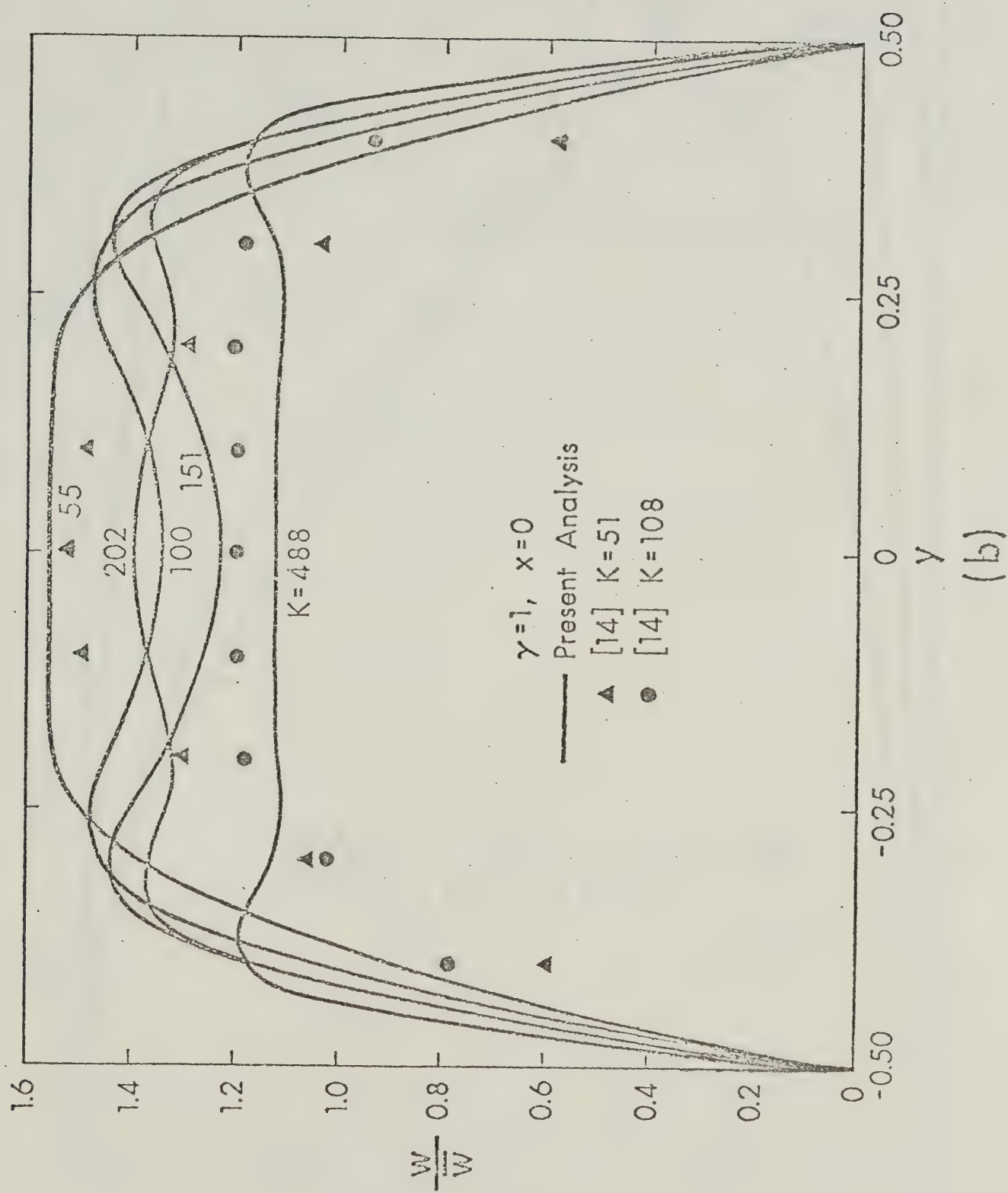


Fig. 8 Axial velocity distributions in square channel with Dean number as parameter and comparison with experimental data



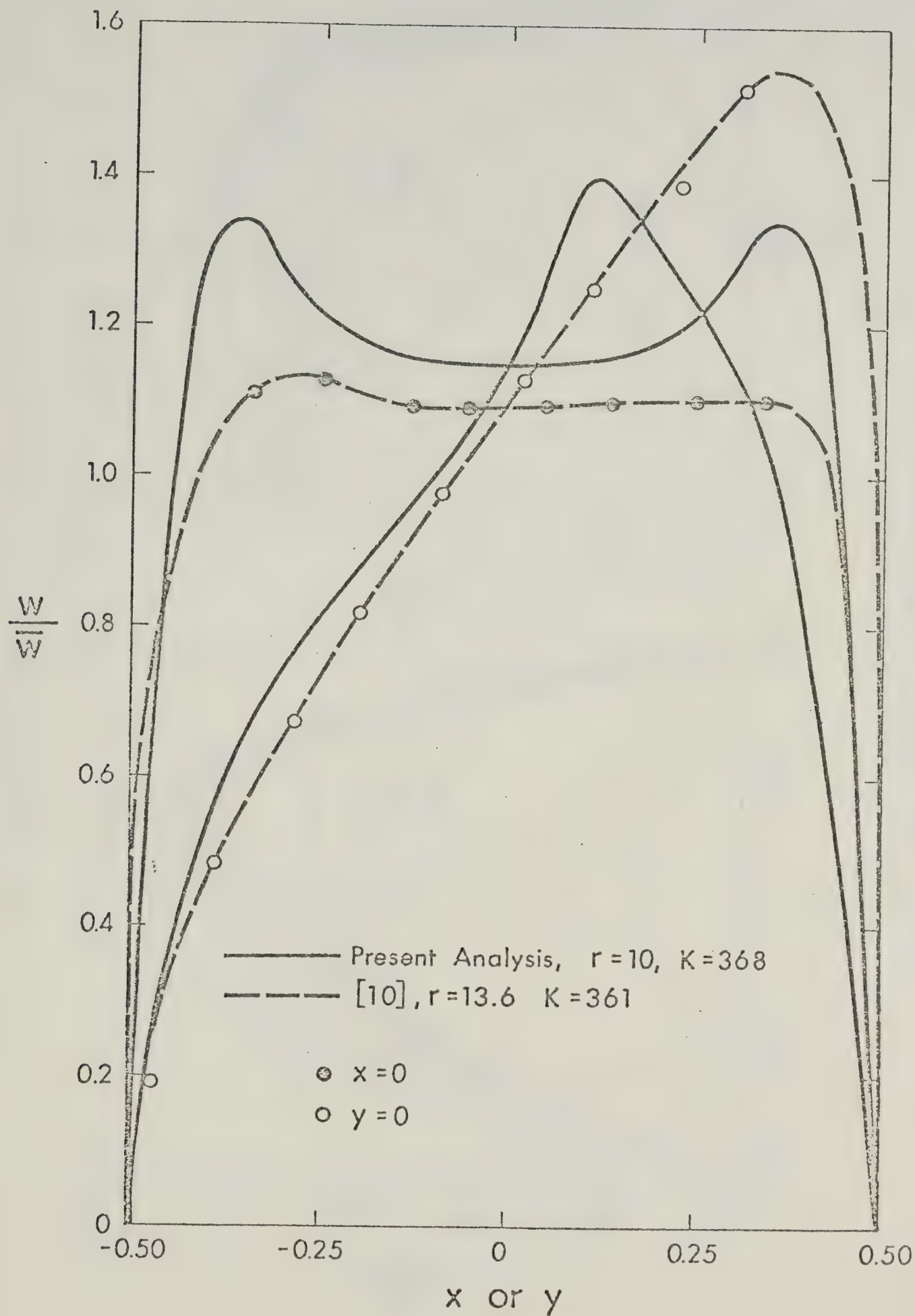


Fig. 9 Axial velocity distributions in square channel and comparison with experimental data

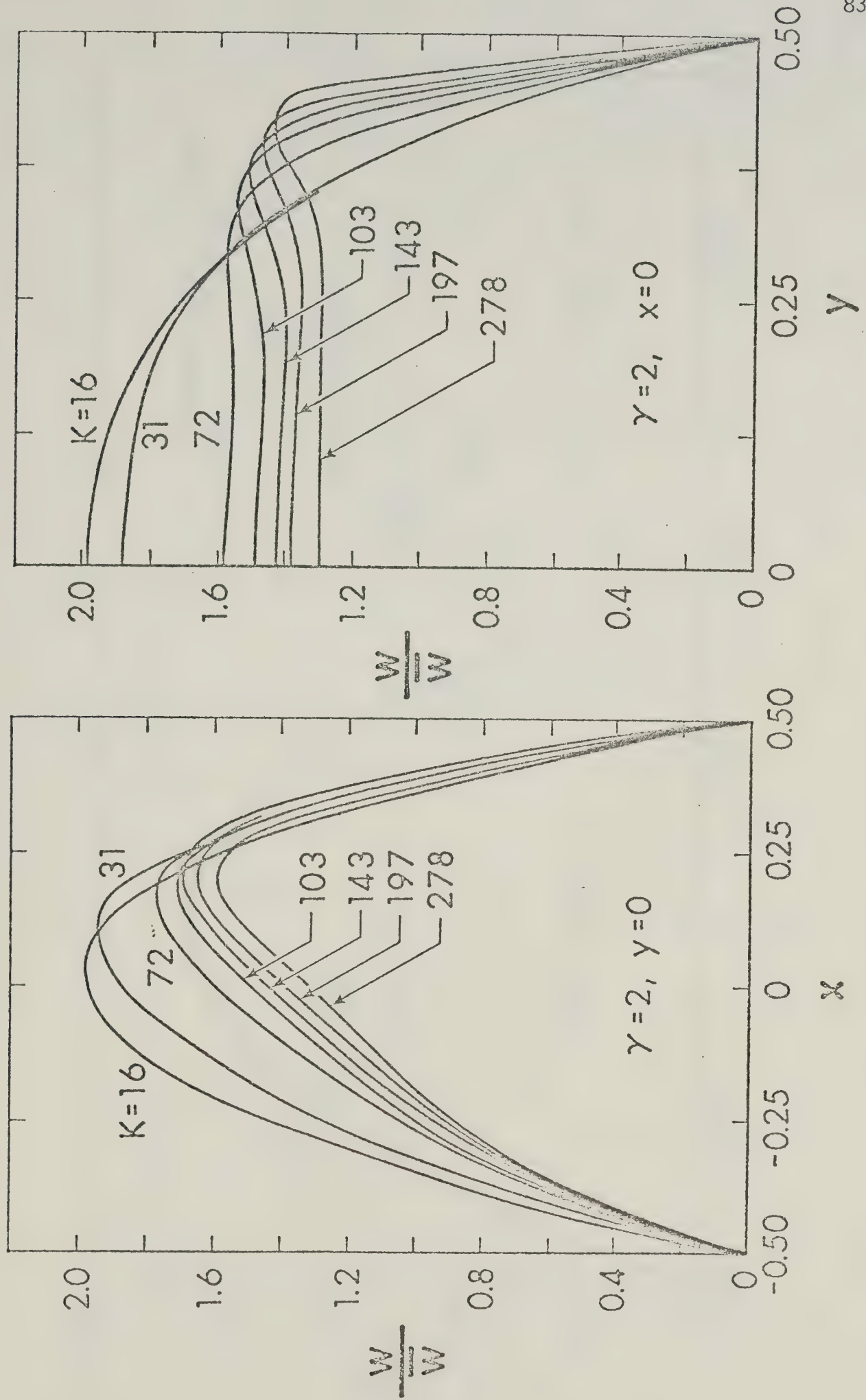


Fig. 10 Axial velocity distributions for $\gamma = 2$ with Deen number as parameter

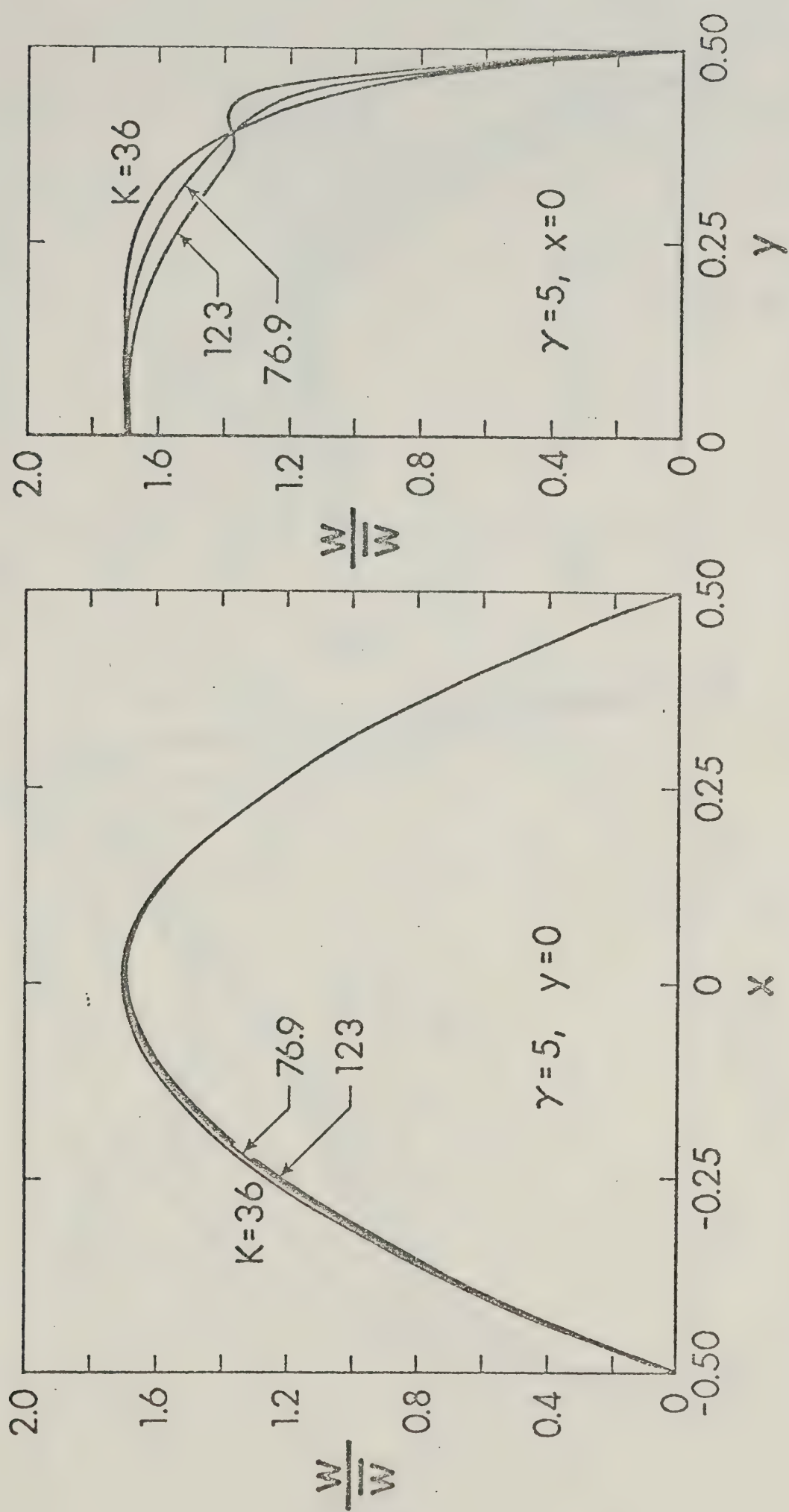


Fig. 11 Axial velocity distributions for $\gamma = 5$ with Dean number as parameter

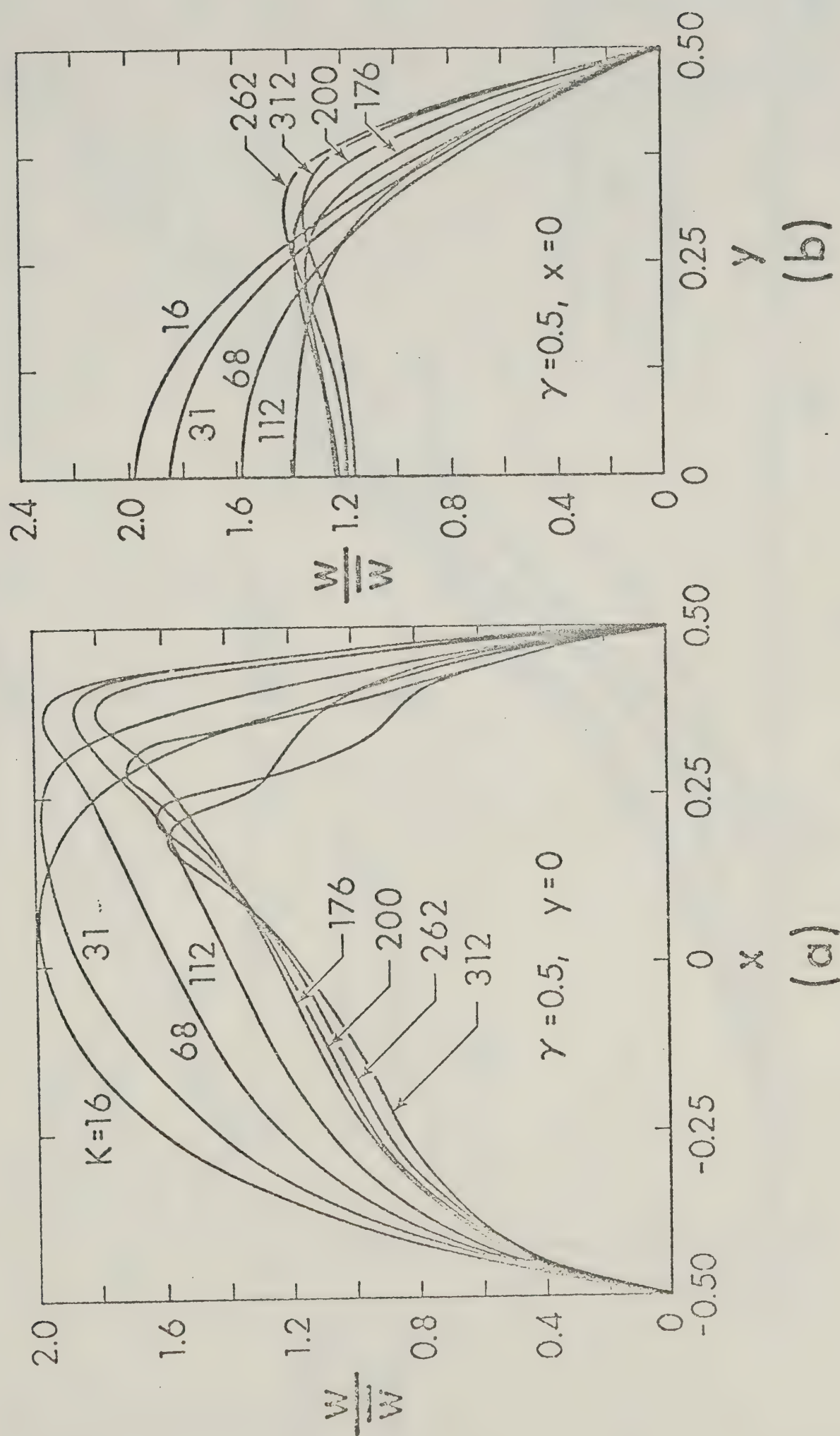


Fig. 12 Axial velocity distributions for $\gamma = 0.5$ with Dean number as parameter

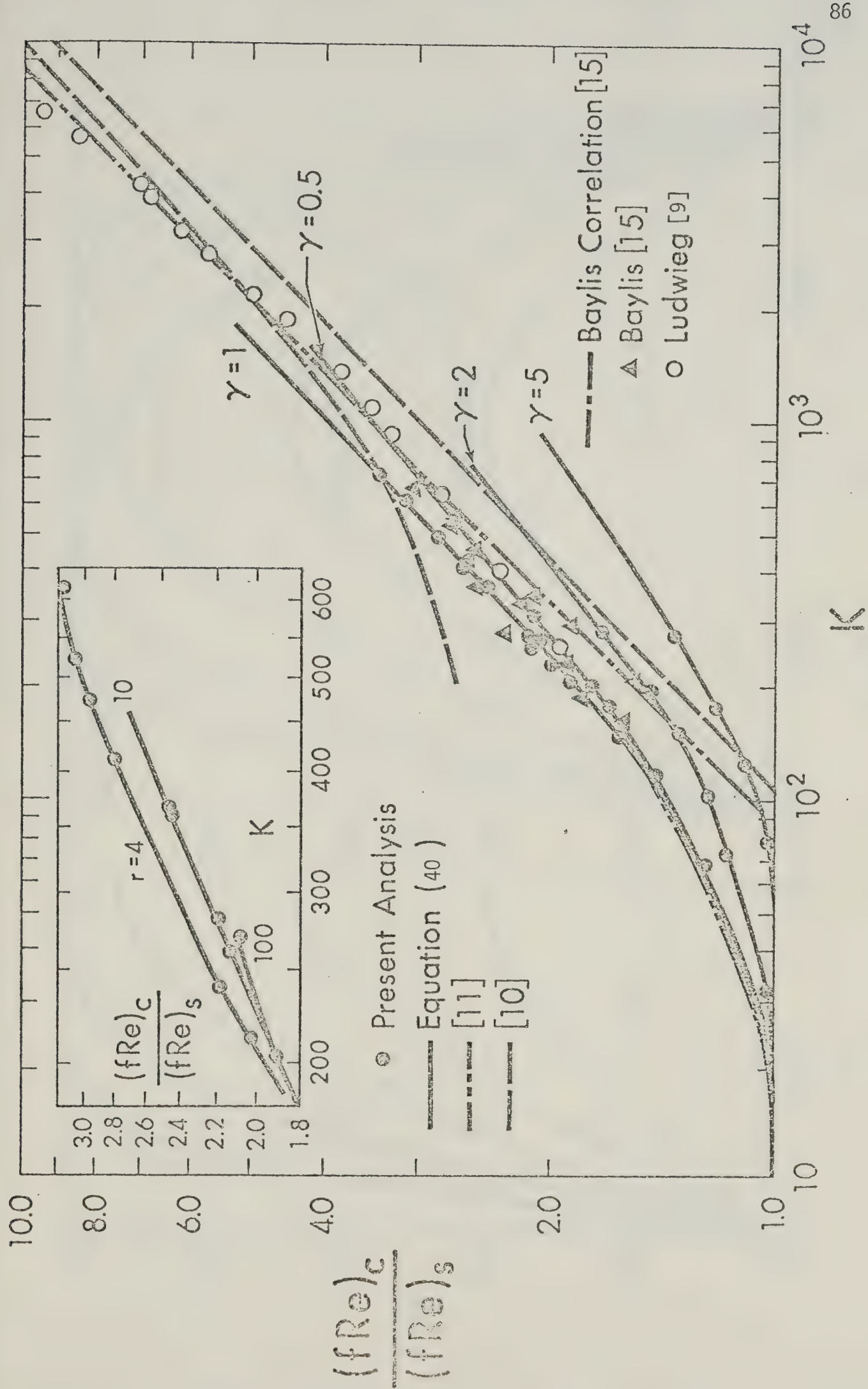


Fig. 13 Friction factor results and comparison with available theoretical and experimental results

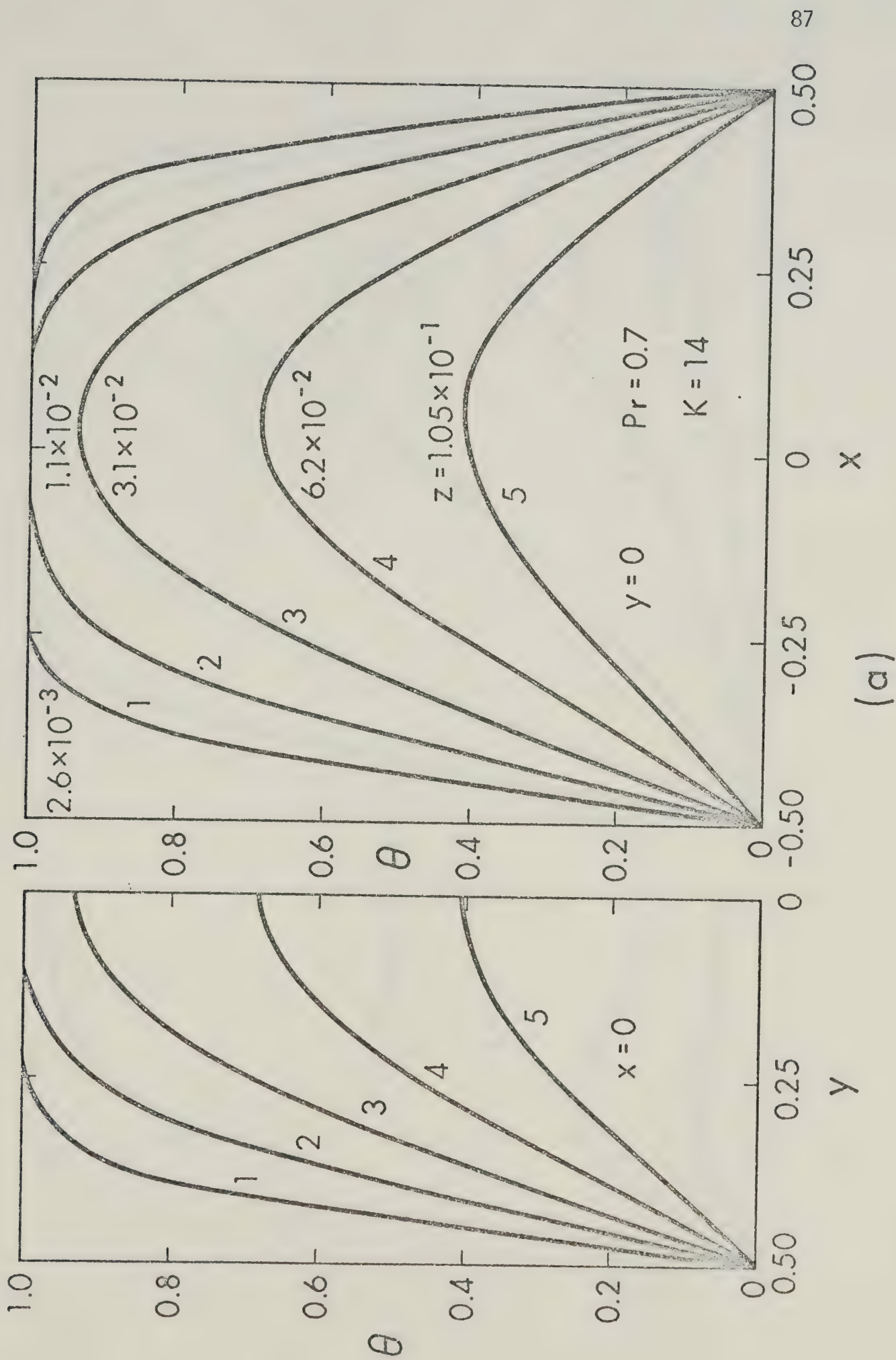
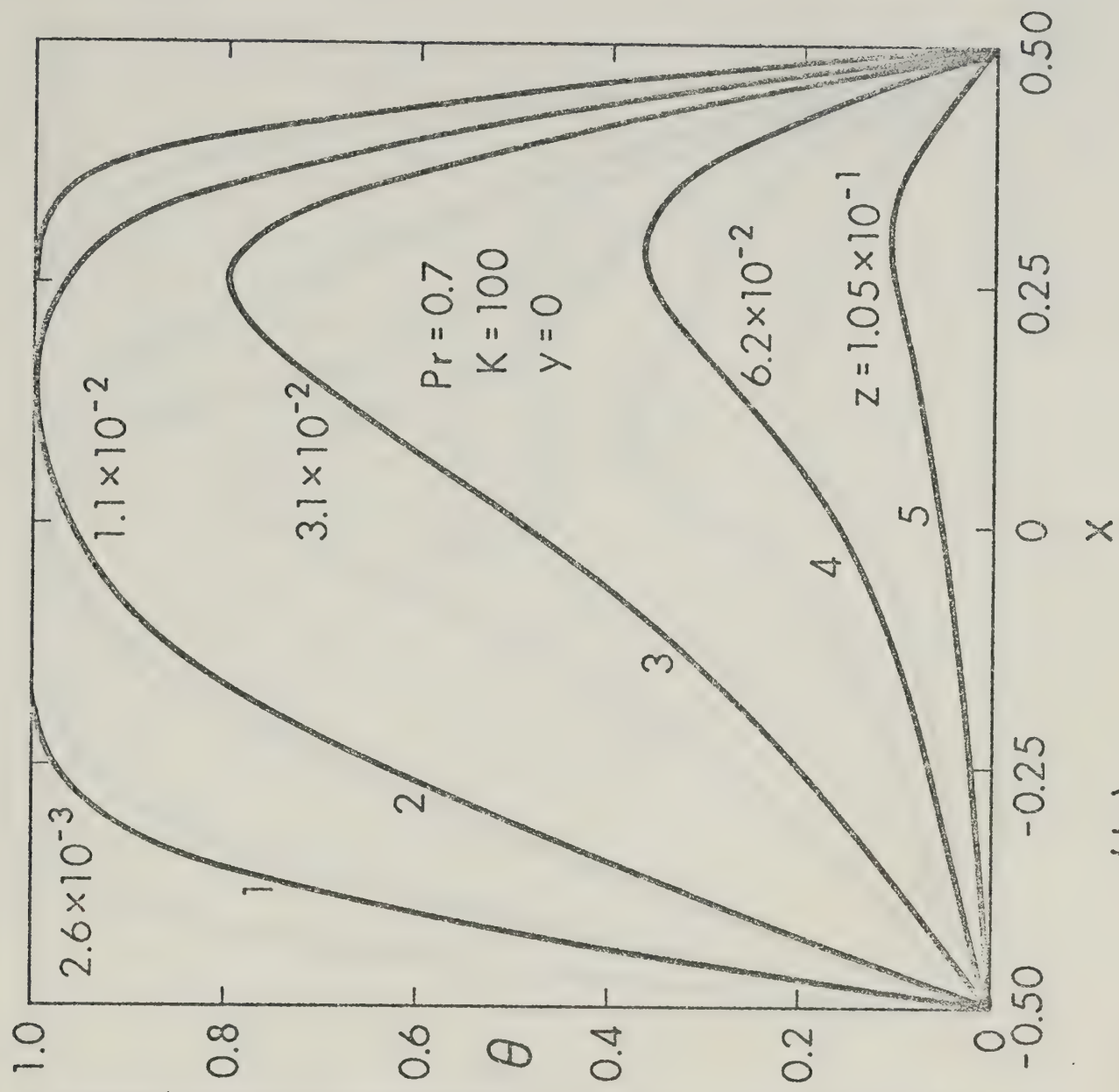
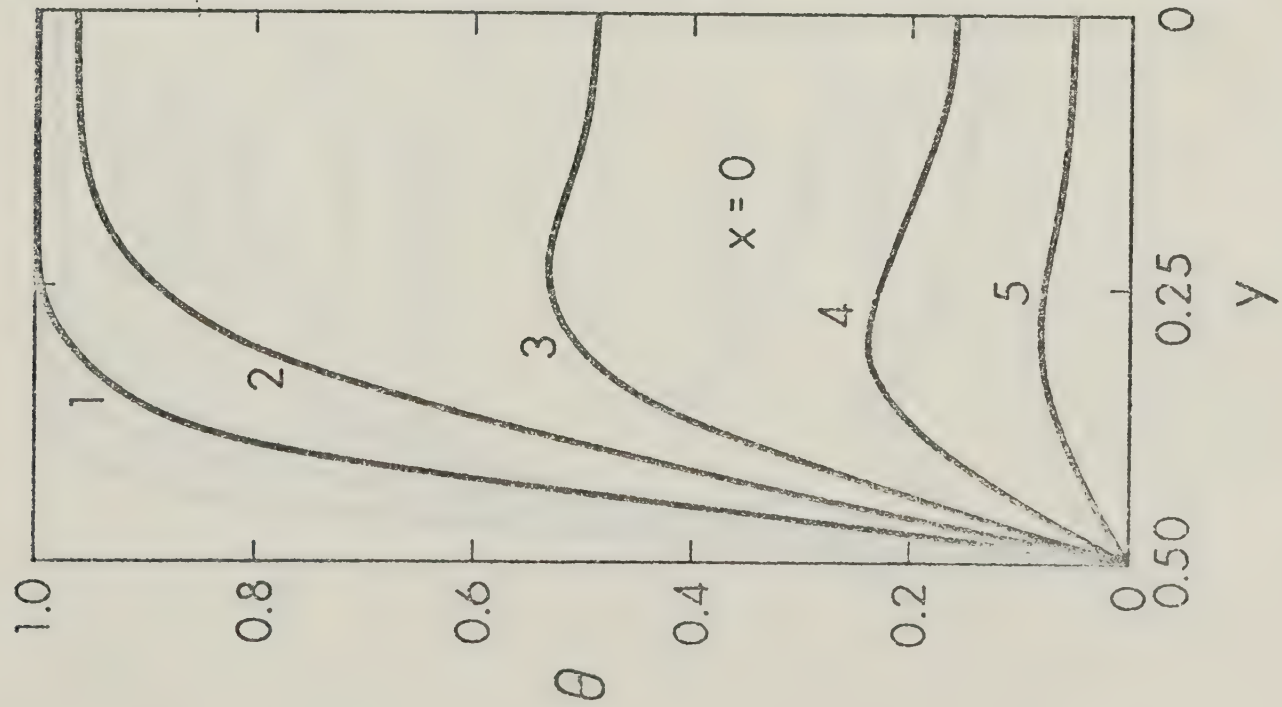
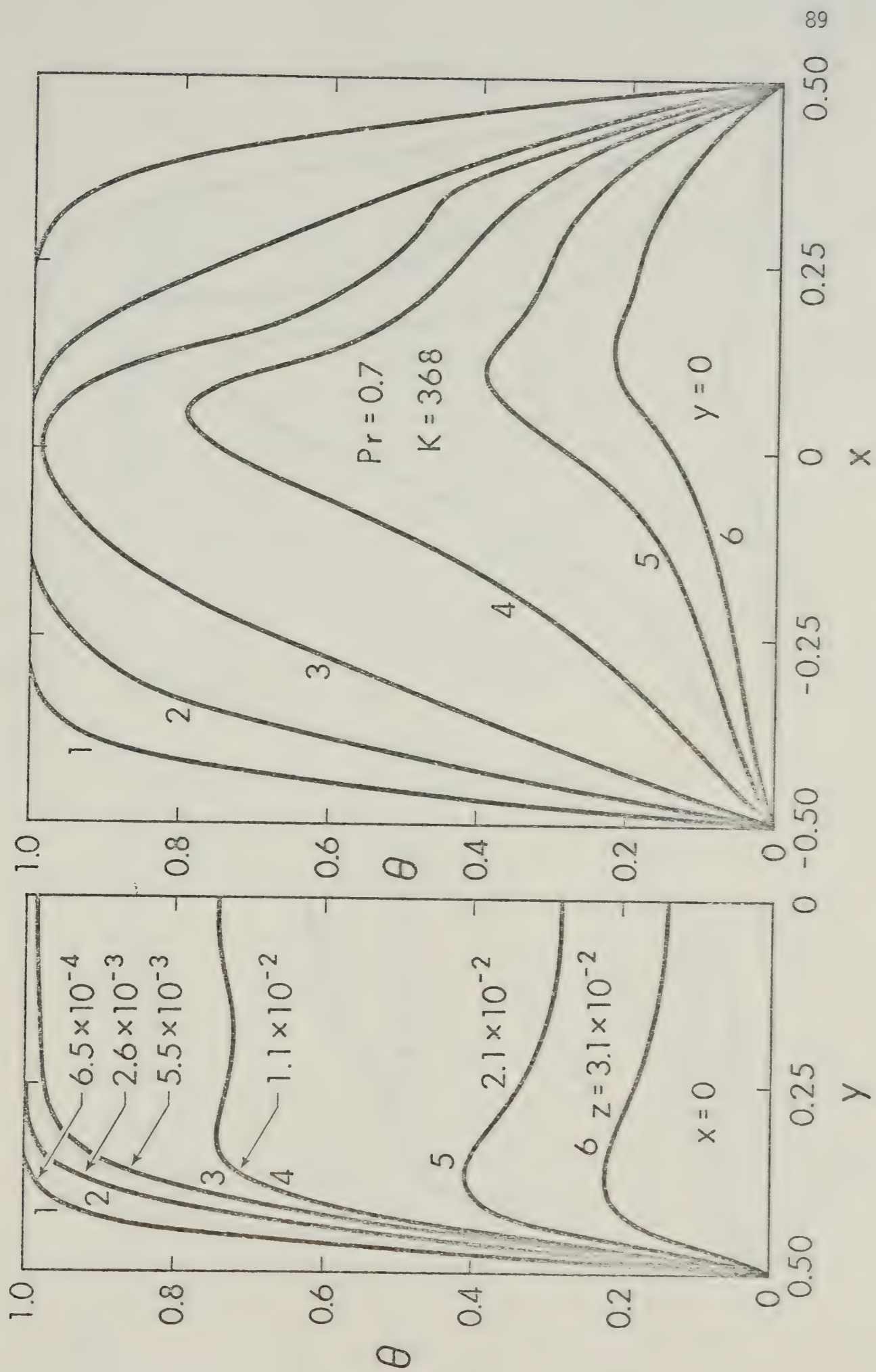


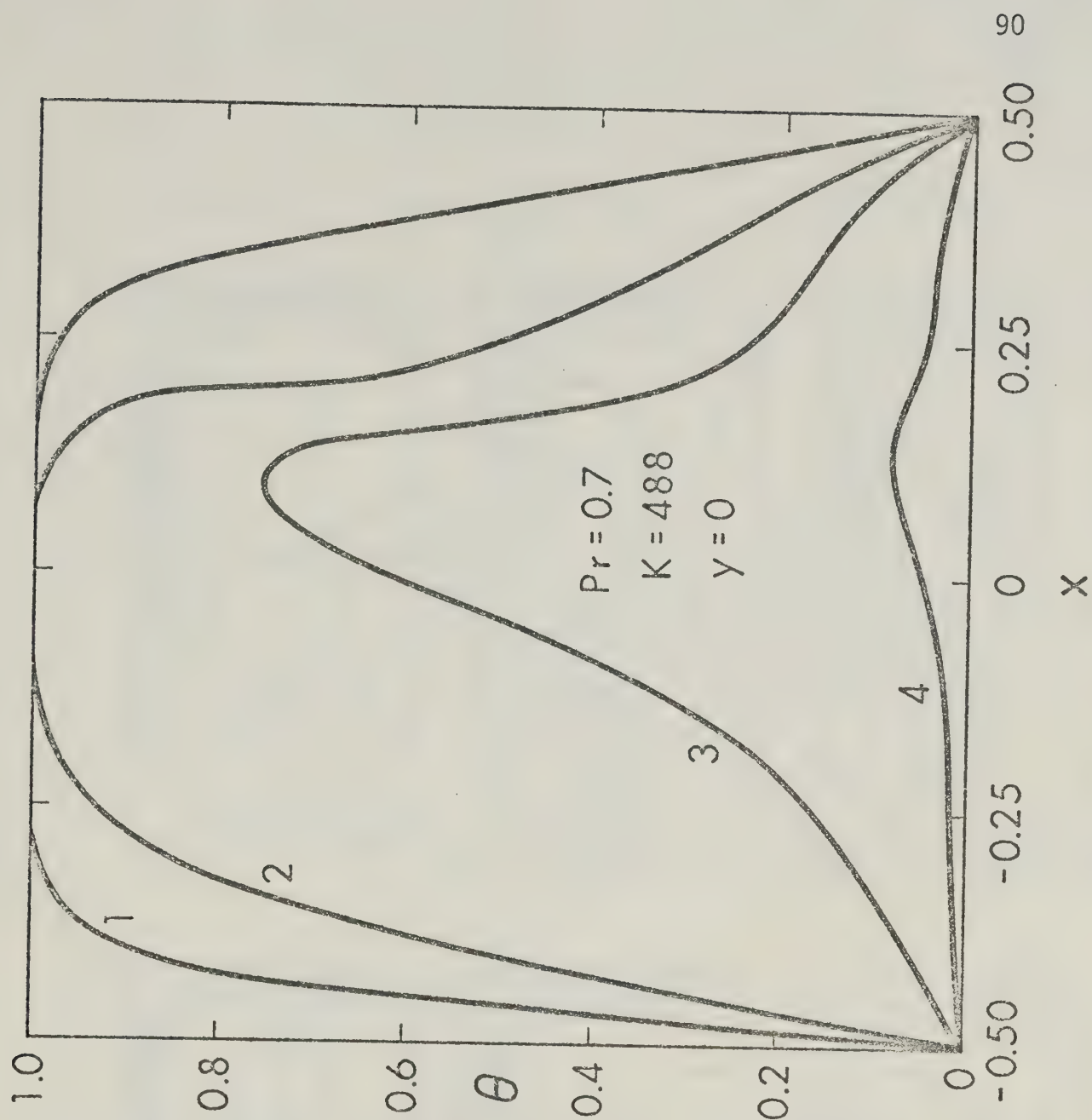
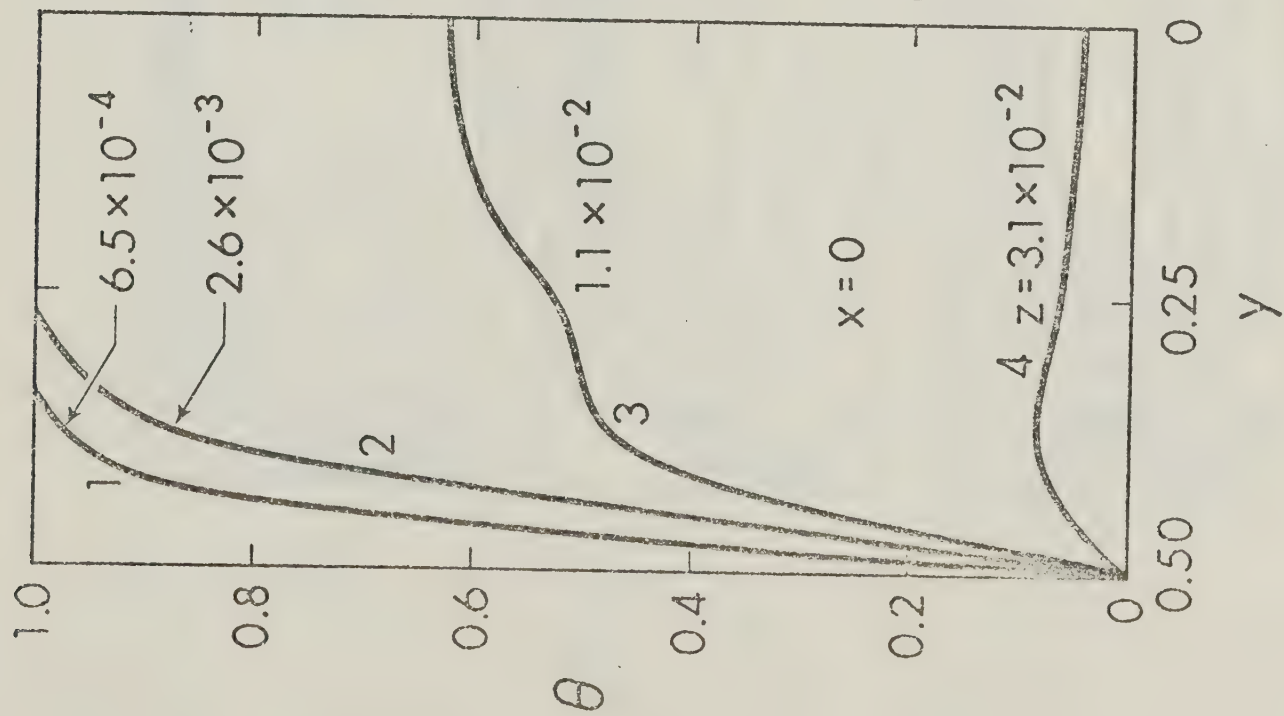
Fig. 14 Typical temperature profile developments at $x=0$ and $y=0$ for constant wall temperature case.



(b)



(c)



(d)

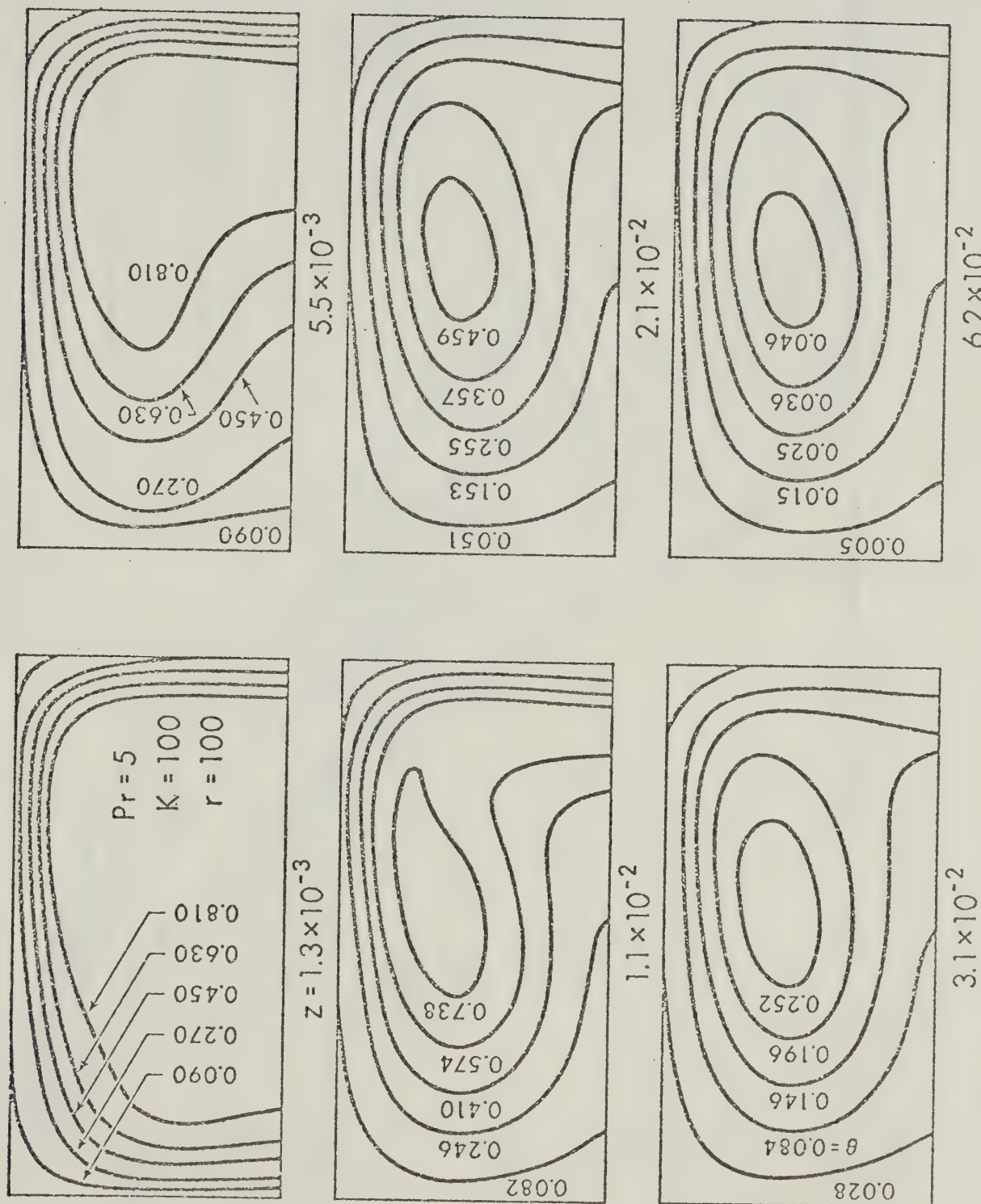


Fig. 15 Development of isotherms with $Pr=5$ and $K=100$ for constant wall temperature case.

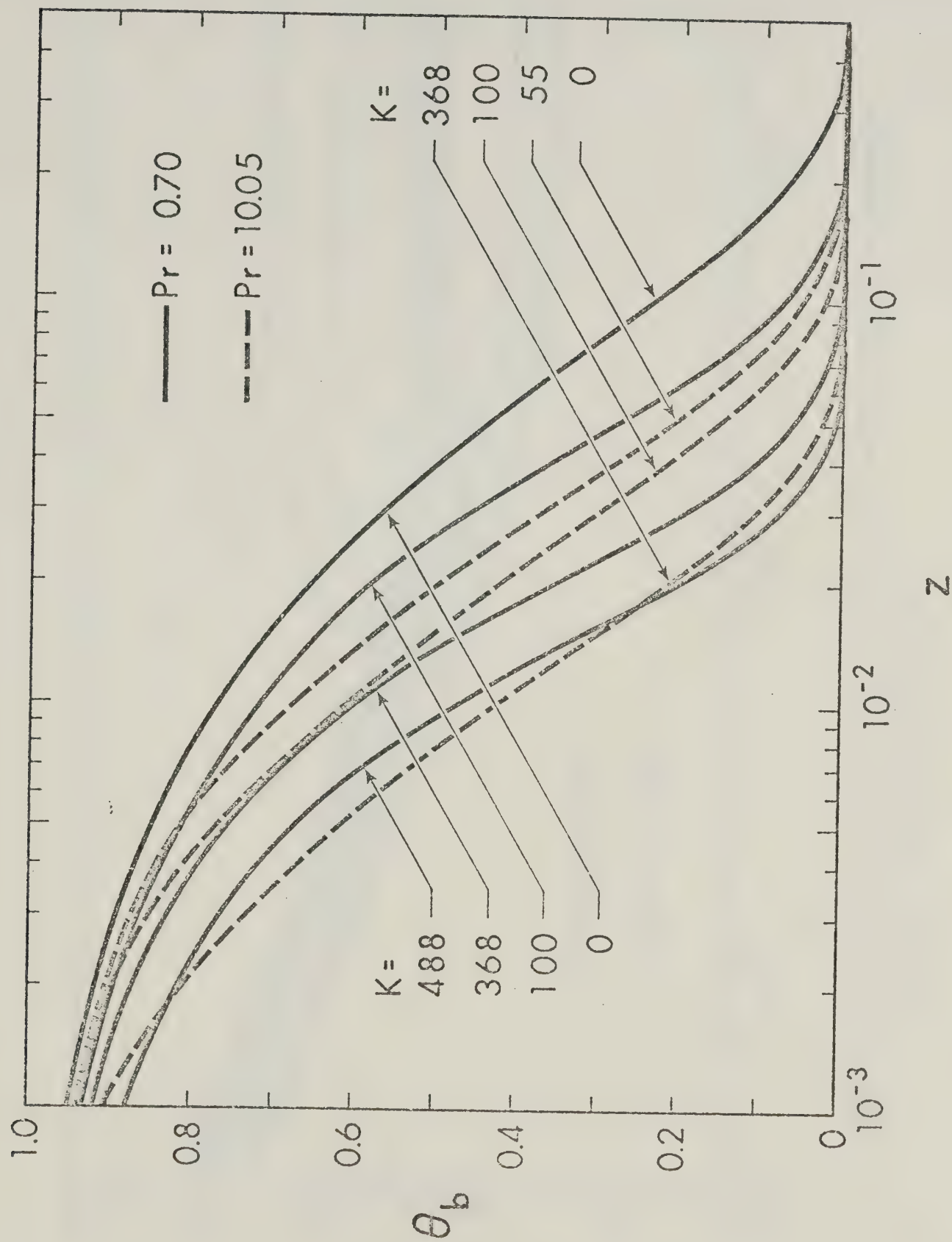


Fig. 16 Axial bulk temperature distribution for $Pr=0.7$ and 10.05 with K as parameter for constant wall temperature case.

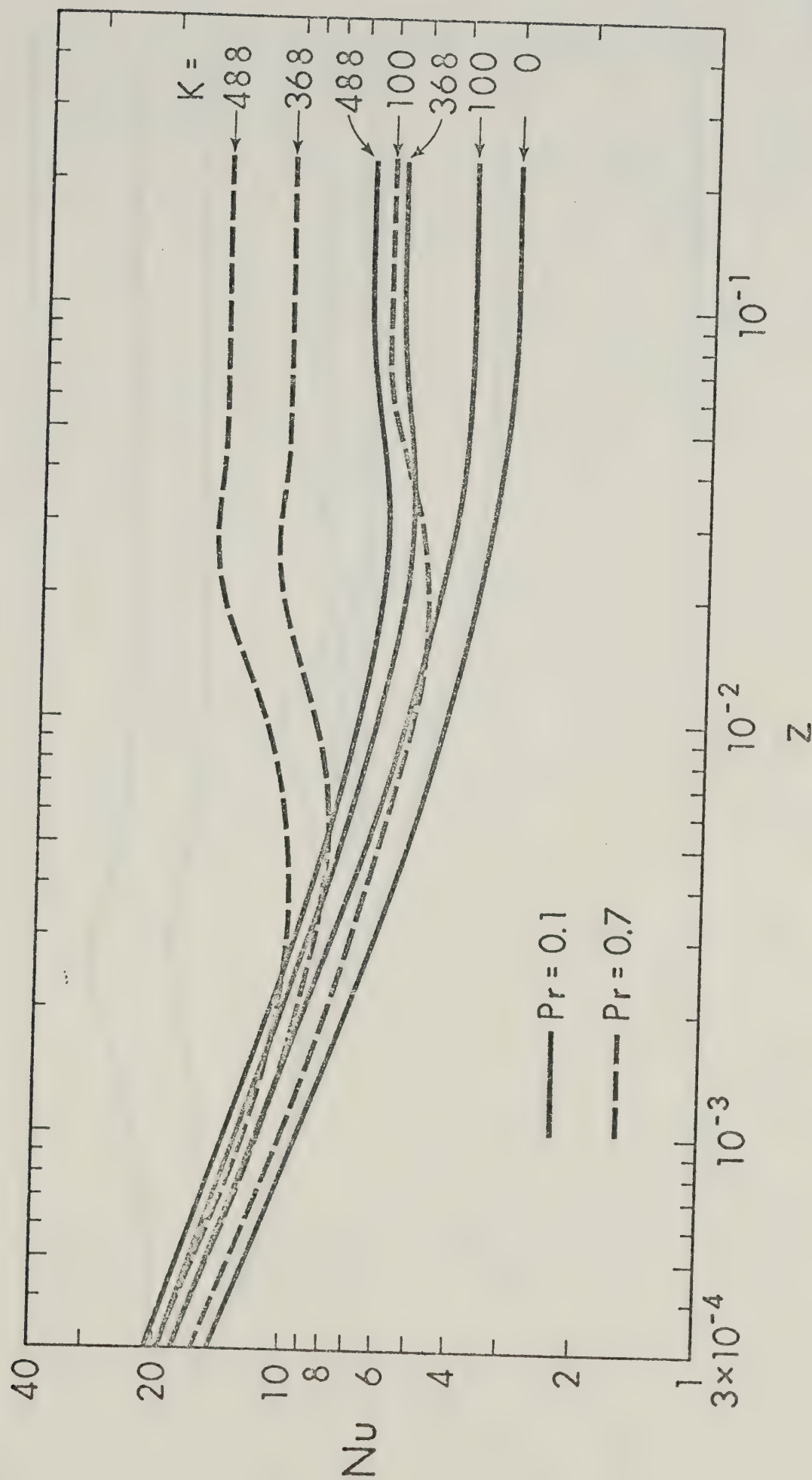


Fig. 17 Local Nusselt number variations for $Pr=0.1$ and 0.7 with K as parameter for constant wall temperature case.

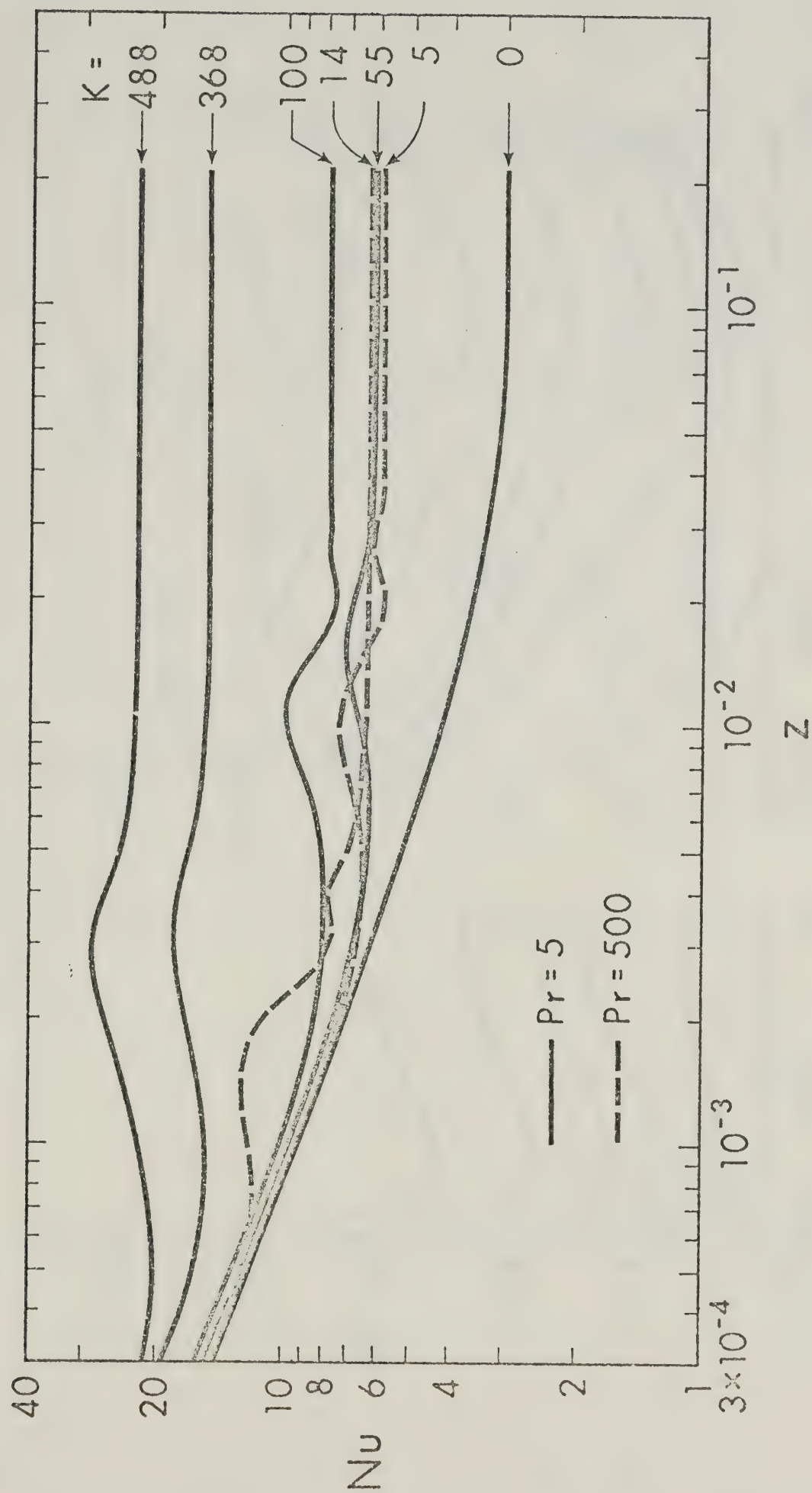
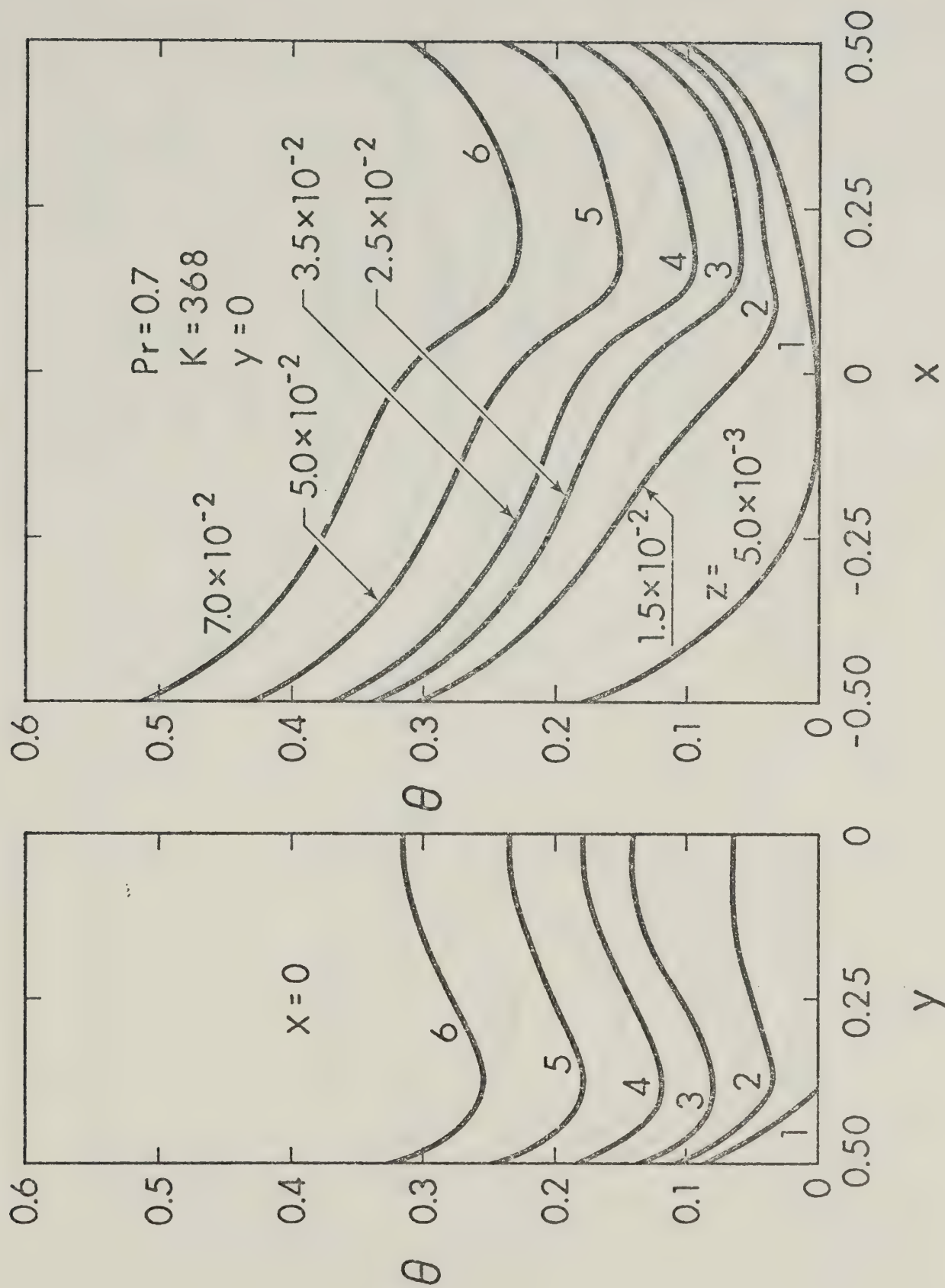
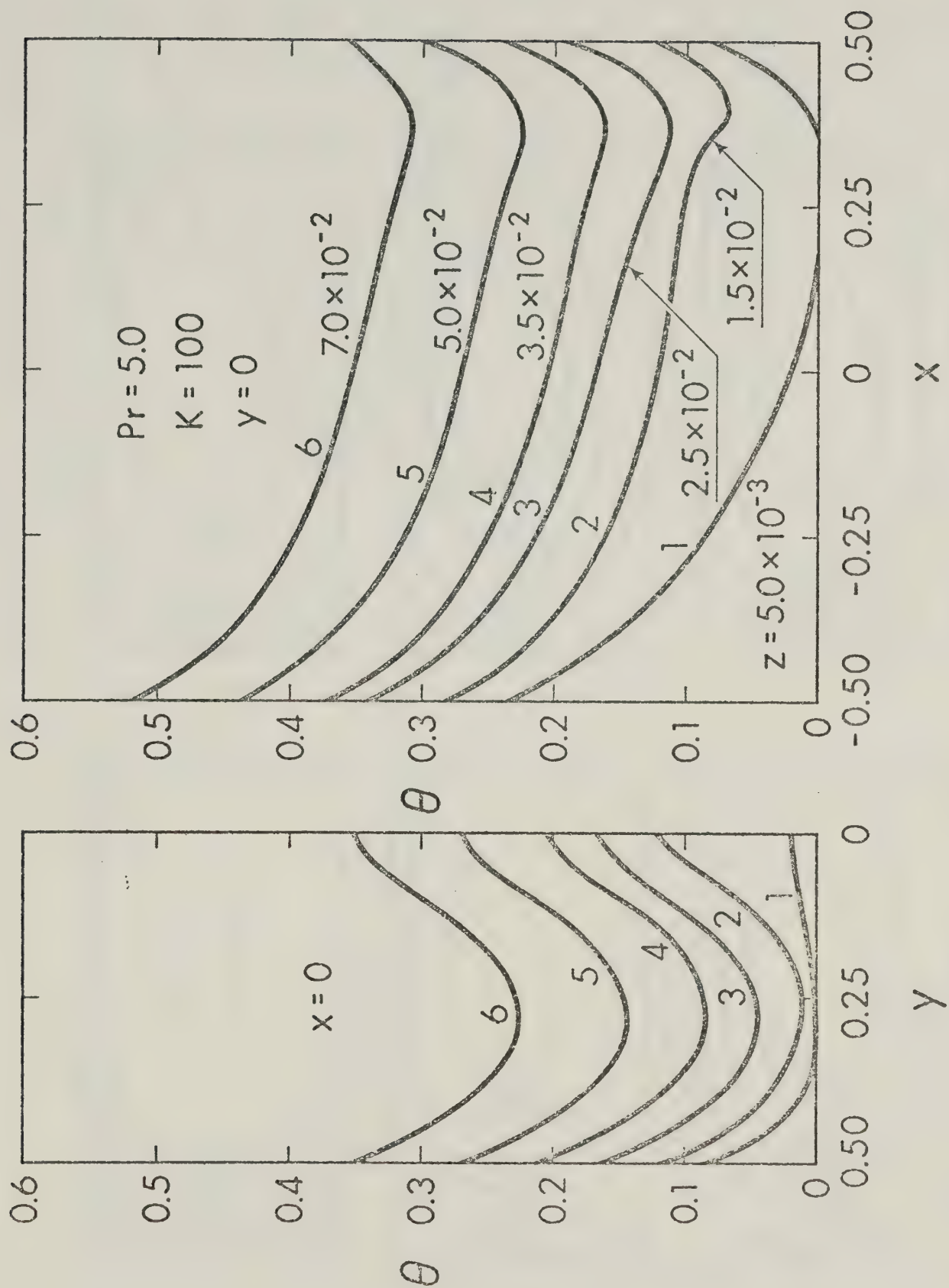


Fig. 18 Local Nusselt number variations for $Pr=5$ and 500 with K as parameter for constant wall temperature.



(a)

Fig. 19 Typical temperature profile development at $x=0$ and $y=0$ for uniform wall heat flux case.



(b)

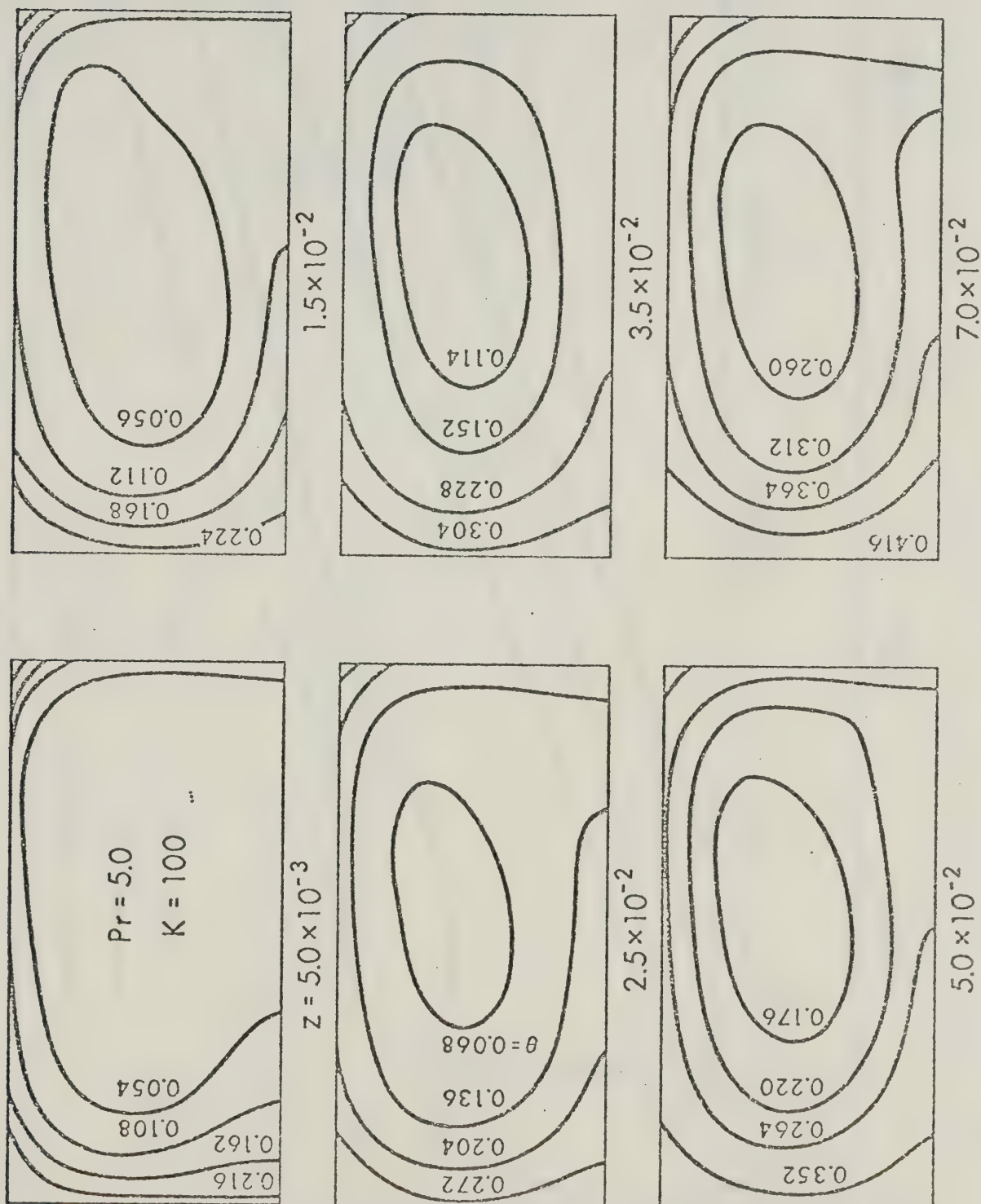


Fig. 20 Development of isotherms with $Pr=5$, and $K=100$ for uniform wall heat flux case.

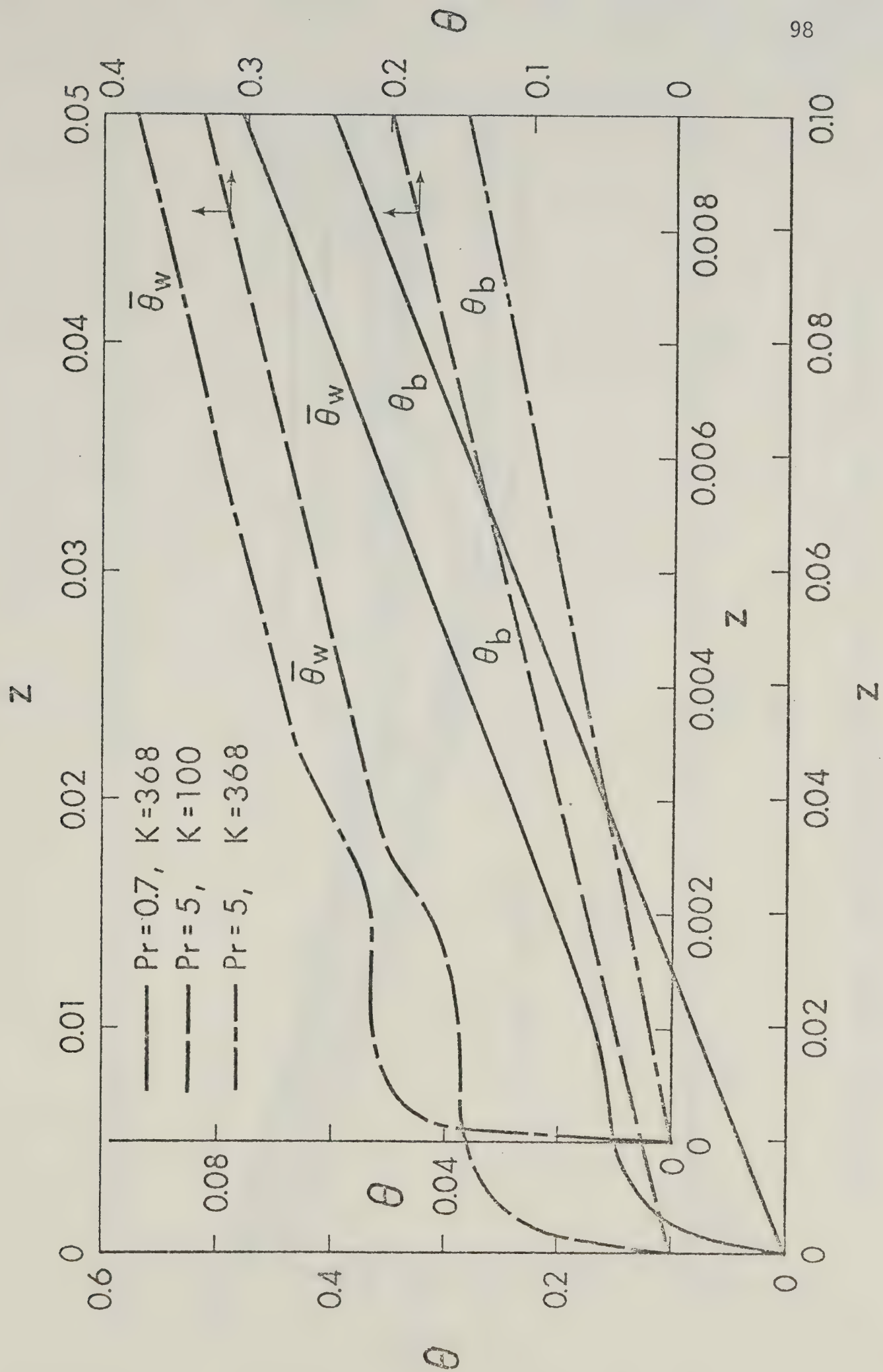


Fig. 21 Axial distributions for $\bar{\theta}_w$ and θ_b for uniform wall heat flux case.

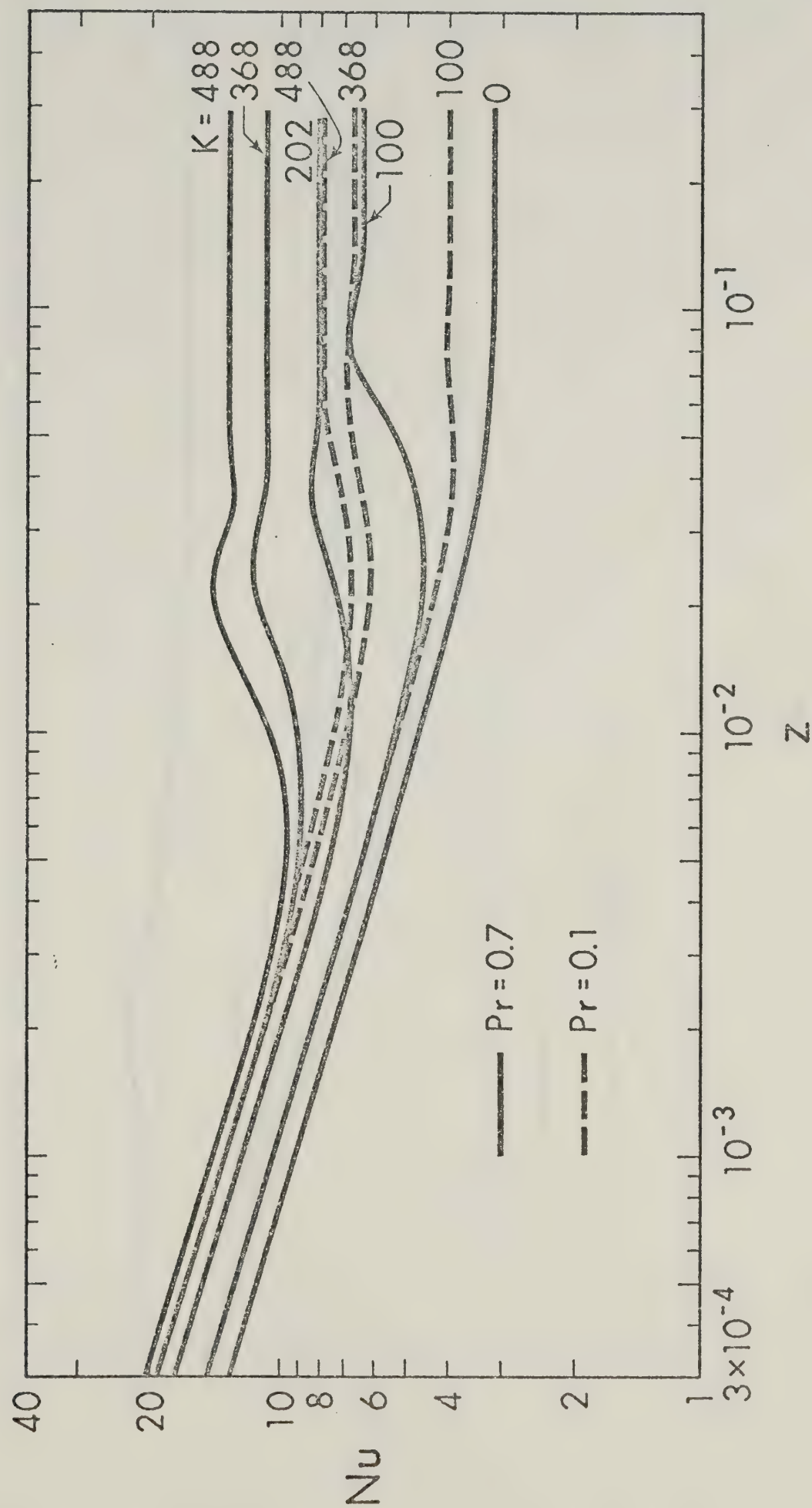


Fig. 22 Local Nusselt number variations for $Pr=0.1$ and 0.7 with K as parameter for uniform wall heat flux case.

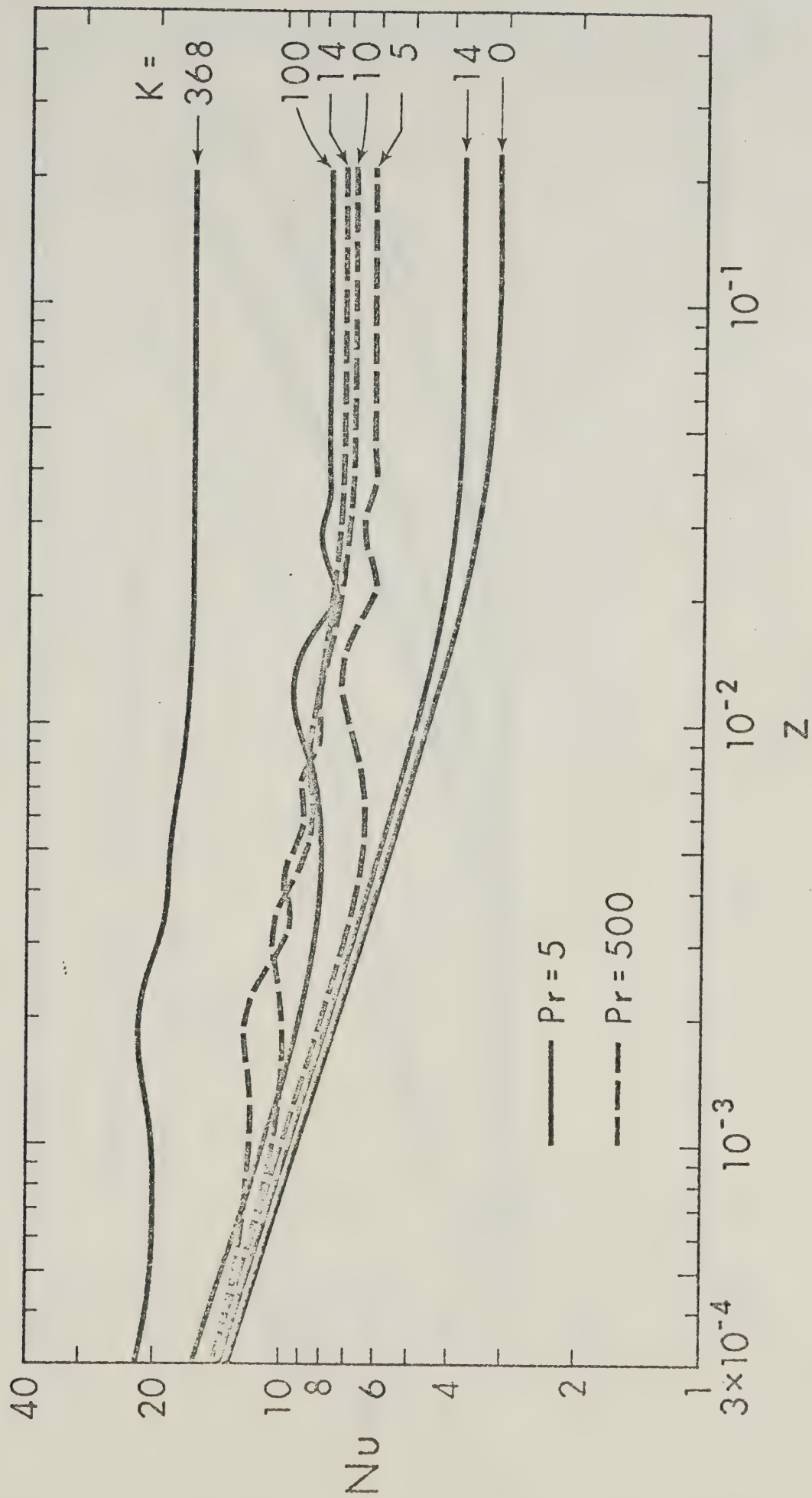


Fig. 23 Local Nusselt number variations for $Pr=5$ and 500 with K as parameter for uniform wall heat flux case.

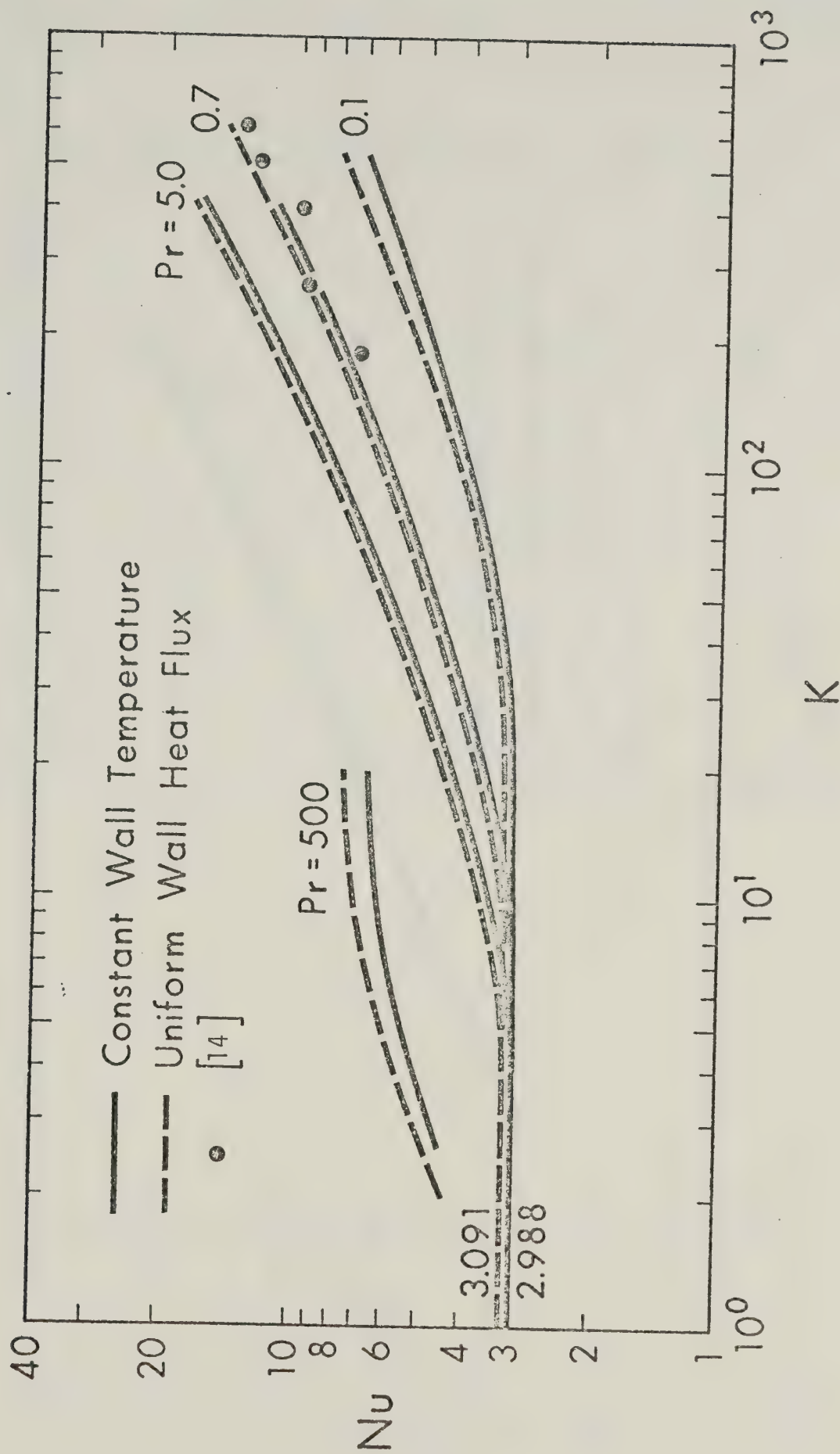


Fig. 24 Heat transfer results for thermally fully developed region and comparison with experimental results.

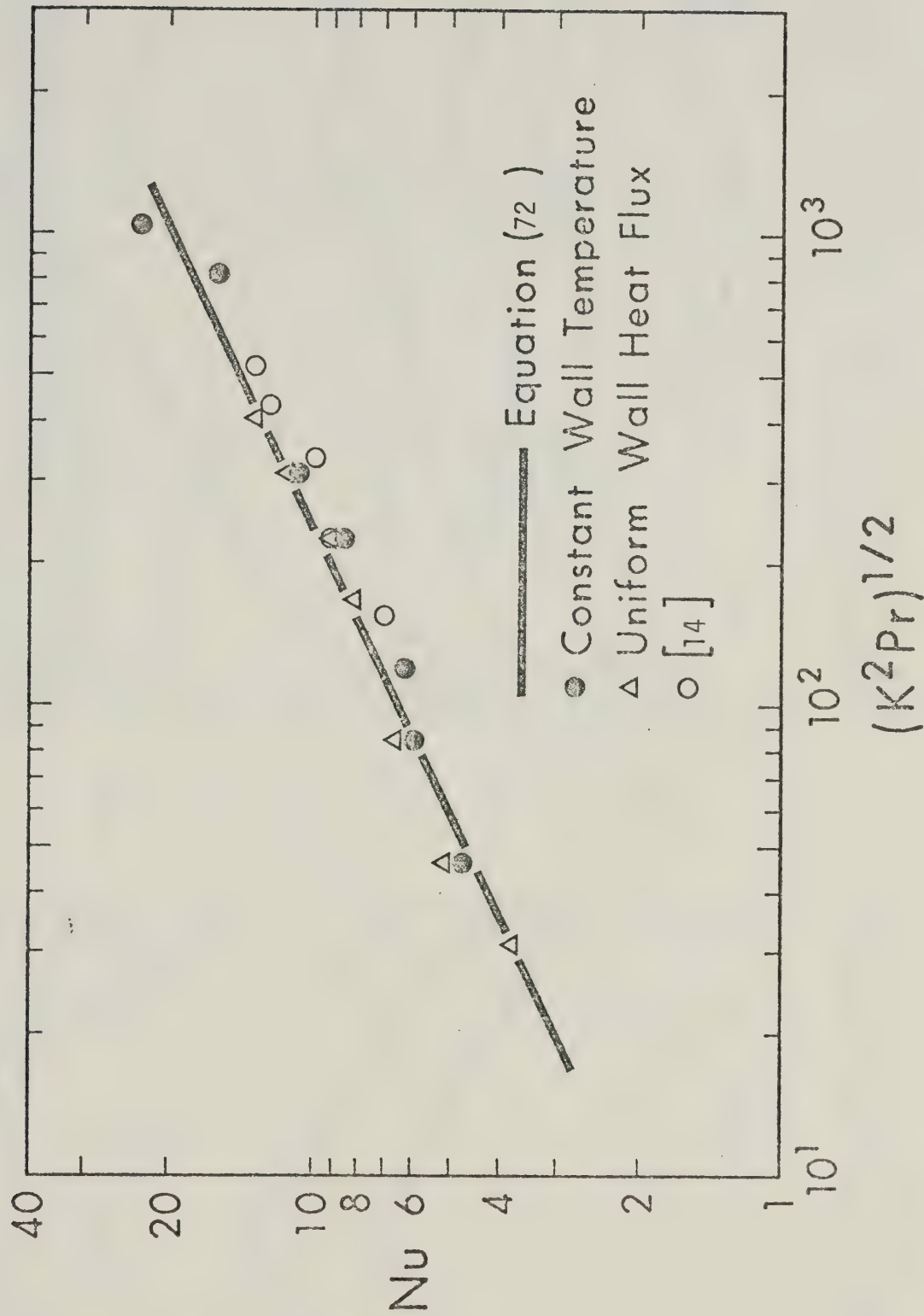


Fig. 25 Correlation equation for the asymptotic heat transfer results and comparison with experimental data.

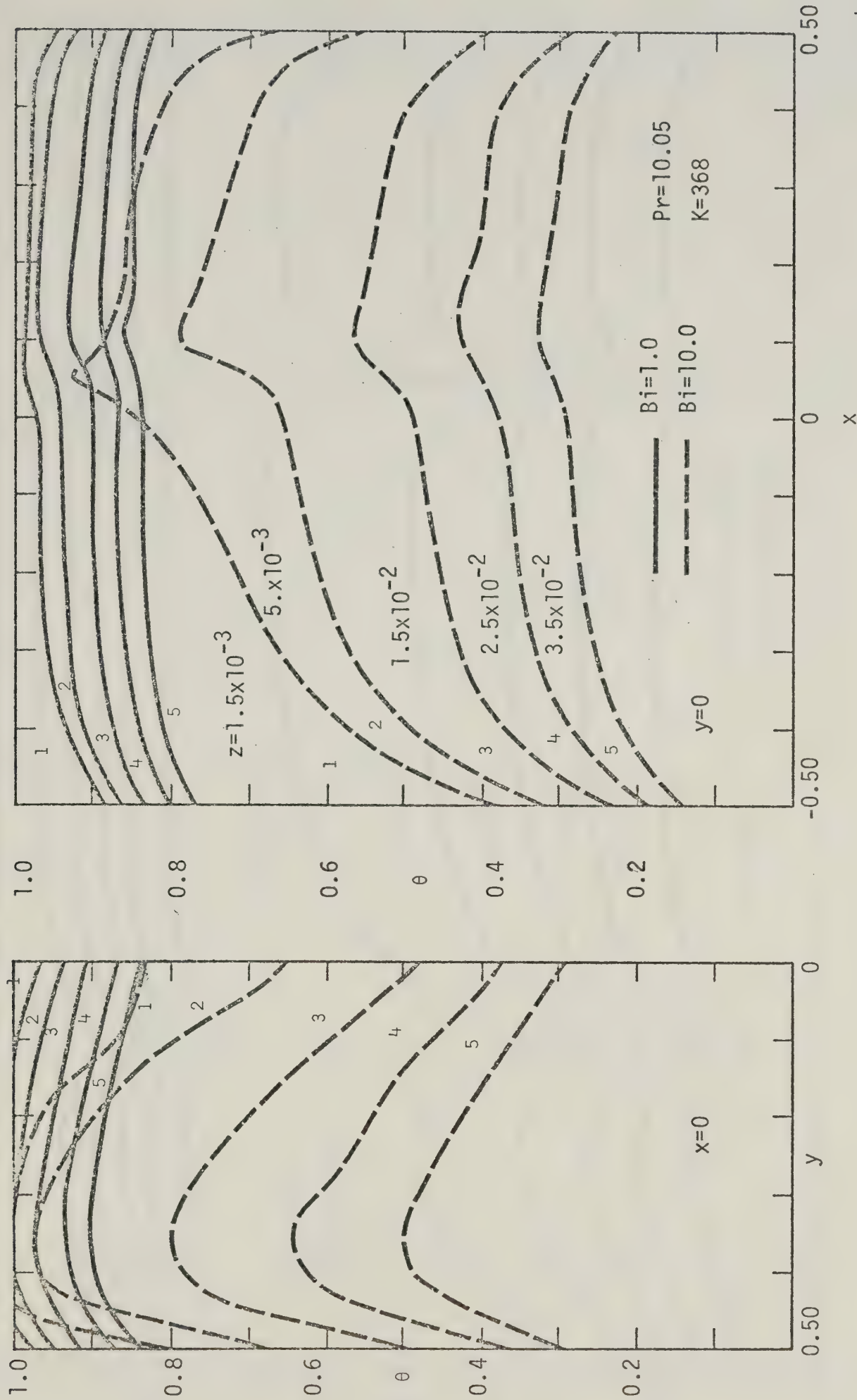
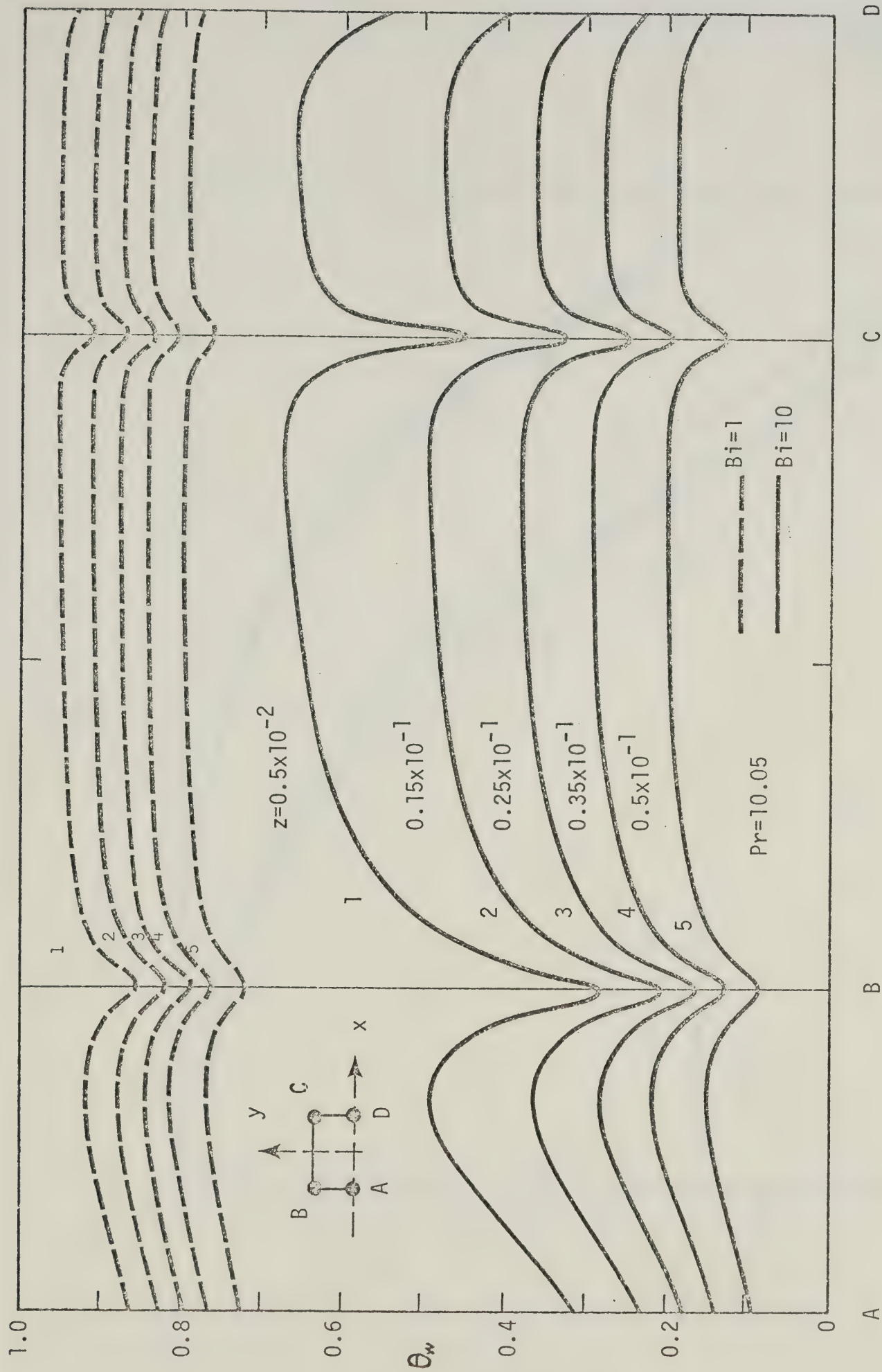


Fig. 26 Temperature profile development at $x=0$ and $y=0$ with Biot numbers 1 and 10 for uniform convective condition at wall.



C

B

A

D

Fig. 27 Development of peripheral wall temperature distribution for Biot numbers 1 and 10.

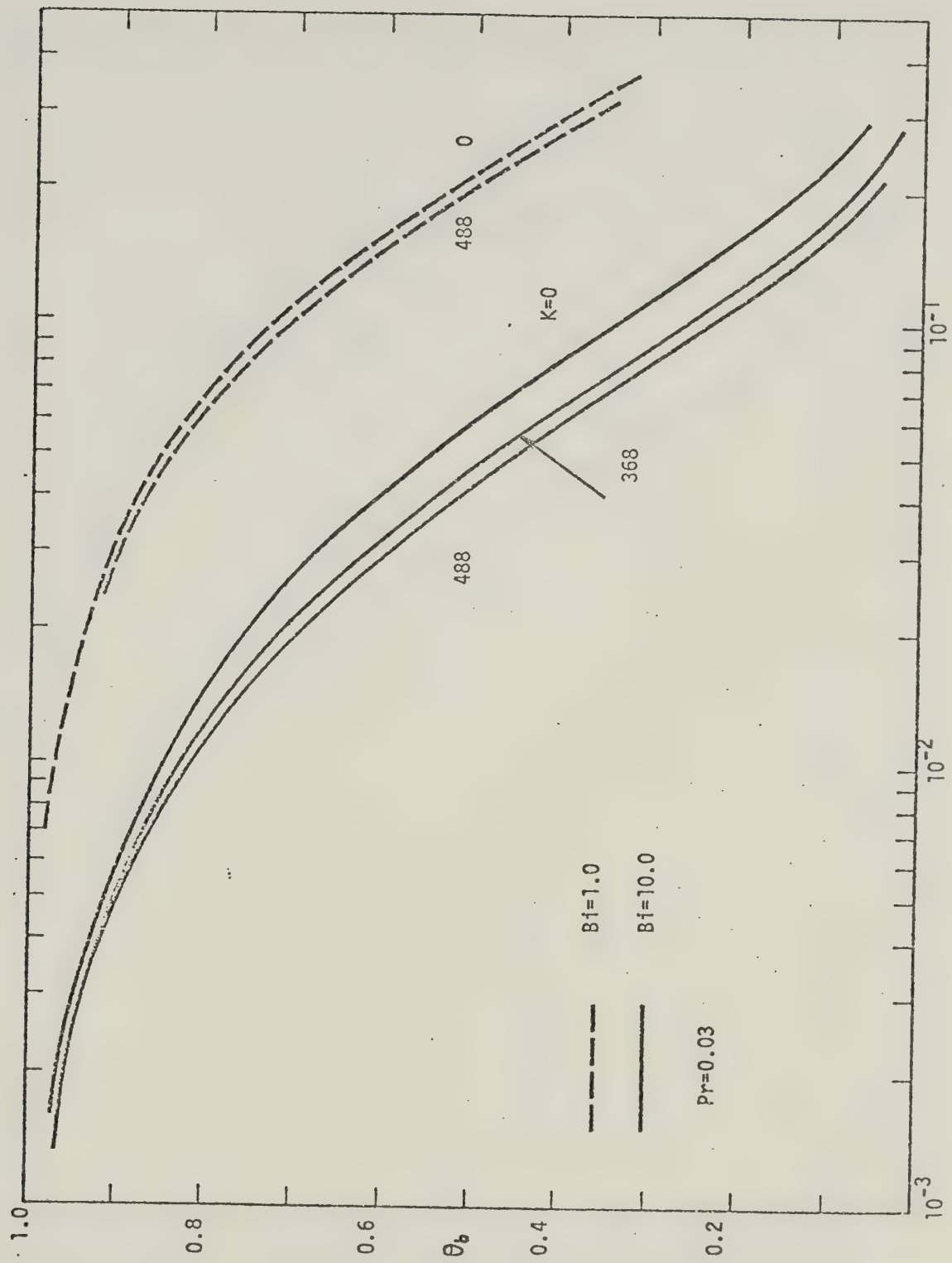


Fig. 28 Axial bulk temperature distribution for $Pr=0.03$ with K as parameter for $Bi=1$ and 10

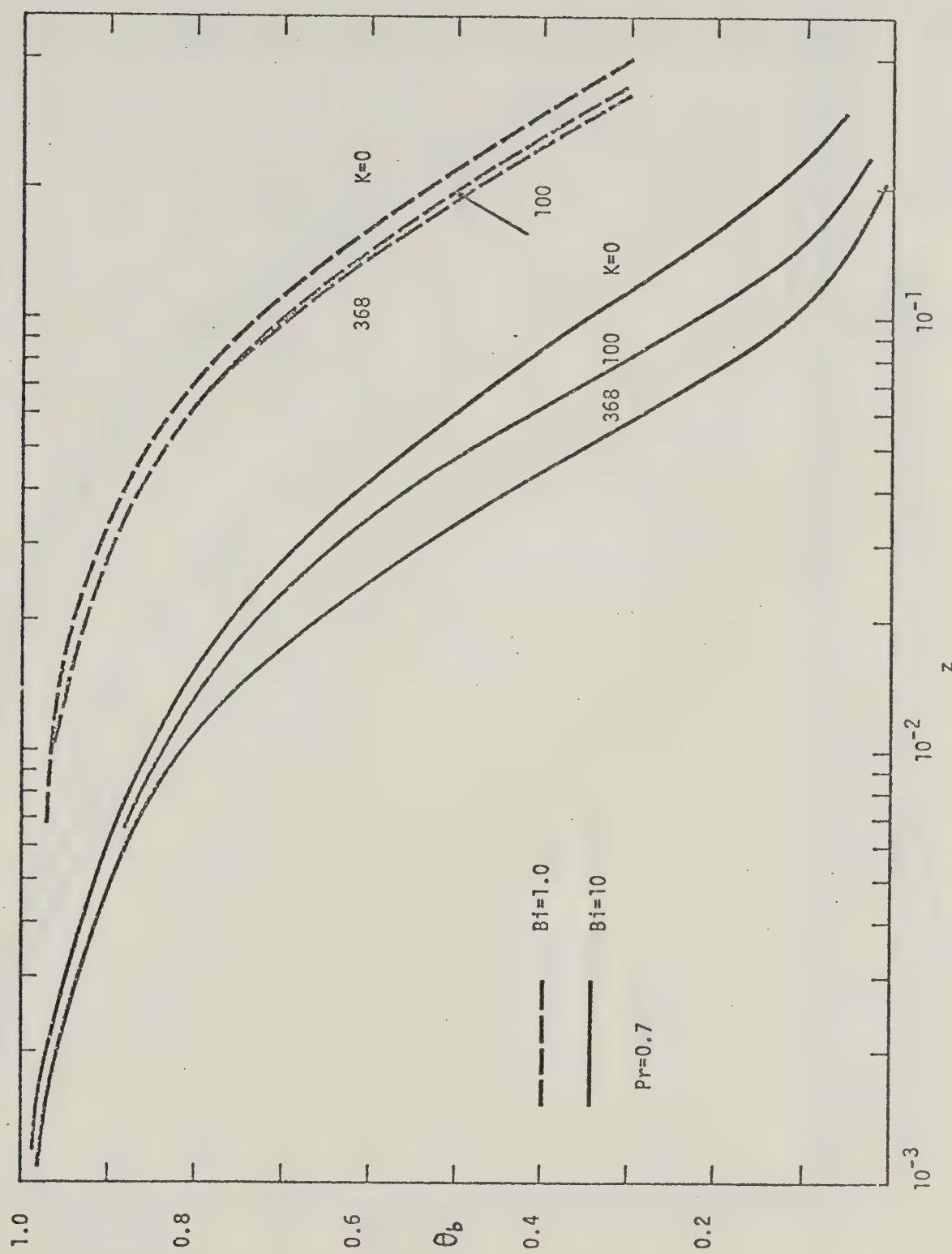


Fig. 29 Axial bulk temperature distribution for $Pr=0.7$ with K as parameter for $Bi=1$ and 10 .

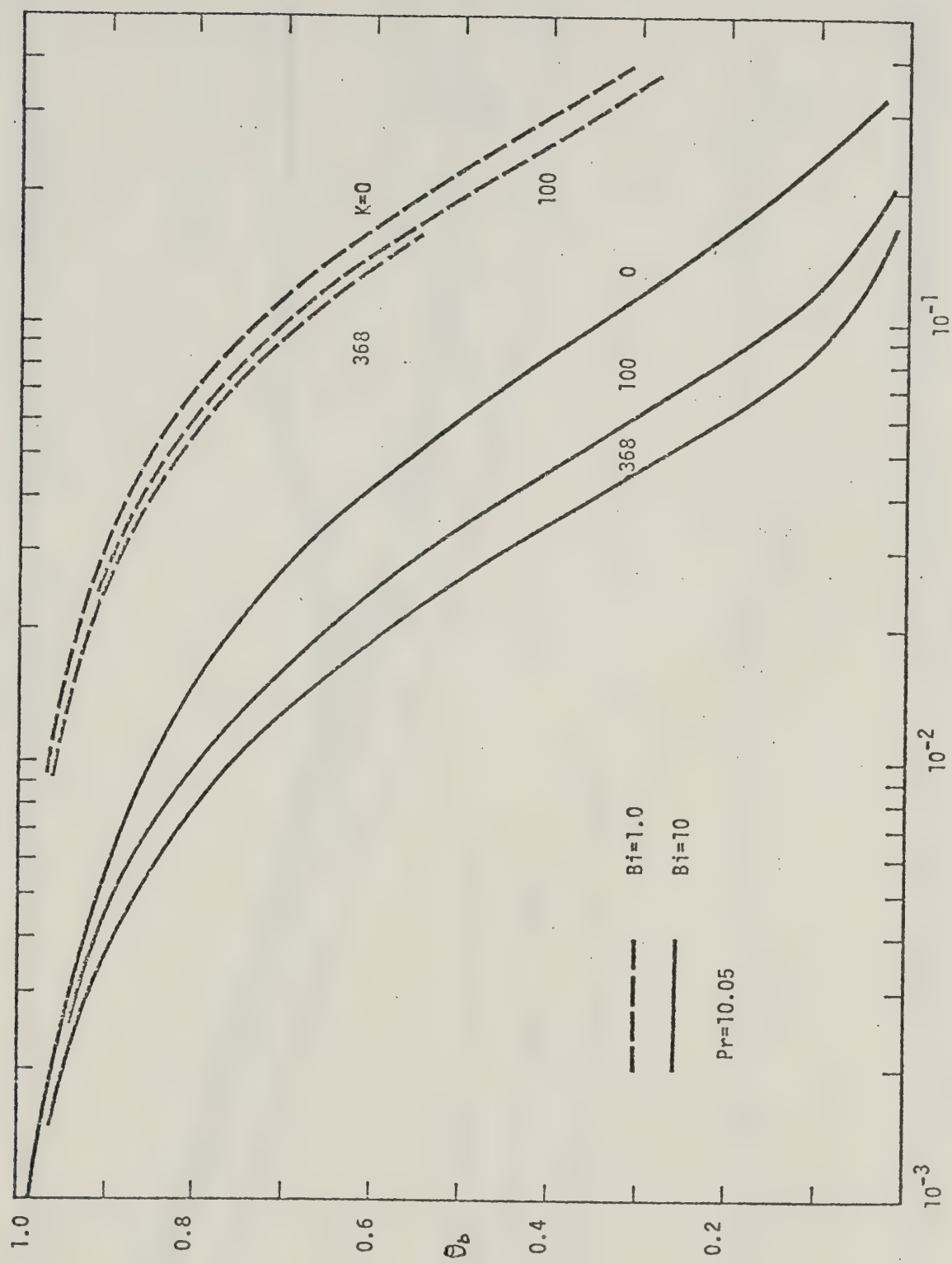


Fig. 30 Axial bulk temperature distribution for $Pr=10.05$ with K as parameter for $Bi=1$ and 10 .

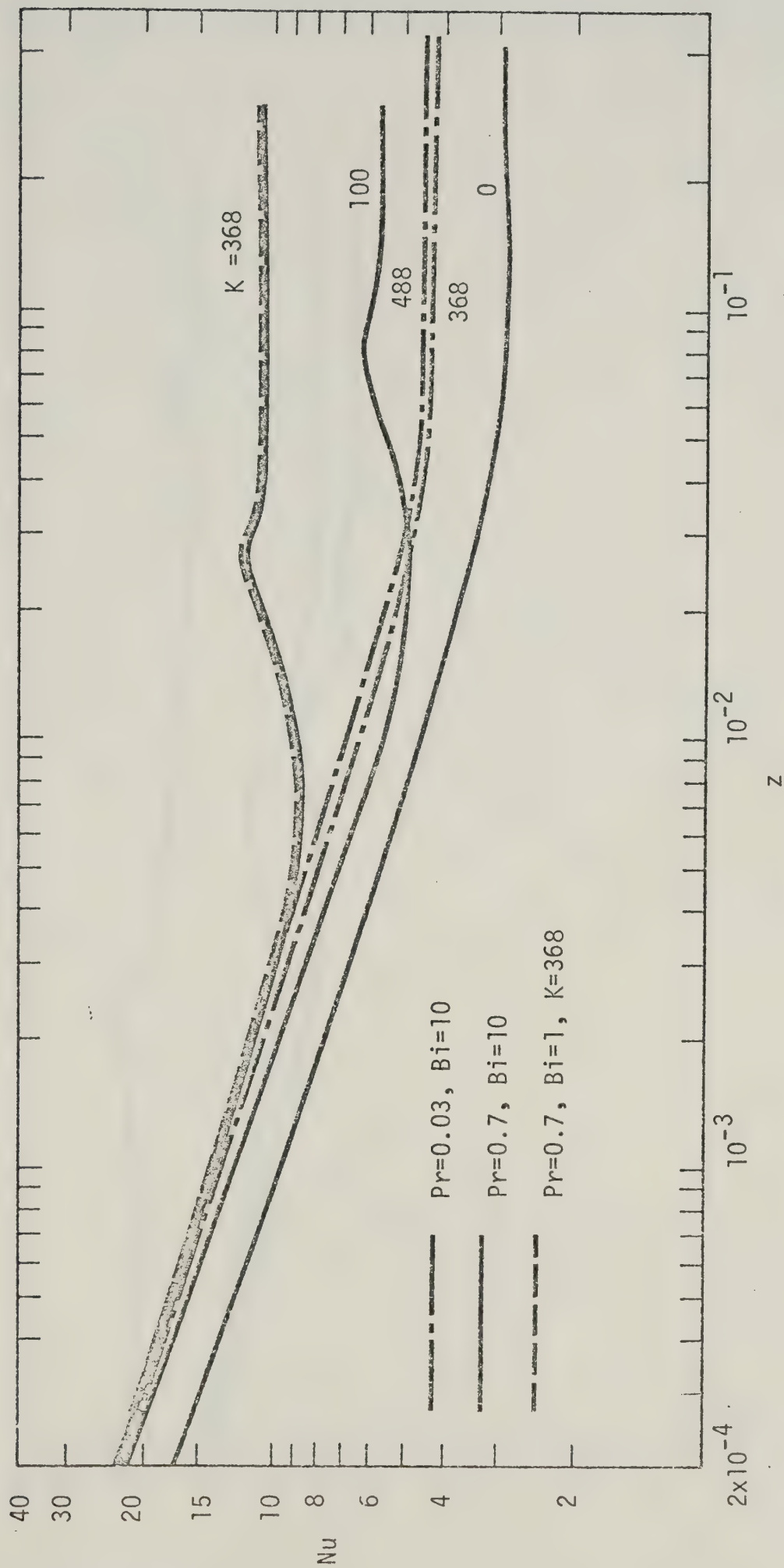


Fig. 31 Local Nusselt number variation for $Pr=0.03$ and 0.7 with Biot number 1 and 10 for uniform convective condition at wall.

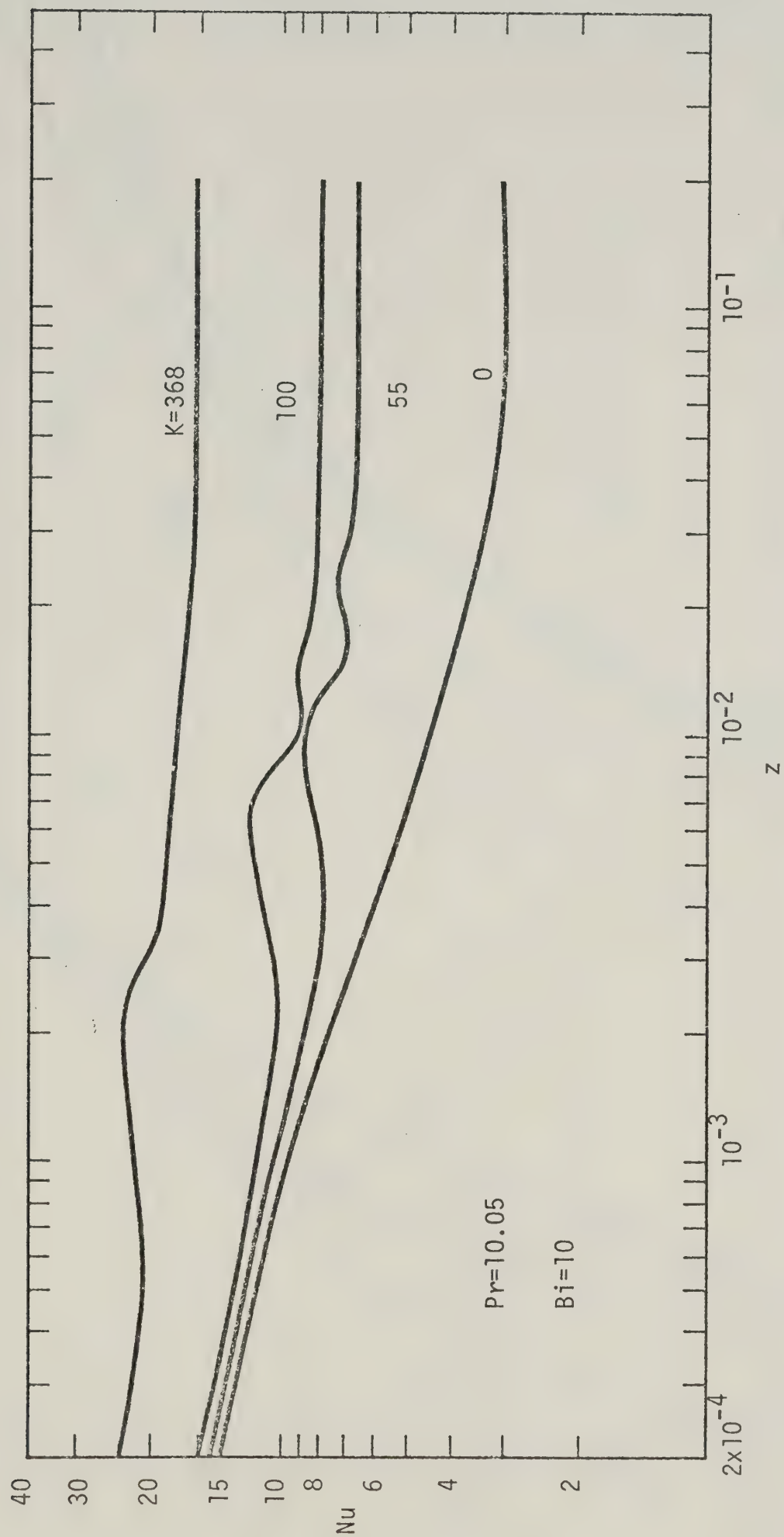


Fig. 32 Local Nusselt number variation with $Pr=10.05$ and Biot number 10 for uniform convective condition at wall.

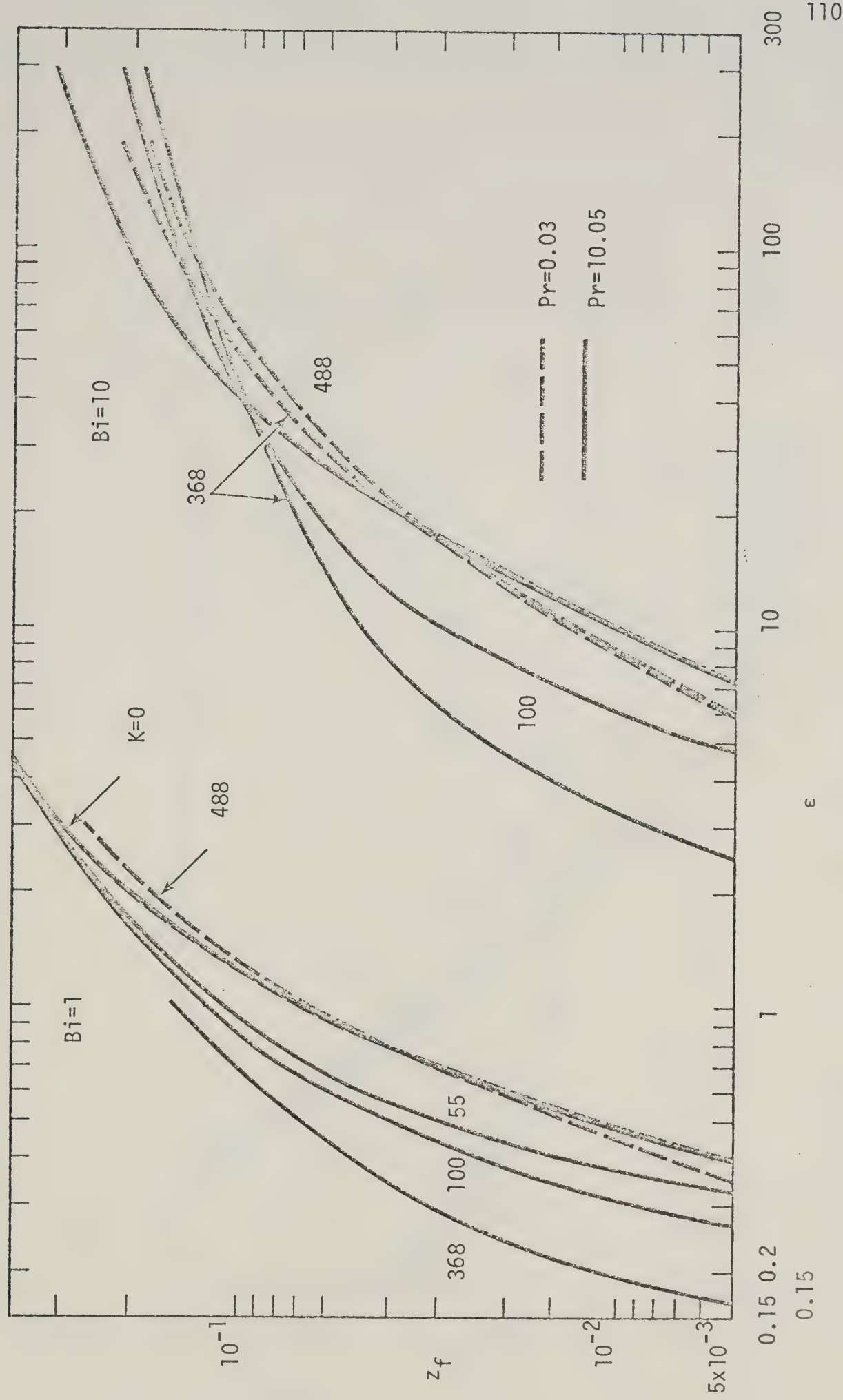


Fig. 33 Length of liquid solidification-free zone with K as parameter for $Pr=0.03$, and 10.05 and $Bi=1, 10$.

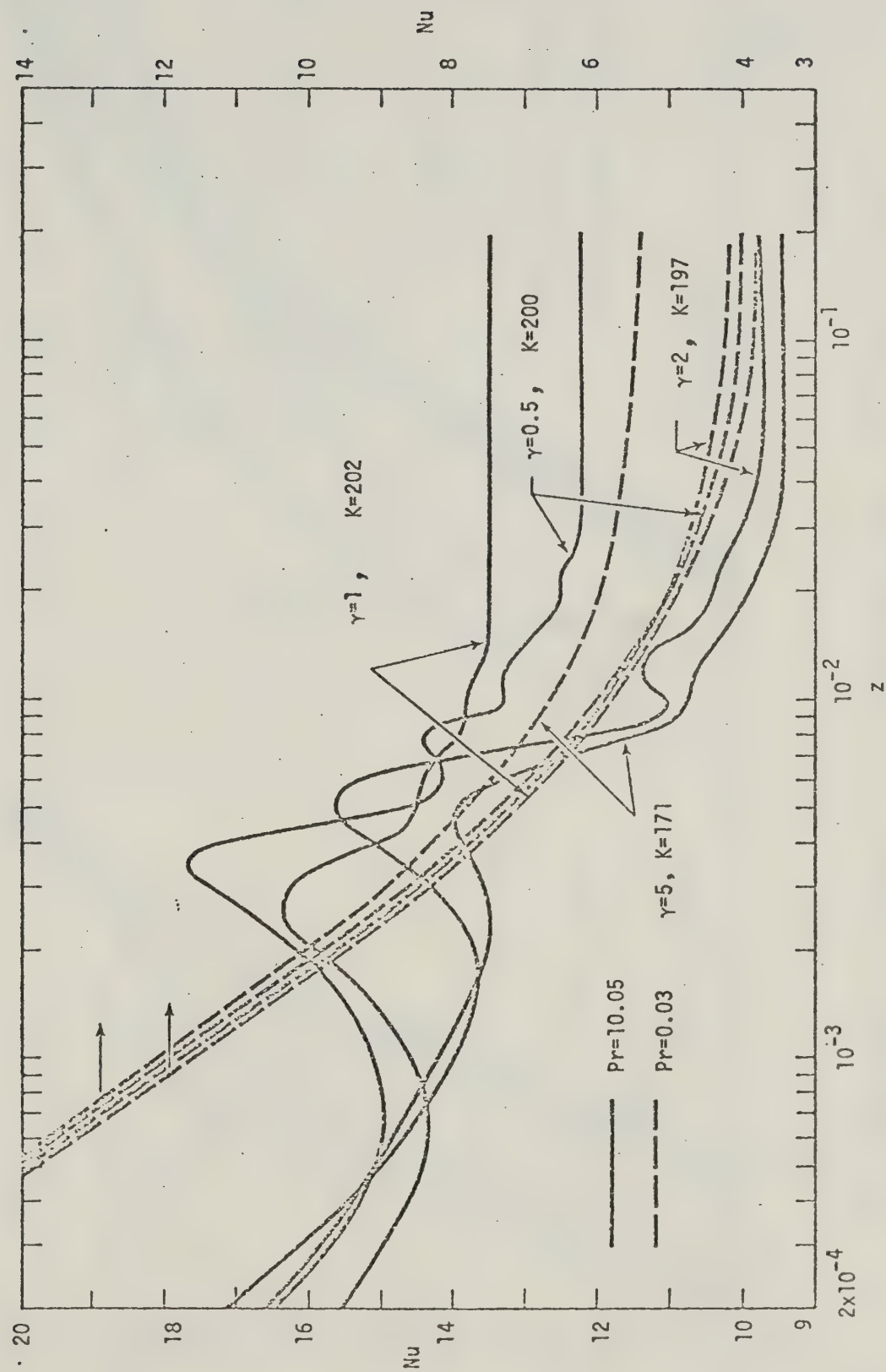


Fig. 34 Local Nusselt number variation for $Pr=0.03, 10.05$ and $Bi=10$ for aspect ratios $\gamma = 1, 2, 5, 0.5$.

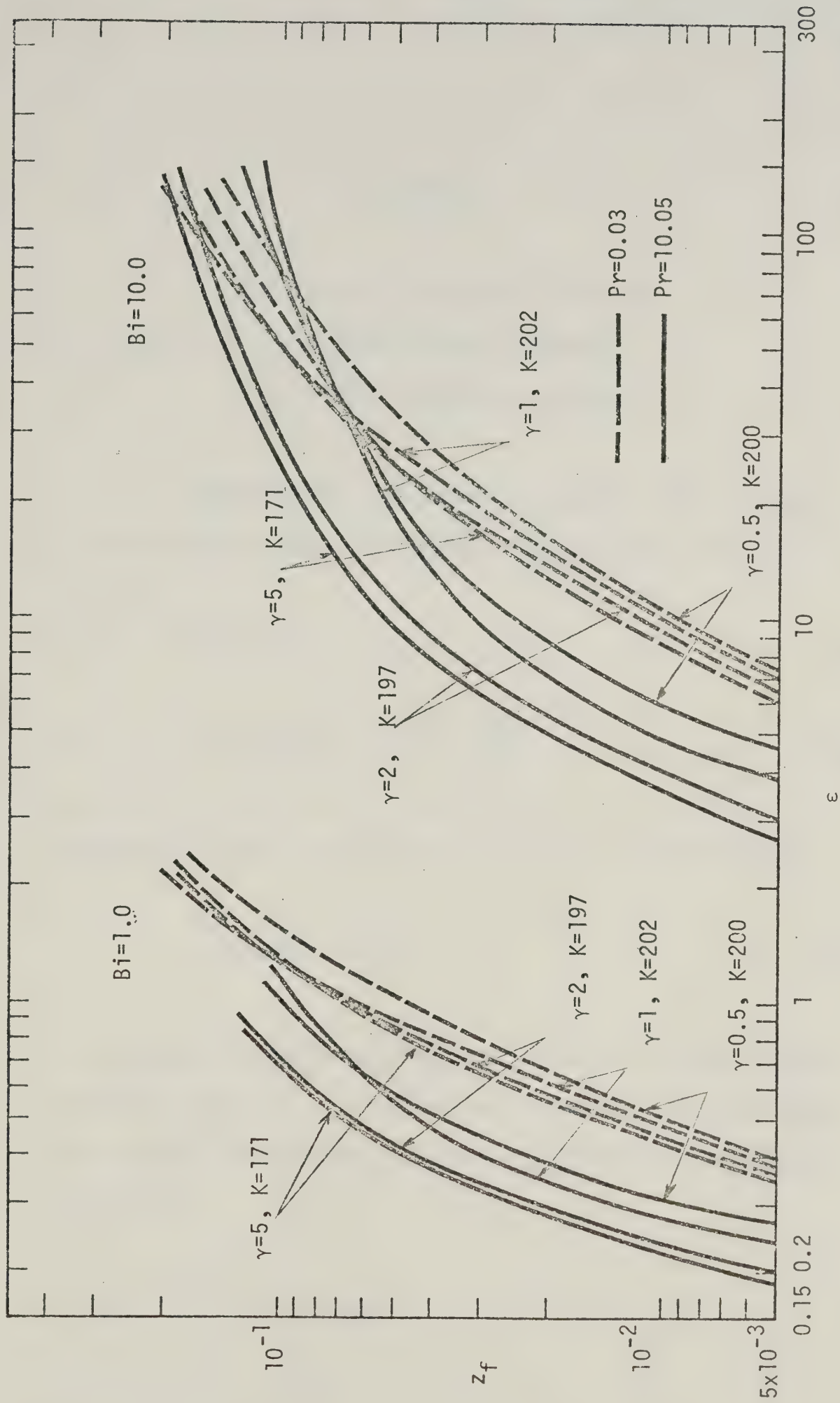


Fig. 35 Length of liquid solidification-free zone for $Pr = 0.03, 10.05$ and $Bi = 1, 10$ for aspect ratios $\gamma = 1, 2, 5, 0.5$.

APPENDIX A

DERIVATION OF THE BASIC EQUATIONS
FOR FLOW AND HEAT TRANSFER
IN A CURVED RECTANGULAR CHANNEL

The governing conservation equations for a steady, incompressible, laminar Newtonian flow in vector form are:

$$\nabla \cdot \vec{V} = 0 \quad (\text{A.1})$$

$$\rho (\vec{V} \cdot \nabla \vec{V}) = - \nabla P + \mu (\nabla^2 \vec{V}) \quad (\text{A.2})$$

Neglecting viscous dissipation, the energy equation becomes

$$\rho C_p (\vec{V} \cdot \nabla T) = k \nabla^2 T \quad (\text{A.3})$$

An orthogonal curvilinear coordinate (toroidal) system X, Y, Z , as shown in Fig. A.1, is introduced. The relationships between the toroidal coordinates (X, Y, Z) and the Cartesian coordinates (x, y, z) are:

$$x = (R + X) \cos \phi$$

$$\begin{aligned}
y &= Y \\
z &= (R + X) \sin \phi \\
\phi &= Z/R
\end{aligned} \tag{A.4}$$

The metric coefficients [32] are:

$$\begin{aligned}
h_1^2 &= \left(\frac{\partial x}{\partial X} \right)^2 + \left(\frac{\partial y}{\partial X} \right)^2 + \left(\frac{\partial z}{\partial X} \right)^2 = 1 \\
h_2^2 &= \left(\frac{\partial x}{\partial Y} \right)^2 + \left(\frac{\partial y}{\partial Y} \right)^2 + \left(\frac{\partial z}{\partial Y} \right)^2 = 1 \\
h_3^2 &= \left(\frac{\partial x}{\partial Z} \right)^2 + \left(\frac{\partial y}{\partial Z} \right)^2 + \left(\frac{\partial z}{\partial Z} \right)^2 = (1+X/R)^2
\end{aligned} \tag{A.5}$$

and \vec{c}_1 , \vec{c}_2 , \vec{c}_3 are the unit base vectors in the X,Y, and Z directions, respectively. The derivatives of unit base vectors are:

$$\begin{aligned}
\frac{\partial \vec{c}_1}{\partial X} &= \frac{\partial \vec{c}_2}{\partial X} = \frac{\partial \vec{c}_3}{\partial X} = 0 \\
\frac{\partial \vec{c}_1}{\partial Y} &= \frac{\partial \vec{c}_2}{\partial Y} = \frac{\partial \vec{c}_3}{\partial Y} = 0 \\
\frac{\partial \vec{c}_1}{\partial Z} &= \frac{1}{R} \vec{c}_3 \\
\frac{\partial \vec{c}_2}{\partial Z} &= 0 \\
\frac{\partial \vec{c}_3}{\partial Z} &= -\frac{1}{R} \vec{c}_1
\end{aligned} \tag{A.6}$$

The del operator is defined as:

$$\nabla = \vec{c}_1 \frac{\partial}{\partial X} + \vec{c}_2 \frac{\partial}{\partial Y} + \frac{\vec{c}_3}{h_3} \frac{\partial}{\partial Z} \quad (\text{A.7})$$

The Laplacian operation $\nabla^2 = \nabla \cdot \nabla$ is obtained by the indicated repeated application of the operator ∇ . Thus, one obtains

$$\nabla^2 = \frac{\partial^2}{\partial X^2} + \frac{\partial^2}{\partial Y^2} + \frac{1}{h_3^2} \frac{\partial^2}{\partial Z^2} + \frac{1}{h_3} \frac{1}{R} \frac{\partial}{\partial X} \quad (\text{A.8})$$

The continuity equation is written as:

$$\nabla \cdot \vec{V} = \vec{c}_1 \frac{\partial \vec{V}}{\partial X} + \vec{c}_2 \cdot \frac{\partial \vec{V}}{\partial Y} + \frac{\vec{c}_3}{h_3} \cdot \frac{\partial \vec{V}}{\partial Z} = 0 \quad (\text{A.9})$$

which combined with equation (A.6) becomes:

$$\nabla \cdot \vec{V} = \frac{\partial U}{\partial X} + \frac{\partial V}{\partial Y} + \frac{1}{1+X/R} \frac{\partial W}{\partial Z} + \frac{1}{1+X/R} \frac{U}{R} = 0 \quad (\text{A.10})$$

The steady state Eulerian derivative $V \cdot \nabla$ in equation (A.2) is a scalar point function and is given as:

$$\vec{V} \cdot \nabla = U \frac{\partial}{\partial X} + V \frac{\partial}{\partial Y} + \frac{W}{h_3} \frac{\partial}{\partial Z} \quad (\text{A.11})$$

The quantity $\vec{V} \cdot \nabla \vec{V}$ is therefore given as:

$$\vec{V} \cdot \nabla \vec{V} = U \frac{\partial \vec{V}}{\partial X} + V \frac{\partial \vec{V}}{\partial Y} + \frac{W}{h_3} \frac{\partial \vec{V}}{\partial Z} \quad (\text{A.12})$$

In expanded form, the expression becomes:

$$\begin{aligned} \vec{V} \cdot \nabla \vec{V} = & U(\vec{c}_1 \frac{\partial U}{\partial X} + \vec{c}_2 \frac{\partial V}{\partial X} + \vec{c}_3 \frac{\partial W}{\partial X}) + \\ & V(\vec{c}_1 \frac{\partial U}{\partial Y} + \vec{c}_2 \frac{\partial V}{\partial Y} + \vec{c}_3 \frac{\partial W}{\partial Y}) + \\ & \frac{W}{h_3} (\vec{c}_1 \frac{\partial U}{\partial Z} + \vec{c}_2 \frac{\partial V}{\partial Z} + \vec{c}_3 \frac{\partial W}{\partial Z} + \frac{U}{R} \vec{c}_3 - \frac{W}{R} \vec{c}_1) \end{aligned} \quad (\text{A.13})$$

The pressure gradient ∇P is:

$$\nabla P = \vec{c}_1 \frac{\partial P}{\partial X} + \vec{c}_2 \frac{\partial P}{\partial Y} + \frac{\vec{c}_3}{h_3} \frac{\partial P}{\partial Z} \quad (\text{A.14})$$

The Laplacian vector $\nabla^2 \vec{V}$ becomes:

$$\begin{aligned} \nabla^2 \vec{V} = & \frac{\partial^2 \vec{V}}{\partial X^2} + \frac{\partial^2 \vec{V}}{\partial Y^2} + \frac{1}{h_3^2} \frac{\partial^2 \vec{V}}{\partial Z^2} + \frac{1}{R} \frac{1}{h_3} \frac{\partial \vec{V}}{\partial X} \\ = & \vec{c}_1 \frac{\partial^2 U}{\partial X^2} + \vec{c}_2 \frac{\partial^2 V}{\partial X^2} + \vec{c}_3 \frac{\partial^2 W}{\partial X^2} + \vec{c}_1 \frac{\partial^2 U}{\partial Y^2} + \vec{c}_2 \frac{\partial^2 V}{\partial Y^2} + \vec{c}_3 \frac{\partial^2 W}{\partial Y^2} \\ & + \frac{1}{Rh_3} (\vec{c}_1 \frac{\partial U}{\partial X} + \vec{c}_2 \frac{\partial V}{\partial X} + \vec{c}_3 \frac{\partial W}{\partial X}) + \frac{1}{h_3^2} (\vec{c}_1 \frac{\partial^2 U}{\partial Z^2} + \\ & \vec{c}_2 \frac{\partial^2 V}{\partial Z^2} + \vec{c}_3 \frac{\partial^2 W}{\partial Z^2} - \frac{U}{R^2} \vec{c}_1 - \frac{2}{R} \frac{\partial W}{\partial Z} \vec{c}_1 - \frac{W}{R^2} \vec{c}_3 + \frac{2}{R} \frac{\partial U}{\partial Z} \vec{c}_3) \end{aligned} \quad (\text{A.15})$$

From equations (A.13), (A.14) and (A.15), equation (A.2) can be written in the following component forms:

\vec{c}_1 component

$$\begin{aligned} \rho \left(U \frac{\partial U}{\partial X} + V \frac{\partial U}{\partial Y} + \frac{W}{1+X/R} \frac{\partial U}{\partial Z} - \frac{1}{R} \frac{W^2}{1+X/R} \right) = - \frac{\partial P}{\partial X} \\ + \mu \left[\frac{\partial^2 U}{\partial X^2} + \frac{\partial^2 U}{\partial Y^2} + \frac{1}{(1+X/R)^2} \frac{\partial^2 U}{\partial Z^2} - \frac{2}{R(1+X/R)^2} \frac{\partial W}{\partial Z} - \frac{U}{R^2(1+X/R)^2} \right. \\ \left. + \frac{1}{R(1+X/R)} \frac{\partial U}{\partial X} \right] \end{aligned} \quad (A.16)$$

\vec{c}_2 component

$$\begin{aligned} \rho \left(U \frac{\partial V}{\partial X} + V \frac{\partial V}{\partial Y} + \frac{W}{1+X/R} \frac{\partial V}{\partial Z} \right) = - \frac{\partial P}{\partial Y} + \mu \left[\frac{\partial^2 V}{\partial X^2} + \frac{\partial^2 V}{\partial Y^2} \right. \\ \left. + \frac{1}{(1+X/R)^2} \frac{\partial^2 V}{\partial Z^2} + \frac{1}{R(1+X/R)} \frac{\partial V}{\partial X} \right] \end{aligned} \quad (A.17)$$

\vec{c}_3 component

$$\begin{aligned} \rho \left(U \frac{\partial W}{\partial X} + V \frac{\partial W}{\partial Y} + \frac{W}{1+X/R} \frac{\partial W}{\partial Z} + \frac{UW}{R(1+X/R)} \right) = - \frac{1}{1+X/R} \frac{\partial P}{\partial Z} \\ + \mu \left[\frac{\partial^2 W}{\partial X^2} + \frac{\partial^2 W}{\partial Y^2} + \frac{1}{(1+X/R)^2} \frac{\partial^2 W}{\partial Z^2} + \frac{1}{R(1+X/R)} \frac{\partial W}{\partial X} + \frac{2}{R(1+X/R)^2} \frac{\partial U}{\partial Z} \right. \\ \left. - \frac{W}{R^2(1+X/R)^2} \right] \end{aligned} \quad (A.18)$$

The equations (A.10), (A.16), (A.17) and (A.18) represent the complete set of governing equations for three-dimensional steady incompressible flow in curved rectangular channels. For the case of fully developed flow, the set of equations can be simplified further by noting that the Z-derivatives are zero. The governing equations then become:

Continuity equation

$$\frac{\partial U}{\partial X} + \frac{\partial V}{\partial Y} + \frac{U}{R(1+X/R)} = 0 \quad (\text{A.19})$$

X - momentum equation

$$\begin{aligned} \rho \left(U \frac{\partial U}{\partial X} + V \frac{\partial U}{\partial Y} - \frac{1}{1+X/R} \frac{U^2}{R} \right) = - \frac{\partial P}{\partial X} + \mu \left[\frac{\partial^2 U}{\partial X^2} + \frac{\partial^2 U}{\partial Y^2} \right. \\ \left. - \frac{U}{R^2(1+X/R)^2} + \frac{1}{R(1+X/R)} \frac{\partial U}{\partial X} \right] \quad (\text{A.20}) \end{aligned}$$

Y - momentum equation

$$\rho \left(U \frac{\partial V}{\partial X} + V \frac{\partial V}{\partial Y} \right) = - \frac{\partial P}{\partial Y} + \mu \left[\frac{\partial^2 V}{\partial X^2} + \frac{\partial^2 V}{\partial Y^2} + \frac{1}{R(1+X/R)} \frac{\partial V}{\partial X} \right] \quad (\text{A.21})$$

Z - momentum equation

$$\begin{aligned} \rho \left(U \frac{\partial W}{\partial X} + V \frac{\partial W}{\partial Y} + \frac{UW}{R(1+X/R)} \right) = - \frac{1}{1+X/R} \frac{\partial P}{\partial Z} \\ + \mu \left[\frac{\partial^2 W}{\partial X^2} + \frac{\partial^2 W}{\partial Y^2} + \frac{1}{R(1+X/R)} \frac{\partial W}{\partial X} - \frac{W}{R^2(1+X/R)^2} \right] \end{aligned} \quad (A.22)$$

The energy equation will be considered next. Using the expression $\vec{V} \cdot \nabla$ from equation (A.11) and the Laplacian operator ∇^2 from equation (A.8), the energy equation (A.3) becomes

$$\begin{aligned} U \frac{\partial T}{\partial X} + V \frac{\partial T}{\partial Y} + \frac{W}{1+X/R} \frac{\partial T}{\partial Z} = \alpha \left[\frac{\partial^2 T}{\partial X^2} + \frac{\partial^2 T}{\partial Y^2} + \frac{1}{(1+X/R)^2} \frac{\partial^2 T}{\partial Z^2} \right. \\ \left. + \frac{1}{R(1+X/R)} \frac{\partial T}{\partial X} \right] \end{aligned} \quad (A.23)$$

where $\alpha = \frac{k}{\rho C_p}$

It is known that the effect of axial conduction term in the energy equation can be neglected practically when the value of Peclet number is large ($Pe \geq 50$). Neglecting the axial conduction term, the energy equation takes the following form:

$$\begin{aligned} U \frac{\partial T}{\partial X} + V \frac{\partial T}{\partial Y} + \frac{W}{1+X/R} \frac{\partial T}{\partial Z} = \alpha \left[\frac{\partial^2 T}{\partial X^2} + \frac{\partial^2 T}{\partial Y^2} \right. \\ \left. + \frac{1}{R(1+X/R)} \frac{\partial T}{\partial X} \right] \end{aligned} \quad (A.24)$$

The Graetz problem (thermal entrance heat transfer) in curved rectangular channels is concerned with the solution of the above parabolic equation with appropriate boundary conditions.

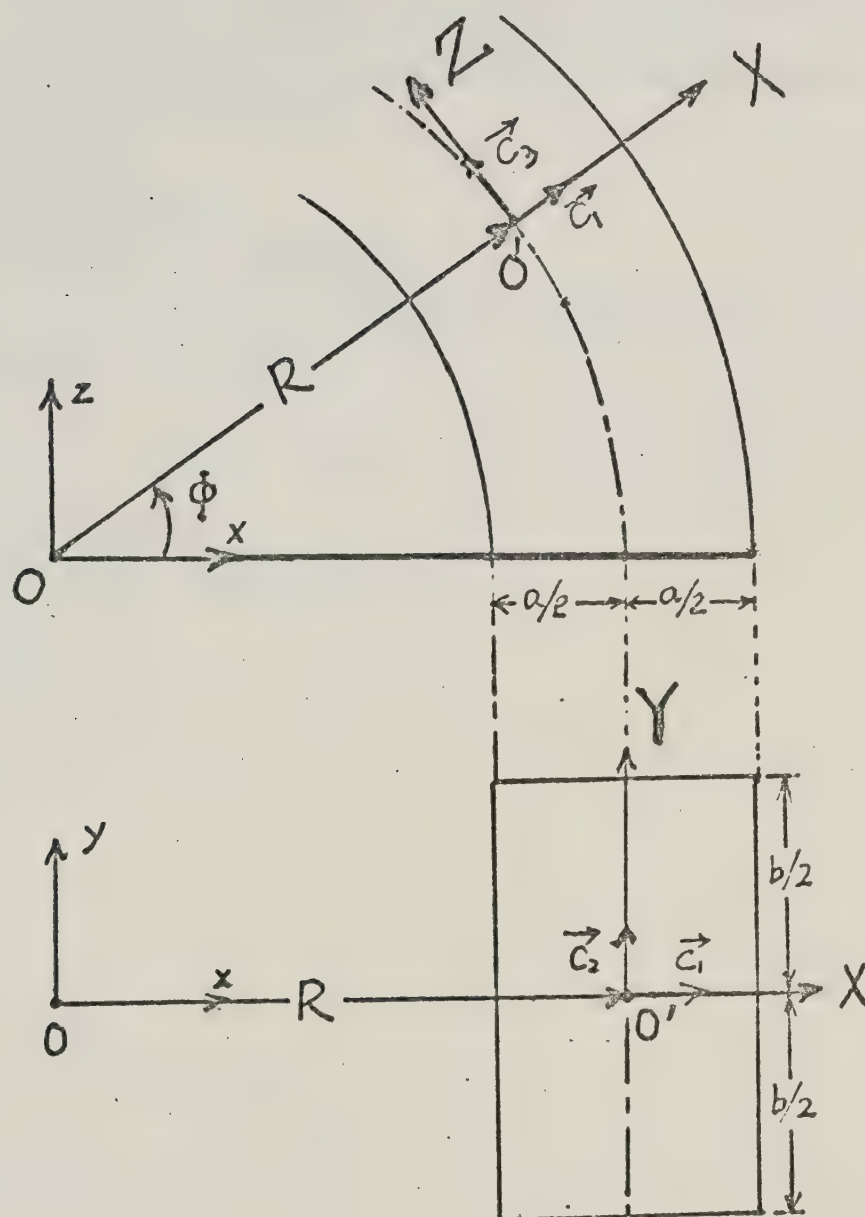


Fig. A.1

APPENDIX B

COMPUTER PROGRAMS

```

C *****
C LAMINAR FLOW IN CURVED RECTANGULAR CHANNELS
C *****
C M,N NUMBER OF GRID POINTS
C R ASPECT RATIO
C D PRESSURE DROP
C RC RADIUS CURVATURE
C MAXIMUM NUMBER OF ITERATION
C ITM, ISM, IVM MAXIMUM NUMBER OF ITERATIONS
C FR1 PRODUCT OF FRICTION FACTOR AND REYNOLD NUMBER
1 FOR STRAIGHT CHANNEL
  DIMENSION X(41),RA1(41),RA2(41),S(41,41),W(41,41),
1VOR(41,41)
*,S1(41,21),W1(41,21),VOR1(41,21),U(41,21),V(41,21),
1A1(41),A2(41)
*,A3(41),A4(41),DW(41,41),FJ(41)
  DIMENSION S2(41,41),VX(41,41)
  COMMON /C4/ M,N
  COMMON /C5/ M1,N1
  REAL MAXS,MAXT
  READ(5,10) M,N,R
10  FORMAT(2I5,F5.1)
  WRITE(6,10) M,N,R
  M1=M+1
  N1=N+1
  MM1=M-1
  NM1=N-1
  VZB=1.0
  READ(5,15) D,RC
15  FORMAT(2F10.0)
  READ(5,16) ITM,ISM,IVM
16  FORMAT(3I10)
  READ(5,17) OMEV,OMES,OMEW
17  FORMAT(3F10.1)
  READ(5,117) FR1
117  FORMAT(F10.3)
  ESS=1.E-4
  PSS=1.E-3
  HI=(1.+1./R)/(2.*M)
  HJ=(1.+R)/(4.*N)

```



```

      HI2=HI*HI
      HJ2=HJ*HJ
      HO=-2.*(1./HI2+1./HJ2)
      DO 5 I=1,M1
      X(I)=- (1.+1./R)/4.+(I-1)*HI
      RA1(I)=1.+X(I)/RC
      RA2(I)=RA1(I)*RA1(I)
5      CONTINUE
      DO 450 I=1,M1
450     READ(5,460) (S(I,J),J=1,N )
      DO 451 I=1,M1
451     READ(5,460) (W(I,J),J=1,N )
      DO 452 I=1,M1
452     READ(5,460) (VOR(I,J),J=1,N1)
      DO 888 I=1,M1
888     READ(5,460) (U(I,J),J=1,N1)
      DO 889 I=1,M1
889     READ(5,460) (V(I,J),J=1,N1)
460     FORMAT(5E16.7)
C      BOUNDARY CONDITUDNS
      DO 110 I=1,M1
      S(I,1)=0.
      S(I,N1)=0.
      V(I,1)=0.
      V(I,N1)=0.
      U(I,N1)=0.
110     W(I,N1)=0.
      DO 111 J=1,N1
      S(1,J)=0.
      U(1,J)=0.
      U(M1,J)=0.
      V(M1,J)=0.
      V(1,J)=0.
      S(M1,J)=0.
      W(M1,J)=0.
      W(1,J)=0.
111     VOR(1,J)=0.
      K=1
660     CONTINUE
      DO 12 I=2,M
      DO 12 J=2,N
      U(I,J)=0.5*(S(I,J+1)-S(I,J-1))/(HJ*RA1(I))
      V(I,J)=0.5*(S(I-1,J)-S(I+1,J))/(HI*RA1(I))
12     DW(I,J)=W(I,J)*(W(I,J+1)-W(I,J-1))/(RC*RA2(I)*HJ)
      DO 13 I=2,M
13     U(I,1)=0.5*(4.*S(I,2)-S(I,3))/(HJ*RA1(I))

```



```

C      VORTICITY AT BOUNDARIESP
      DO 20 J=1,N1
      VOR(1,J)=-2.*S(2,J)*VZB/(RA2(1)*HI2)+(1.-VZB)*VOR(1,J)
20     VOR(M1,J)=-2.*S(M,J)*VZB/(RA2(M1)*HI2)+(1.-VZB)*VOR(M1,J)
      DO 21 I=1,M1
21     VOR(I,N1)=-2.*S(I,N)*VZB/(RA2(I)*HJ2)+(1.-VZB)*
1     VOR(I,N1)
C      SOLVE VORTICITY FUNCTION
      IV=1
160     CONTINUE
      DO 22 I=2,M
      DO 22 J=2,N
22     S1(I,J)=VOR(I,J)
      DO 25 J=2,N
      DO 23 I=2,M
      L=I-1
      A1(L)=(1./HI2-1.5/(RC*HI*RA1(I))+0.5*U(I,J)/HI)
      A2(L)=HO
      A3(L)=(1./HI2+1.5/(RC*HI*RA1(I))-0.5*U(I,J)/HI)
      A4(L)=DW(I,J)-(1./HJ2-0.5*V(I,J)/HJ)*VOR(I,J+1)
      *      -(1./HJ2+0.5*V(I,J)/HJ)*VOR(I,J-1)
23     CONTINUE
      A4(1)=A4(1)-A1(1)*VOR(1,J)
      A4(MM1)=A4(MM1)-A3(MM1)*VOR(M1,J)
      CALL GAUSS(A1,A2,A3,A4,MM1,X)
      DO 24 I=2,M
      VX(I,J)=X(I-1)
24     VOR(I,J)=S1(I,J)+OMEV*(VX(I,J)-S1(I,J))
25     CONTINUE
      DV=0.
      FEV=0.
      DO 30 I=2,M
      DO 30 J=2,N
      VN=ABS(VOR(I,J))
      VR=ABS(VOR(I,J)-S1(I,J))
      DV=AMAX1(DV,VR)
      FEV=AMAX1(FEV,VN)
30     CONTINUE
      DV=DV/FEV
      IF(DV.LE.ESS.OR.IV.GT.IVM) GO TO 31
760     IV=IV+1
      GO TO 160
31     CONTINUE
C      SOLVE STREAM FUNCTION
      DO 310 I=2,M
      DO 310 J=2,N

```



```

310  S2(I,J)=S(I,J)
      IS=1
300  CONTINUE
      DO 32 I=2,M
      DO 32 J=2,N
32    S1(I,J)=S(I,J)
      DO 35 J=2,N
      DO 33 I=2,M
      AVP=-RA2(I)*VOR(I,J)
      L=I-1
      A1(L)=(1./HI2+0.5/(RC*HI*RA1(I)))
      A2(L)=H0
      A3(L)=(1./HI2-0.5/(HI*RC*RA1(I)))
      A4(L)=AVP-(1./HJ2)*(S(I,J+1)+S(I,J-1))
33    CONTINUE
      CALL GAUSS(A1,A2,A3,A4,MM1,X)
      DO 34 I=2,M
      VX(I,J)=X(I-1)
34    S(I,J)=S1(I,J)+OMES*(VX(I,J)-S1(I,J))
35    CONTINUE
      DS=0.
      FES=0.
      DO 39 I=2,M
      DO 39 J=2,N
      SN=ABS(S(I,J))
      SR=ABS(S(I,J)-S1(I,J))
      DS=AMAX1(DS,SR)
      FES=AMAX1(FES,SN)
39    CONTINUE
      DS=DS/FES
      IF(DS.LE.ESS.OR.IS.GT.ISM) GO TO 40
      IS=IS+1
      GO TO 300
40    CONTINUE
      WRITE(6,350) IS,DS
C    UP-DATING COEFF
      DO 41 I=2,M
      DO 41 J=2,N
      U(I,J)=0.5*(S(I,J+1)-S(I,J-1))/(HJ*RA1(I))
41    V(I,J)=0.5*(S(I-1,J)-S(I+1,J))/(HI*RA1(I))
      DO 42 I=2,M
42    U(I,1)=0.5*(4.*S(I,2)-S(I,3))/(HJ*RA1(I))
      DSS=0.
      DO 711 I=1,M1
      DO 711 J=1,N1
      SRR=ABS(S(I,J)-S2(I,J))

```



```

DSS=AMAX1(DSS,SRR)
711  CONTINUE
SD=DSS/FES
C      SOLVE AXIAL VELOCITY
DO 712 I=2,M
DO 712 J=2,N
712  S2(I,J)=W(I,J)
IW=1
750  CONTINUE
DO 51 I=2,M
DO 51 J=2,N
51  S1(I,J)=W(I,J)
DO 52 I=2,M
52  W(I,1)=(4.*W(I,2)-W(I,3))/3.
DO 55 J=2,N
DO 53 I=2,M
L=I-1
A1(L)=(1./HI2+0.5*U(I,J)/HI-0.5/(RC*HI*RA1(I)))
A2(L)=(HO-1.0*U(I,J)/(RC*RA1(I))-1.0/(RC*RC*RA2(I)))
A3(L)=(1./HI2-0.5*U(I,J)/HI+0.5/(HI*RC*RA1(I)))
C=D/RA1(I)
A4(L)=C-(1./HJ2-0.5*V(I,J)/HJ)*W(I,J+1)-(1./HJ2+
10.5*V(I,J)/HJ)*W(I,J-1)
53  CONTINUE
CALL GAUSS(A1,A2,A3,A4,MM1,X)
DO 54 I=2,M
VX(I,J)=X(I-1)
5000 FORMAT(11E10.3)
54  W(I,J)=S1(I,J)+OMEW*(VX(I,J)-S1(I,J))
55  CONTINUE
PW=0.
FEW=0.
DO 59 I=2,M
DO 59 J=2,N
WN=ABS(W(I,J))
WR=ABS(W(I,J)-S1(I,J))
PW=AMAX1(WR,PW)
FEW=AMAX1(FEW,WN)
59  CONTINUE
PW=PW/FEW
IF(PW.LE.ESS.OR.IW.GT.ISM) GO TO 64
IW=IW+1
GO TO 750
64  CONTINUE
WRITE(6,350) IW,PW
350  FORMAT(/,I5,E20.5)

```



```

PWW=0.
DO 714 I=2,M
  DO 714 J=2,N
    WD=ABS(W(I,J)-S2(I,J))
    PWW=AMAX1(WD,PWW)
714 CONTINUE
WD=PWW/FEW
WRITE(6,223) SD,WD
223 FORMAT('SD =',E15.5,/, 'WD =',E15.5)
WRITE(6,222) K
222 FORMAT('OUTER ITERATION TIMES =',I5)
113 FORMAT(I5,15X,E15.5,/,I5,15X,E15.5)
DO 65 I=2,M
  DO 65 J=2,N
    65 DW(I,J)=W(I,J)*(W(I,J+1)-W(I,J-1))/(RC*RA2(I)*HJ)
    IF(WD.LE.PSS.AND.SD.LE.PSS) GO TO 200
    IF(K.GE.ITM) GO TO 200
    K=K+1
    GO TO 660
200 CONTINUE
6666 CONTINUE
C CALCULATION OF DEAN NUMBER
WRITE(6,1005)
1005 FORMAT('STREAM FUNCTION')
DO 1006 I=1,M1
1006 WRITE(6,601) (S(I,J),J=1,N)
DO 3001 I=1,M1
WRITE(6,601) (VOR(I,J),J=1,N1)
3001 CONTINUE
WRITE(6,1)
1 FORMAT('AXIAL VELOCITY')
DO 600 I=1,M1
600 WRITE(6,601) (W(I,J),J=1,N)
WRITE(6,1001)
1001 FORMAT('V COMPONENT')
DO 177 I=1,M1
177 WRITE(6,601) (V(I,J),J=1,N)
WRITE(6,1002)
1002 FORMAT('U COMPONENT')
DO 173 I=1,M1
173 WRITE(6,601) (U(I,J),J=1,N)
CALL SIMPS(W,M,N,HI,HJ,SUMM)
AREA=(1.+R)*(1.+1./R)/8
SUMM=SUMM/AREA
WRITE(6,501) SUMM
501 FORMAT('REYNOLD NUMBER =',10X,E15.5)

```



```

      SUPP=SUMM/SQRT(RC)
      WRITE(6,1000) SUPP
1000  FORMAT(/,,'DEAN NUMBER =', F20.5)
      DO 130 I=1,M1
130   FJ(I)=-0.5*(-4.*W(I,N)+W(I,NM1))/ HJ *RA1(I)
      CALL SIMP(FJ,M,HI,SUM)
      SUM1=SUM
      DO 132 J=1,N1
132   FJ(J)=-0.5*(-4.*W(M,J)+W(MM1,J))/HI*(1.+0.5/RC)
      CALL SIMP(FJ,N,HI,SUM)
      SUM2=SUM
      DO 135 J=1,N1
135   FJ(J)=-0.5*(-4.*W(2,J)+W(3,J))/HI *(1.-0.5/RC)
      CALL SIMP(FJ,N,HI,SUM)
      SUM3=SUM
      PRE=0.5*(1.+R)+0.5*(1.+1./R)
      FRE=(SUM1+SUM2+SUM3)/PRE
      FRE1=2.*FRE/SUMM
      FRA1=FRE1/FR1
      FRE2=-0.5*D/SUMM
      FRA2=FRE2/FR1
      WRITE(6,666) FRE1,FRE2, FRA1, FRA2
666   FORMAT(///,,'FRE1 =',F15.5,5X,'FRE2 =',F15.5,/,/,
* 'FRA1 =',F15.5,5X,'FRA2 =',F15.5)
601   FORMAT(/ ,7E18.5)
603   FORMAT(' ',I3,10E12.3)
      DO 401 I=1,M1
401   WRITE(7,410) (S(I,J),J=1,N )
      DO 402 I=1,M1
402   WRITE(7,410) (W(I,J),J=1,N )
      DO 403 I=1,M1
403   WRITE(7,410) (VOR(I,J),J=1,N1)
      DO 190 I=1,M1
190   WRITE(7,281) (U(I,J),J=1,N1)
      DO 191 I=1,M1
191   WRITE(7,281) (V(I,J),J=1,N1)
281   FORMAT(5E16.7)
410   FORMAT(5E16.7)
      CALL CCC2(II,JJ,MAXT,XT,T,HI,HJ)
      WRITE(6,531) MAXT,II,JJ
      CALL CCC1(XT,T,HI,HJ)
531   FORMAT('0',20X,'MAXIMUM OF TEMPERATURE',10X,E14.7
1,5X,'IN I-D',2X,I5,5X,'IN J-D',2X,I5)
      STOP

```



```

C      SUBROUTINE FOR THE SELECTING OF THE MAXIMUM VALUE
1  IN THE NUMERICAL CALCULATION DOMAIN
      SUBROUTINE CCC2(II,JJ,MAXTS,DE,ST,HI,HJ)
      DIMENSION ST(41,21),DE(10)
      COMMON /C3/ M,N
      REAL MAXTS,MAXST
      FES=0.
      DO 1 I=2,M
      DO 1 J=2,N
      SC=ABS(ST(I,J))
1  FES=AMAX1(FES,SC)
      DO 2 I=2,M
      DO 2 J=2,N
      SC=ABS(ST(I,J))
      IF(SC.EQ.FES) II=I
      IF(SC.EQ.FES) JJ=J
2  CONTINUE
      MAXTS=FES
      MAXST=FES
      EH=0.
      NJ=1
7  IM=2
      IF(MAXST.LT.0.00001.OR.MAXST.GT.100) GO TO 50
      IF(MAXST.GE.0.00001.AND.MAXST.LT.0.0001) DB=0.00001
      IF(MAXST.GE.0.0001.AND.MAXST.LT.0.001) DB=0.0001
      IF(MAXST.GE.0.001.AND.MAXST.LT.0.01) DB=0.001
      IF(MAXST.GE.0.01.AND.MAXST.LT.0.1) DB=0.01
      IF(MAXST.GE.0.1.AND.MAXST.LT.1.0) DB=0.1
      IF(MAXST.GE.1.0.AND.MAXST.LT.10.) DB=1.0
      IF(MAXST.GE.10..AND.MAXST.LE.100.) DB=10.
      DA=DB
      DO 4 I=2,9
      DM=AMIN1(MAXST,DA)
      IF(DM.EQ.DA) DD=DM
      DA=DB*I
4  CONTINUE
      EH=DD+EH
      IF(NJ.EQ.2) GO TO 8
      MAXST=MAXST-DD
      NJ=NJ+1
      GO TO 7
8  DC=EH/10.
      DO 5 J=1,10
      DE(J)=DC*J
5  CONTINUE

```



```

50  IM=1
    RETURN
    END

```

```

C    SUBROUTINE FOR THE CONSTANT STREAM LINE
    SUBROUTINE CCC1 (CF,F,HI,HJ)
    DIMENSION CF(10),F(41,21),DF(41),CJ(41),PF(41)
1,RI(41),PJ(41),      QI(41)
    COMMON /C3/ M,N
    DO 6 K=1,10
    WRITE(6,120) K,CF(K)
    WRITE(6,105)
    DO 81 I=2,M
    JK=1
    IF(I.GE.2) GO TO 93
93  DF(1)=CF(K)-F(I,1)
    DO 83 J=2,N
    DF(J)=CF(K)-F(I,J)
    EE=DF(J)*DF(J-1)
    IF(EE.GT.0.) GO TO 83
    EF=DF(J-1)/(F(I,J)-F(I,J-1))
    CJ(JK)=J-1+EF
    JK=JK+1
83  CONTINUE
    IF(JK.EQ.1) GO TO 81
    JKD=JK-1
    QI(I)=HI*(I-1)
    WRITE(6,107) I,QI(I),(CJ(JK),JK=1,JKD )
81  CONTINUE
    WRITE(6,108)
    DO 71 J=2,N
    IK=1
    IF(J.GE.2) GO TO 74
74  PF(1)=CF(K)-F(1,J)
    DO 72 I=2,M
    PF(I)=CF(K)-F(I,J)
    QF=PF(I)*PF(I-1)
    IF(QF.GT.0.) GO TO 72
    RF=PF(I-1)/(F(I,J)-F(I-1,J))
    RI(IK)=I-1+RF
    IK=IK+1
72  CONTINUE
    IF(IK.EQ.1) GO TO 71
    IKD=IK-1

```



```

      PJ(J)=HJ*(J-1)
      WRITE(6,107) J,PJ(J),(RI(IK),IK=1,IKD)
71    CONTINUE
      6    CONTINUE
105   FORMAT('0',30X,'COORDINATE IN X-DIRECTION',20X,'I
      1N Y-DIRECTION')
107   FORMAT(' ',30X,I5,5X,F10.4,20X,4F10.4)
108   FORMAT('0',30X,'COORDINATE IN Y-DIRECTION',20X,
      1 'X-DIRECTION')
120   FORMAT('0',20X,'NO OF CONSTANT LINE',10X,I5,10X,
      1 'CONSTANT VALUE',10X,F20.5)
      RETURN
      END

```

```

C      *****
C      HEAT TRANSFER OF UNIFORM WALL TEMPERATURE
C      *****
C      R  ASPECT RATIO
C      REY  REYNOLD NUMBER
C      DEAN  DEAN NUMBER
C      PR  PRANDTL NUMBER
      DIMENSION T(41,21),T1(41,21),TK(41,21) ,T2(41,21)
      DIMENSION A1(41,21),A2(41,21),A3(41,21),B1(41,21),
      *B2(41,21),B3(41,21)
      DIMENSION S(41,21),VOR(41,21) ,FJ(41)
      DIMENSION X(41),RA1(41),SWT(200)
      DIMENSION U(41,21),V(41,21),W(41,21)
      DIMENSION GZW(41,21),WT(41,21) ,SDZ(200)
      DIMENSION XT(41,21)
      COMMON /C1/ ZZ(1500),DX,KZ ,BI
      COMMON /C2/ A(41,21),B,C(41,21),D(41,21),E,F(41,21)
1    WW(41,21)
      COMMON /C4/ M1,N1
      COMMON /C3/ M,N
      COMMON /C6/ AREA
      REAL MAXS,MAXT
      READ(5,10) M,N,R
      WRITE(6,10) M,N,R
10   FORMAT(2I5,F5.1)
      READ(5,314) PR,RC,DEAN,REY
314  FORMAT(4F20.5)
      WRITE(6,14) PR,RC,DEAN,REY
14   FORMAT(//,'PRANDTL NUMBER =',F15.5,/,
      1 'CURVATURE =',F15.5,/,

```



```

*'DEAN NUMBER =' ,F15.5,/, 'REYNOLD NUMBER =' ,F15.5)
M1=M+1
N1=N+1
MM1=M-1
NM1=N-1
HI=(1.+1./R)/(2.*M)
HJ=(1.+R)/(4.*N)
DX=HI/2.
DX2=HI*HI
DO 450 I=1,M1
450 READ(5,460) (S(I,J),J=1,N )
DO 451 I=1,M1
451 READ(5,460) (W(I,J),J=1,N )
DO 452 I=1,M1
452 READ(5,460) (VOR(I,J),J=1,N1)
DO 888 I=1,M1
888 READ(5,460) (U(I,J),J=1,N1)
DO 889 I=1,M1
889 READ(5,460) (V(I,J),J=1,N1)
460 FORMAT(5E16.7)
C ENTRANCE CONDITIONS
DO 15 I=1,M1
W(I,N1)=0.
DO 15 J=1,N1
15 T(I,J)=1.0
DO 16 I=1,M1
16 T(I,N1)=0.
DO 26 J=1,N1
T(1,J)=0.
26 T(M1,J)=0.
DO 12 I=1,M1
DO 12 J=1,N1
12 W(I,J)=W(I,J)/REY
DO 100 I=1,M1
X(I)=-(1.+1./R)/4.+(I-1)*HI
100 RA1(I)=1.+X(I)/RC
DO 18 I=1,M1
DO 18 J=1,N1
18 WW(I,J)=2.*W(I,J)*DX2/RA1(I) /PR
PR1=1./PR
DO 11 I=1,M1
DO 11 J=1,N1
A(I,J)=PR1-DX*(U(I,J)-1./(RC*RA1(I)) )
B=-2.*PR1
C(I,J)=PR1+DX*(U(I,J)-1./(RC*RA1(I)) )
D(I,J)=-PR1+DX*V(I,J)

```



```

      E=2.*PR1
      F(I,J)=-PR1-DX*V(I,J)
11    CONTINUE
      AREA=(1.+R)*(1.+1./R)/8.
      KMAX=1000
      Z=0.
      KZ=0
      KK=1
      DO 19 I=1,M1
      DO 19 J=1,N1
19    TK(I,J)=T(I,J)
      DX=HI
      20    KZ=KZ+1
C    AXIAL STEP
      DZ=5.E-5
      IF(KZ.GT.100) DZ=1.E-4
      IF(KZ.GT.450) DZ=2.E-4
      IF(KZ.GT.650) DZ=5.E-5
      IF(KZ.GT.850) DZ=1.E-3
21    Z=Z+DZ
      ZZ(KZ)=DZ
      DO 22 I=1,M1
      DO 22 J=1,N1
22    TK(I,J)=T(I,J)
      CALL TEMP(T,TK)
      WRITE(6,201) KZ,Z
      DO 23 I=1,M1
      DO 23 J=1,N1
23    T1(I,J)=T(I,J)*W(I,J)
      CALL SIMPS(T1,M,N,HI,HJ,SUMM)
      TBK=SUMM
      DO 130 I=1,M1
130    FJ(I)=-0.5*(-4.*T(I,N)+T(I,NM1))/HJ
      CALL SIMP(FJ,M,HI,SUM)
      SUM1=SUM
      DO 132 J=1,N1
132    FJ(J)=-0.5*(-4.*T(M,J)+T(MM1,J))/HI
      CALL SIMP(FJ,N,HJ,SUM)
      SUM2=SUM
      DO 133 J=1,N1
133    FJ(J)=-0.5*(-4.*T(2,J)+T(3,J))/HI
      CALL SIMP(FJ,N,HJ,SUM)
      SUM3=SUM
      PRE=0.5*(1.+R)+0.5*(1.+1./R)
      SUMM=(SUM1+SUM2+SUM3)/PRE
      ANU1=-SUMM/TBK

```



```

C      CALCULATIONS OF TEMP. GRADIEND IN FLOW DIRECTION
      DO 50 I=1,M1
      DO 50 J=1,N1
50     T1(I,J)=(T(I,J)-TK(I,J))/ZZ(KZ)
      DO 51 J=1,N1
      DO 51 I=1,M1
51     T1(I,J)=T1(I,J)*W(I,J)
      CALL SIMPS (T1,M,N,HI,HJ,SUMM)
      ANU2=-0.25 * SUMM/TBK
      AVNU=0.5*(ANU1+ANU2)
      DNU=100*ABS(ANU1-ANU2)/AVNU
      IF(KZ.LE.1) GO TO 66
      BNU2=0.5*(ANU2+BNU2)
      BNU =0.5*(BNU1+BNU2)
      BP=100.*ABS(BNU2-BNU1)/BNU
      WRITE(6,202) BNU1,BNU2,BNU,BP
66     CONTINUE
      BNU1=ANU1
      BNU2=ANU2
      WRITE(6,501) ANU1,ANU2,AVNU,DNU
      WRITE(6,502) TBK
      WRITE(6,503)
201    FORMAT(/,'NO. OF SECTION',I5,10X,'DISTANCE FROM
1 ENTRANCE',F10.6)
202    FORMAT(30X,'***',3F15.6,E20.5)
501    FORMAT('NU1',F10.6,10X,'NU2',F10.6,10X,'AVERAGE
1 NU',F10.6,10X,E20.4)
      KKK=KZ/30
      IF(KKK.NE.KK) GO TO 500
      KK=KK+1
      WRITE(6,503)
      DO 61 I=1,M1
      WRITE(6,504) I
61     WRITE(6,505) (T(I,J),J=1,N1)
502    FORMAT('BULK TEMP.', E15.5 )
503    FORMAT('// 'TEMP. DISTRIBUTIONS'//)
504    FORMAT('I',I5)
505    FORMAT(' ',10E12.4)
500    CONTINUE
      IF(KZ.GE.KMAX) GO TO 90
      GO TO 20
90     CONTINUE
      STOP
      END
      SUBROUTINE TEMP(T,TK)
      DIMENSION T(41,21),TK(41,21),TKH(41,21),X(41)

```



```

DIMENSION A1(41),A2(41),A3(41),A4(41),A5(41)
COMMON /C1/ ZZ(1500),DX,KZ      ,BI
COMMON /C2/ A(41,21),B,C(41,21),D(41,21),E,F(41,21)
1,WW(41,21)
COMMON /C3/ M,N
COMMON /C4/ M1,N1
  M1=M+1
  MM1=M-1
  DO 20 J=1,N
DO 10 I=2,M
  L=I-1
  A1(L)=C(I,J)
  A2(L)=B-WW(I,J)/ZZ(KZ)
  A3(L)=A(I,J)
  IF(J.EQ.1) GO TO 15
  A4(L)=D(I,J)*TK(I,J+1)+(E-WW(I,J)/ZZ(KZ))*TK(I,J)+
1F(I,J)*TK(I,J-1)
  GO TO 10
15  A4(L)=(D(I,J)+F(I,J))*TK(I,J+1)+(E-WW(I,J)/ZZ(KZ))
1*TK(I,J)
10  CONTINUE
  CALL GAUSS(A1,A2,A3,A4,MM1,X)
DO 20 I=2,M
20  TKH(I,J)=X(I-1)
DO 21 J=1,N
  TKH(1,J)=0.
21  TKH(M1,J)=0.
DO 40 I=2,M
DO 30 J=1,N
  A1(J)=F(I,J)
  A2(J)=E+WW(I,J)/ZZ(KZ)
  A3(J)=D(I,J)
  A4(J)=A(I,J)*TKH(I+1,J)+(B+WW(I,J)/ZZ(KZ))*T
1KH(I,J)+C(I,J)*TKH(I-1,J)
30  CONTINUE
  A3(1)=F(I,1)+D(I,1)
  CALL GAUSS(A1,A2,A3,A4,N,X)
DO 40 J=1,N
40  T(I,J)=X(J)
  RETURN
  END

```

```

C *****
C HEAT TRANSFER OF UNIFORM HEAT FLUX

```



```

C *****
C R ASPECT RATIO
C REY REYNOLD NUMBER
C DEAN DEAN NUMBER
C PR PRANDTL NUMBER
  DIMENSION T(41,21),T1(41,21),TK(41,21) ,T2(41,21)
    DIMENSION S(41,21),VOR(41,21) ,FJ(41)
      DIMENSION X(41),RA1(41),SWT(200)
  DIMENSION U(41,21),V(41,21),W(41,21)
    DIMENSION GZW(41,21),WT(41,21) ,SDZ(200)
  DIMENSION XT(41,21)
  COMMON /C1/ ZZ(1500),DX,KZ
  COMMON /C2/ A(41,21) ,C(41,21),D(41,21) ,F(41,21)
1  ,WW(41,21),B(41,21),E(41,21)
  COMMON /C4/ M1,N1
  COMMON /C3/ M,N
  COMMON /C6/ AREA
  REAL MAXS,MAXT
  READ(5,10) M,N,R
  WRITE(6,10) M,N,R
10  FORMAT(2I5,F5.1)
  READ(5,314) PR,RC,DEAN,REY
314  FORMAT(4F20.5)
  WRITE(6,14) PR,RC,DEAN,REY
14  FORMAT(//,'PRANDTL NUMBER =',F15.5,/,
1  'CURVATURE =',F15.5,/,
* 'DEAN NUMBER =',F15.5,/, 'REYNOLD NUMBER =',F15.5)
  M1=M+1
  N1=N+1
  MM1=M-1
  NM1=N-1
  HI=(1.+1./R)/(2.*M)
  HJ=(1.+R)/(4.*N)
  DX=HI/2.
  DX2=HI*HI
C  ENTRANCE CONDITIONS
  DO 15 I=1,M1
    W(I,N1)=0.
  DO 15 J=1,N1
15  T(I,J)=0.0
    DX=HI
  DO 450 I=1,M1
450  READ(5,460) (S(I,J),J=1,N )
    DO 451 I=1,M1
451  READ(5,460) (W(I,J),J=1,N )
    DO 452 I=1,M1

```



```

452 READ(5,460) (VOR(I,J),J=1,N1)
      DO 888 I=1,M1
888  READ(5,460) (U(I,J),J=1,N1)
      DO 889 I=1,M1
889  READ(5,460) (V(I,J),J=1,N1)
460  FORMAT(5E16.7)
      DO 100 I=1,M1
        X(I)=-((1.+1./R)/4.+(I-1)*HI
100  RA1(I)=1.+X(I)/RC
      DO 12 I=1,M1
      DO 12 J=1,N1
12  W(I,J)=W(I,J)/REY
      DO 18 I=1,M1
      DO 18 J=1,N1
18  WW(I,J)=2.0*W(I,J)*DX2/RA1(I)  /PR
      PR1=1./PR
      DO 11 I=1,M1
      DO 11 J=1,N1
        A(I,J)=PR1-DX*(U(I,J)-1./(RC*RA1(I)) )
        B(I,J)=-2.*PR1
        C(I,J)=PR1+DX*(U(I,J)-1./(RC*RA1(I)) )
        D(I,J)=-PR1+DX*V(I,J)
        E(I,J)=2.*PR1
        F(I,J)=-PR1-DX*V(I,J)
11  CONTINUE
      AREA=(1.+R)*((1.+1./R)/8.
      KMAX=1000
      Z=0.
      KZ=0
      KK=1
20  KZ=KZ+1
C  AXIAL STEP
      DO 19 I=1,M1
      DO 19 J=1,N1
19  TK(I,J)=T(I,J)
C  AXIAL STEP
      DZ=5.E-5
      IF(KZ.GT.100) DZ=1.E-4
      IF(KZ.GT.450) DZ=2.E-4
      IF(KZ.GT.650) DZ=5.E-4
      IF(KZ.GT.850) DZ=1.E-3
21  Z=Z+DZ
      ZZ(KZ)=DZ
      DO 22 I=1,M1
      DO 22 J=1,N1
22  TK(I,J)=T(I,J)

```



```

CALL TEMP (T,TK)
WRITE(6,201) KZ,Z
DO 23 I=1,M1
DO 23 J=1,N1
23  T1(I,J)=T(I,J)*W(I,J)
CALL SIMPS(T1,M,N,HI,HJ,SUMM)
TBK=SUMM
SUT=0.
DO 42 I=1,M1
42  SUT=SUT+T(I,N1)
DO 44 J=1,N
44  SUT=SUT+T(1,J)+T(M1,J)
SUT=2.*SUT-T(1,1)-T(M1,1)
AVET      =SUT/(2*(M+2*N))
TAW=AVET
DO 651 I=1,M1
DO 651 J=1,N1
651  T1(I,J)=(AVET-T(I,J))*W(I,J)
CALL SIMPS(T1,M,N,HI,HJ,SUMM)
ANU1=1./SUMM
TMW=SUMM
C  CALCULATIONS OF TEMP. GRADIEND IN FLOW DIRECTION
DO 25 J=1,N1
DO 25 I=1,M1
GZW(I,J)=(T(I,J)-TK(I,J))*W(I,J)/ZZ(KZ)
25  CONTINUE
CALL SIMPS(GZW,M,N,HI,HJ,SGWT)
ANU2      =0.25 * SGWT/TMW
AVNU=0.5*(ANU1+ANU2)
DNU=100.*ABS(ANU1-ANU2)/AVNU *0.5
WRITE(6,501) ANU1      ,ANU2      ,AVNU,DNU
WRITE(6,502) TBK ,TAW ,TMW
KKK=KZ/30
IF(KKK.NE.KK) GO TO 500
KK=KK+1
WRITE(6,503)
DO 61 I=1,M1
WRITE(6,504) I
61  WRITE(6,505) (T(I,J),J=1,N1)
201  FORMAT(/,'NO. OF SECTION',I5,10X,'DISTANCE FROM
1 ENTRANCE',F10.6)
202  FORMAT(30X,'***',3F15.6,E20.5)
501  FORMAT('NU1',F10.6,10X,'NU2',F10.6,10X,'AVERAGE
1 NU',F10.6,10X,E20.4)
502  FORMAT('BULK TEMP.',E15.5 , 'WALL TEMP.',E15.5,
1 'MEAN WALL DIFFERENCE',E15.5)

```



```

503  FORMAT(// 'TEMP. DISTRIBUTIONS'//)
504  FORMAT('I',I5)
505  FORMAT(' ',9E12.4)
500  CONTINUE
      IF(KZ.GE.KMAX) GO TO 90
      GO TO 20
90    CONTINUE
      STOP
      END
      SUBROUTINE TEMP(T,TK)
      DIMENSION T(41,21),TK(41,21),TKH(41,21),X(41)
      DIMENSION A1(41),A2(41),A3(41),A4(41),A5(41)
      COMMON /C1/ ZZ(1500),DX,KZ
      COMMON /C2/ A(41,21),C(41,21),D(41,21),F(41,21)
1     ,WW(41,21),B(41,21),E(41,21)
      COMMON /C3/ M,N
      COMMON /C4/ M1,N1
      DO 20 J=1,N
      DO 10 I=2,M
      A1(I)=C(I,J)
      A2(I)=B(I,J)-WW(I,J)/ZZ(KZ)
      A3(I)=A(I,J)
      IF(J.EQ.1) GO TO 15
      A4(I)=D(I,J)*TK(I,J+1)+(E(I,J)-WW(I,J)/ZZ(KZ))*TK(I,J)
      *+F(I,J)*TK(I,J-1)
      GO TO 10
15    A4(I)=(D(I,J)+F(I,J))*TK(I,J+1)+(E(I,J)-WW(I,J)
1     /ZZ(KZ))*TK(I,J)
10    CONTINUE
      A2(1)=-2.
      A3(1)=2.
      A1(M1)=2.
      A2(M1)=-2.
      IF(J.EQ.1) GO TO 16
      A4(1)=-TK(1,J+1)+2.*TK(1,J)-TK(1,J-1) -2.*DX
      A4(M1)=-TK(M1,J+1)+2.*TK(M1,J) -TK(M1,J-1) -2.*DX
16    A4(1)=-2.*TK(1,2)+2.*TK(1,1) -2.*DX
      A4(M1)=-2.*TK(M1,2)+2.*TK(M1,1)-2.*DX
      CALL GAUSS(A1,A2,A3,A4,M1,X)
      DO 17 I=1,M1
17    TKH(I,J)=X(I)
20    CONTINUE
      DO 21 I=1,M1
      A1(I)=1.
      A2(I)=-4.
      A3(I)=1.

```



```

21  A4(I)=-2.*TKH(I,N)-2.*DX
    A3(1)=2.
    A1(M1)=2.
    A4(M1)=A4(M1)-2.*DX
    A4(1)=A4(1)-2.*DX
    CALL GAUSS (A1,A2,A3,A4,M1,X)
    DO 22 I=1,M1
22  TKH(I,N1)=X(I)
    DO 40 I=2,M
    DO 30 J=1,N
    A1(J)=F(I,J)
    A2(J)=E(I,J)+WW(I,J)/ZZ(KZ)
    A3(J)=D(I,J)
    A4(J)=A(I,J)*TKH(I+1,J)+(B(I,J)+WW(I,J)/ZZ(KZ))*T
    *KH(I,J)+C(I,J)*TKH(I-1,J)
30  CONTINUE
    A1(N1)=2.
    A2(N1)=-2.
    A3(1)=F(I,1)+D(I,1)
    A4(N1)=-TKH(I+1,N1)+2.*TKH(I,N1)-TKH(I-1,N1)-2.*DX
    CALL GAUSS(A1,A2,A3,A4,N1,X)
    DO 40 J=1,N1
40  T(I,J)=X(J)
    DO 50 J=1,N1
    A1(J)=1.
    A2(J)=-4.
    A3(J)=1.
    A4(J)=-2.*T(2,J)-2.*DX
50  A5(J)=-2.*T(M,J)-2.*DX
    A3(1)=2.
    A1(N1)=2.
    A4(N1)=A4(N1)-2.*DX
    CALL GAUSS (A1,A2,A3,A4,N1,X)
    DO 52 J=1,N1
52  T(1,J)=X(J)
    A5(N1)=A5(N1)-2.*DX
    CALL GAUSS(A1,A2,A3,A5,N1,X)
    DO 54 J=1,N1
54  T(M1,J)=X(J)
    RETURN
    END

```

```

C *****
C HEAT TRANSFER OF WALL CONVECTION

```



```

C *****
C R ASPECT RATIO
C REY REYNOLD NUMBER
C DEAN DEAN NUMBER
C PR PRANDTL NUMBER
C BI BIOT NUMBER
C DIMENSION T(41,21),T1(41,21),TK(41,21) ,T2(41,21)
  DIMENSION S(41,21),VOR(41,21) ,FJ(41)
  DIMENSION X(41),RA1(41),SWT(200)
  DIMENSION U(41,21),V(41,21),W(41,21)
  DIMENSION GZW(41,21),WT(41,21) ,SDZ(200)
  DIMENSION XT(41,21)
  COMMON /C1/ ZZ(1500),DX,KZ ,BI
  COMMON /C2/ A(41,21),B,C(41,21),D(41,21),E,F(41,21)
1,WW(41,21)
  COMMON /C4/ M1,N1
  COMMON /C3/ M,N
  COMMON /C6/ AREA
  REAL MAXS,MAXT
  READ(5,10) M,N,R
  WRITE(6,10) M,N,R
10  FORMAT(2I5,F5.1)
  READ(5,214) PR,RC,REY,DEAN,BI
214  FORMAT(5F15.5)
  WRITE(6,14) PR,RC,DEAN,REY
  WRITE(6,114) BI
114  FORMAT('BIOT NUMBER =',F25.3)
14  FORMAT('/', 'PRANDTL NUMBER =',F15.5,/,
1 'CURVATURE =',F15.5,/,
* 'DEAN NUMBER =',F15.5,/, 'REYNOLD NUMBER =',F15.5)
  M1=M+1
  N1=N+1
  MM1=M-1
  NM1=N-1
  HI=(1.+1./R)/(2.*M)
  HJ=(1.+R)/(4.*N)
  DX=HI/2.
  DX2=HI*HI
  DO 450 I=1,M1
450  READ(5,460) (S(I,J),J=1,N )
  DO 451 I=1,M1
451  READ(5,460) (W(I,J),J=1,N )
  DO 452 I=1,M1
452  READ(5,460) (VOR(I,J),J=1,N1)
  DO 888 I=1,M1
888  READ(5,460) (U(I,J),J=1,N1)

```



```

DO 889 I=1,M1
889 READ(5,460) (V(I,J),J=1,N1)
460 FORMAT(5E16.7)
C ENTRANCE CONDITIONS
DO 15 I=1,M1
  W(I,N1)=0.
DO 15 J=1,N1
15 T(I,J)=1.0
DO 100 I=1,M1
  X(I)=-(1.+1./R)/4.+(I-1)*HI
100 RA1(I)=1.+X(I)/RC
DO 12 I=1,M1
DO 12 J=1,N1
12 W(I,J)=W(I,J)/REY
DO 18 I=1,M1
DO 18 J=1,N1
18 WW(I,J)=2.*W(I,J)*DX2/RA1(I) /PR
PR1=1./PR
DO 11 I=1,M1
DO 11 J=1,N1
A(I,J)=PR1-DX*(U(I,J)-1./(RC*RA1(I)))
B=-2.*PR1
C(I,J)=PR1+DX*(U(I,J)-1./(RC*RA1(I)))
D(I,J)=-PR1+DX*V(I,J)
E=2.*PR1
F(I,J)=-PR1-DX*V(I,J)
11 CONTINUE
AREA=(1.+R)*(1.+1./R)/8.
KMAX=1000
Z=0.
DX=HI
Z=0.
KZ=0
KK=1
20 KZ=KZ+1
DO 19 I=1,M1
DO 19 J=1,N1
19 TK(I,J)=T(I,J)
C AXIAL STEP
  DZ=5.E-5
  IF(KZ.GT.100) DZ=1.E-4
  IF(KZ.GT.450) DZ=2.E-4
  IF(KZ.GT.650) DZ=5.E-4
  IF(KZ.GT.850) DZ=1.E-3
21 Z=Z+DZ
  ZZ(KZ)=DZ

```



```

WRITE(6,201) KZ,Z
DO 22 I=1,M1
DO 22 J=1,N1
22 TK(I,J)=T(I,J)
CALL TEMP (T,TK)
DO 23 I=1,M1
DO 23 J=1,N1
23 T1(I,J)=T(I,J)*W(I,J)
CALL SIMPS(T1,M,N,HI,HJ,SUMM)
TBK=SUMM
SUT=0.
DO 42 I=1,M1
42 SUT=SUT+T(I,N1)
DO 44 J=1,N
44 SUT=SUT+T(1,J)+T(M1,J)
SUT=2.*SUT-T(1,1)-T(M1,1)
AVET =SUT/(2*(M+2*N))
TAW=AVET
ANU1=-BI*TAW/(TAW-TBK)
C CALCULATIONS OF TEMP. GRADIEND IN FLOW DIRECTION
DO 25 J=1,N1
DO 25 I=1,M1
GZW(I,J)=(T(I,J)-TK(I,J))*W(I,J)/ZZ(KZ)
25 CONTINUE
CALL SIMPS(GZW,M,N,HI,HJ,SGWT)
ANU2 = 0.25* SGWT/ (TAW-TBK)
AVNU=0.5*(ANU1+ANU2)
DNU=100.*ABS(ANU1-ANU2)/AVNU *0.5
WRITE(6,501) ANU1 ,ANU2 ,AVNU,DNU
TW=T(1,N1)
SUPER=(1.-TW)/TW
WRITE(6,502) TBK ,TAW ,SUPER
KKK=KZ/30
IF(KKK.NE.KK) GO TO 500
KK=KK+1
WRITE(6,503)
DO 61 I=1,M1
WRITE(6,504) I
61 WRITE(6,505) (T(I,J),J=1,N1)
201 FORMAT(/,'NO. OF SECTION',I5,10X,'DISTANCE FROM
1 ENTRANCE',F10.6)
202 FORMAT(30X,'***',3F15.6,E20.5)
501 FORMAT('NU1',F10.6,10X,'NU2',F10.6,10X,'AVERAGE
1 NU',F10.6,10X,E20.4)
502 FORMAT('BULK TEMP.',E15.5 , 'WALL TEMP.',E15.5,
1 'SUPERHEATED RATIO',E15.3)

```



```

503  FORMAT(// 'TEMP. DISTRIBUTIONS'//)
504  FORMAT('I',I5)
505  FORMAT(' ',9E12.4)
500  CONTINUE
      IF(KZ.GE.KMAX) GO TO 90
      GO TO 20
90   CONTINUE
      STOP
      END
      SUBROUTINE TEMP(T,TK)
      DIMENSION T(41,21),TK(41,21),TKH(41,21),X(41)
      DIMENSION A1(41),A2(41),A3(41),A4(41),A5(41)
      COMMON /C1/ ZZ(1500),DX,KZ      ,BI
      COMMON /C2/ A(41,21),B,C(41,21),D(41,21),E,F(41,21)
1     ,WW(41,21)
      COMMON /C3/ M,N
      COMMON /C4/ M1,N1
      DO 20 J=1,N
      DO 10 I=2,M
      A1(I)=C(I,J)
      A2(I)=B-WW(I,J)/ZZ(KZ)
      A3(I)=A(I,J)
      IF(J.EQ.1) GO TO 15
      A4(I)=D(I,J)*TK(I,J+1)+(E-WW(I,J)/ZZ(KZ))*TK(I,J)+
1     F(I,J)*TK(I,J-1)
      GO TO 10
15   A4(I)=(D(I,J)+F(I,J))*TK(I,J+1)+(E-WW(I,J)/ZZ(KZ))*
1     TK(I,J)
10   CONTINUE
      A2(1)=-2. -2.*DX*BI
      A3(1)=2.
      A1(M1)=2.
      A2(M1)=-2.-2.*DX*BI
      IF(J.EQ.1) GO TO 16
      A4(1)=-TK(1,J+1)+2.*TK(1,J)-TK(1,J-1)
      A4(M1)=-TK(M1,J+1)+2.*TK(M1,J) -TK(M1,J-1)
16   A4(1)=-2.*TK(1,2)+2.*TK(1,1)
      A4(M1)=-2.*TK(M1,2)+2.*TK(M1,1)
      CALL GAUSS(A1,A2,A3,A4,M1,X)
      DO 17 I=1,M1
17   TKH(I,J)=X(I)
20   CONTINUE
      DO 21 I=1,M1
      A1(I)=1.
      A2(I)=-4. -2.*DX*BI
      A3(I)=1.

```



```

21  A4(I)=-2.*TKH(I,N)
    A3(1)=2.
    A1(M1)=2.
    A2(1)=A2(1)-2.*DX*B I
    A2(M1)=A2(M1)-2.*DX*B I
    CALL GAUSS (A1,A2,A3,A4,M1,X)
    DO 22 I=1,M1
22  TKH(I,N1)=X(I)
    DO 40 I=2,M
    DO 30 J=1,N
    A1(J)=F(I,J)
    A2(J)=E+WW(I,J)/ZZ(KZ)
    A3(J)=D(I,J)
    A4(J)=A(I,J)*TKH(I+1,J)+(B+WW(I,J)/ZZ(KZ))*
1 TKH(I,J)+C(I,J)*TKH(I-1,J)
30  CONTINUE
    A1(N1)=2.
    A2(N1)=-2. -2.*DX*B I
    A3(1)=F(I,1)+D(I,1)
    A4(N1)=-TKH(I+1,N1)+2.*TKH(I,N1)-TKH(I-1,N1)
    CALL GAUSS(A1,A2,A3,A4,N1,X)
    DO 40 J=1,N1
40  T(I,J)=X(J)
    DO 50 J=1,N1
    A1(J)=1.
    A2(J)=-4. -2.*DX*B I
    A3(J)=1.
    A4(J)=-2.*T(2,J)
50  A5(J)=-2.*T(M,J)
    A3(1)=2.
    A1(N1)=2.
    A2(N1)=A2(N1)-2.*DX*B I
    CALL GAUSS (A1,A2,A3,A4,N1,X)
    DO 52 J=1,N1
52  T(1,J)=X(J)
    CALL GAUSS(A1,A2,A3,A5,N1,X)
    DO 54 J=1,N1
54  T(M1,J)=X(J)
    RETURN
    END

```

```

C  SUBROUTINE FOR GAUSSIAN ELIMINATION
    SUBROUTINE GAUSS(A,B,C,D,N1,X)
    DIMENSION A(61),B(61),C(61),D(61),X(41),BETA(61),

```



```

1 GAMMA(61)
  N=N1-1
  BETA(1)=B(1)
  GAMMA(1)=D(1)/B(1)
  DO 10 I=2,N1
    BETA(I)=B(I)-A(I)*C(I-1)/BETA(I-1)
10  GAMMA(I)=(D(I)-A(I)*GAMMA(I-1))/BETA(I)
    X(N1)=GAMMA(N1)
    I=N1
    DO 20 K=1,N
      I=I-1
20  X(I)=GAMMA(I)-C(I)*X(I+1)/BETA(I)
    RETURN
  END

```

```

C  SIMPSON'S RULE FOR SINGLE INTEGRATION--(F(J),J=1,N1)
  SUBROUTINE SIMP(F,N,HJ,SUM)
  DIMENSION F(61)
  N1=N+1
  NM1=N-1
  SUM=F(1)+F(N1)
  DO 10 J=2,N,2
10  SUM=SUM+4.0*F(J)
  DO 12 J=3,NM1,2
12  SUM=SUM+2.0*F(J)
  SUM=SUM*HJ/3.
  RETURN
  END

```

```

C  SIMPSON'S RULE FOR DOUBLE INTEGRATION--((F(I,J),
1 J=1,N1),I=1,M1)
  SUBROUTINE SIMPS(F,M,N,HI,HJ,SUMM)
  DIMENSION SUM(61),F(41,41)
  M1=M+1
  N1=N+1
  MM1=M-1
  NM1=N-1
  DO 8 I=1,M1
    SUM(I)=F(I,1)+F(I,N1)
    DO 4 J=2,N,2
4  SUM(I)=SUM(I)+4.0*F(I,J)

```



```
      DO 6 J=3,NM1,2
6     SUM(I)=SUM(I)+2.0*F(I,J)
8     SUM(I)=HJ*SUM(I)/3.
      SUMM=SUM(1)+SUM(M1)
      DO 10 I=2,M,2
10    SUMM=SUMM+4.0*SUM(I)
      DO 12 I=3,MM1,2
12    SUMM=SUMM+2.0*SUM(I)
      SUMM=HI*SUMM/3.
      RETURN
      END
```


APPENDIX C.1

NUMERICAL RESULTS IN THERMAL ENTRANCE REGION WITH
UNIFORM WALL TEMPERATURE

Pr = 0.7 , K = 368

z	Nu ₁	z	Nu ₁
0.5x10 ⁻³	14.748	0.15x10 ⁻¹	9.837
0.60	13.694	0.18	10.364
0.70	12.953	0.20	10.631
0.1x10 ⁻²	11.576	0.21	10.734
0.12	10.983	0.23	10.880
0.15	10.323	0.25	10.953
0.20	9.578	0.28	10.966
0.25	9.092	0.30	10.936
0.30	8.765	0.32	10.893
0.35	8.544	0.35	10.828
0.40	8.399	0.38	10.778
0.50	8.261	0.40	10.755
0.60	8.258	0.45	10.731
0.70	8.339	0.50	10.735
0.80	8.473	0.60	10.757
0.90x10 ⁻²	8.641	0.65	10.763
0.1x10 ⁻¹	8.828	0.70	10.765
0.12	9.230	0.90x10 ⁻¹	10.768

Pr = 5, K = 100

z	Nu ₁	z	Nu ₁
0.5x10 ⁻³	12.398	0.12x10 ⁻¹	9.860
0.80	10.732	0.15	8.709
0.1x10 ⁻²	10.079	0.18	7.915
0.15	9.058	0.20	7.828
0.20	8.494	0.23	7.980
0.25	8.183	0.25	8.043
0.30	8.030	0.28	7.984
0.35	7.984	0.30	7.909
0.40	8.011	0.35	7.864
0.50	8.210	0.40	7.891
0.60	8.537	0.50	7.783
0.70x10 ⁻²	8.944	0.60	7.873
0.1x10 ⁻¹	9.995	0.70	7.873
		0.80x10 ⁻¹	7.873

Pr = 500, K = 14

z	Nu ₁	z	Nu ₁
0.5×10^{-3}	12.107	0.6×10^{-2}	6.955
0.6	11.862	0.7	6.697
0.7	11.807	0.8	6.588
0.9×10^{-3}	11.950	0.9×10^{-2}	6.510
0.1×10^{-2}	12.090	0.1×10^{-1}	6.451
0.15	12.784	0.15	6.359
0.20	11.496	0.18	6.349
0.25	8.900	0.20	6.347
0.30	7.748	0.25	6.347
0.35	7.850	0.30×10^{-1}	6.347
0.40	8.018		
0.50×10^{-2}	7.045		

APPENDIX C.2

NUMERICAL RESULTS IN THERMAL ENTRANCE REGION WITH
UNIFORM WALL HEAT FLUX

Pr = 0.7 , K = 368

z	Nu ₁	z	Nu ₁
0.5x10 ⁻³	16.931	0.1x10 ⁻¹	9.136
0.8	14.651	0.15	10.028
0.1x10 ⁻²	13.687	0.20	11.011
0.15	12.128	0.25	11.499
0.20	11.177	0.28	11.463
0.30	10.078	0.30	11.354
0.40	9.493	0.35	11.023
0.5	9.168	0.40	10.826
0.7	8.941	0.50	10.854
0.8	8.955	0.60	10.945
0.9	9.025	0.70	10.932
0.95	9.076	0.80x10 ⁻¹	10.921
0.98x10 ⁻²	9.111	0.10x10 ⁰	10.921

$Pr = 5$, $K = 100$

z	Nu_1	z	Nu_1
0.5×10^{-3}	14.100	0.12×10^{-1}	9.710
0.8	12.142	0.15	9.136
0.1×10^{-2}	11.327	0.18	8.173
0.15	10.035	0.20	7.880
0.20	9.273	0.23	7.932
0.25	8.786	0.25	8.108
0.30	8.471	0.28	8.245
0.35	8.277	0.30	8.176
0.40	8.170	0.35	7.913
0.50	8.137	0.40	7.975
0.60	8.257	0.50	7.936
0.70×10^{-2}	8.468	0.60	7.958
0.1×10^{-1}	9.327	0.70	7.949
		0.80×10^{-1}	7.947

Pr = 5, K = 368

z	Nu ₁	z	Nu ₁
0.5×10^{-3}	20.800	0.1×10^{-1}	17.500
0.8	20.619	0.15	17.137
0.1×10^{-2}	20.791	0.20	17.008
0.15	21.624	0.25	16.956
0.20	22.277	0.28	16.939
0.25	21.813	0.30	16.931
0.30	20.104	0.35	16.920
0.35	19.115	0.40	16.910
0.40	18.991	0.50	16.903
0.50	18.888	0.60	16.902
0.70	18.032	0.70	16.902
0.90×10^{-2}	17.616	0.90×10^{-1}	16.902

Pr = 500, K = 14

z	Nu ₁	z	Nu ₁
0.5×10^{-3}	12.884	0.1×10^{-1}	8.440
0.8	12.023	0.15	7.932
0.1×10^{-2}	11.842	0.20	7.677
0.15	12.050	0.25	7.536
0.20	12.191	0.30	7.454
0.25	11.425	0.35	7.406
0.30	10.293	0.40	7.377
0.35	9.757	0.50	7.350
0.40	8.757	0.60	7.340
0.50	9.709	0.70	7.340
0.70	8.983	0.90×10^{-1}	7.340
0.90×10^{-2}	8.491	0.1×10^0	7.340

APPENDIX C.3

NUMERICAL RESULTS IN THERMAL ENTRANCE WITH
CONVECTIVE BOUNDARY CONDITION

Pr = 0.03 , K = 368 , Bi = 10

z	Nu ₁	z	Nu ₁
0.5x10 ⁻³	16.815	0.1x10 ⁻¹	6.392
0.80	14.422	0.15	5.691
0.1x10 ⁻²	13.402	0.20	5.277
0.20	10.664	0.25	5.003
0.30	9.336	0.30	4.811
0.40	8.504	0.40	4.573
0.50	7.917	0.50	4.441
0.60	7.473	0.70	4.328
0.70	7.123	0.90x10 ⁻¹	4.294
0.80	6.836	0.1x10 ⁰	4.283
0.90x10 ⁻²	6.596	0.15	4.283

$Pr = 0.03$, $K = 368$, $Bi = 1.0$

z	Nu_1	z	Nu_1
0.5×10^{-3}	16.851	0.1×10^{-1}	6.550
0.80	14.511	0.15	5.865
0.1×10^{-2}	13.509	0.20	5.445
0.20	10.811	0.25	5.164
0.30	9.498	0.30	4.964
0.40	8.672	0.40	4.705
0.50	8.089	0.50	4.553
0.60	7.648	0.70	4.402
0.70	7.299	0.90×10^{-1}	4.342
0.80	7.013	0.1×10^0	4.327
0.90×10^{-2}	6.776	0.15	4.300
		0.20	4.300

$Pr = 10.05$, $K = 368$, $Bi = 1.0$

z	Nu_1	z	Nu_1
0.5×10^{-3}	20.923	0.1×10^{-1}	17.476
0.80	20.778	0.15	17.098
0.1×10^{-2}	20.966	0.20	16.963
0.15	21.773	0.25	16.906
0.20	22.388	0.30	16.879
0.25	21.856	0.35	16.865
0.30	20.115	0.40	16.856
0.35	19.157	0.50	16.842
0.40	19.052	0.60	16.838
0.50	18.893	0.70	16.836
0.70	18.031	0.80	16.836
0.9×10^{-2}	17.598	0.90×10^{-1}	16.836

$Pr = 10.05$, $K = 368$, $Bi = 10$

z	Nu_1	z	Nu_1
0.5×10^{-3}	21.556	0.1×10^{-1}	17.284
0.80	21.609	0.15	16.818
0.1×10^{-2}	21.870	0.20	16.635
0.15	22.553	0.25	16.548
0.20	22.280	0.35	16.470
0.30	20.333	0.40	16.450
0.35	19.381	0.50	16.404
0.40	19.298	0.60	16.390
0.50	18.925	0.70×10^{-1}	16.390
0.70	17.969		
0.90×10^{-2}	17.446		

TABLE 1
NUMERICAL RESULTS FOR FRICTION FACTOR, $\gamma=1$

$\partial p/\partial z$	r	Re	K	$(f_c/f_s)_1$	$(f_c/f_s)_2$	M X N
-4×10^3	100	139.4	13.94	1.000	1.007	20 x 10
-9×10^3	100	295.3	29.53	1.055	1.071	"
-1.9×10^4	100	548.2	54.82	1.212	1.218	"
-4×10^4	100	1000	100.0	1.416	1.406	"
-7×10^4	100	1511	151.1	1.667	1.629	"
-1.1×10^5	100	2026	202.6	2.177	1.909	"
-1.6×10^5	100	2743	274.3	2.620	2.060	"
-5×10^4	10	830.6	262.7	2.561	2.112	"
-5.5×10^4	10	896.1	283.4	2.521	2.154	"
-8×10^4	10	1164	368.1	3.077	2.415	"
-8×10^4	10	1152	364.3	2.370	2.441	40 x 20
-2.5×10^4	4	429.6	214.8	2.136	2.042	20 x 10
-3×10^4	4	482.4	241.2	2.300	2.180	"
-6×10^4	4	823.8	411.9	3.090	2.550	"
-8×10^4	4	976.7	488.4	3.726	2.880	"
-8×10^4	4	950.7	475.3	2.882	2.957	40 x 20
-9×10^4	4	1041	520.2	3.03	3.04	20 x 10
-1.1×10^5	4	1238	618.8	3.677	3.124	"
-1.4×10^5	4	1431	715.4	4.25	3.43	"

TABLE 2
NUMERICAL RESULTS FOR FRICTION FACTOR, $\gamma=2$

$\partial p / \partial z$	r	Re	K	$(f_c/f_s)_1$	$(f_c/f_s)_2$	M X N
-5×10^3	100	159.4	15.94	1.000	1.014	16 x 16
-1×10^4	100	314.8	31.48	1.022	1.027	"
-2.6×10^4	100	721.5	72.15	1.160	1.165	"
-4×10^4	100	1035	103.5	1.252	1.249	"
-6×10^4	100	1438	143.8	1.362	1.350	"
-9×10^4	100	1973	197.3	1.517	1.476	"
-8×10^4	30	1526	278.6	1.809	1.695	"

TABLE 3
NUMERICAL RESULTS FOR FRICTION FACTOR, $\gamma=5$

$\partial p / \partial z$	r	Re	K	$(f_c/f_s)_1$	$(f_c/f_s)_2$	M X N
-8×10^3	100	208.2	20.82	1.000	1.001	12 x 30
-1.4×10^4	100	360.1	36.00	1.001	1.020	"
-3×10^4	100	769.0	76.90	1.019	1.024	"
-5×10^4	100	1231	123.1	1.059	1.067	"
-8×10^4	100	1718	171.8	1.276	1.224	"
-8×10^4	30	1544	281.8	1.547	1.361	"

TABLE 4
 NUMERICAL RESULTS FOR FRICTION FACTOR, $\gamma=0.5$

$\partial p/\partial z$	r	Re	K	$(f_c/f_s)_1$	$(f_c/f_s)_2$	M X N
-5×10^3	100	160.1	16.00	1.000	1.010	32 x 8
-1×10^4	100	311.0	31.10	1.028	1.039	"
-2.6×10^4	100	680.6	68.06	1.238	1.235	"
-5×10^4	100	1126	112.6	1.463	1.436	"
-9×10^4	100	1766	176.6	1.729	1.648	"
-1.1×10^5	100	2007	200.7	1.942	1.772	"
-9×10^4	30	1435	262.0	2.306	2.028	"
-1.1×10^5	30	1713	312.7	2.383	2.077	"

TABLE 5

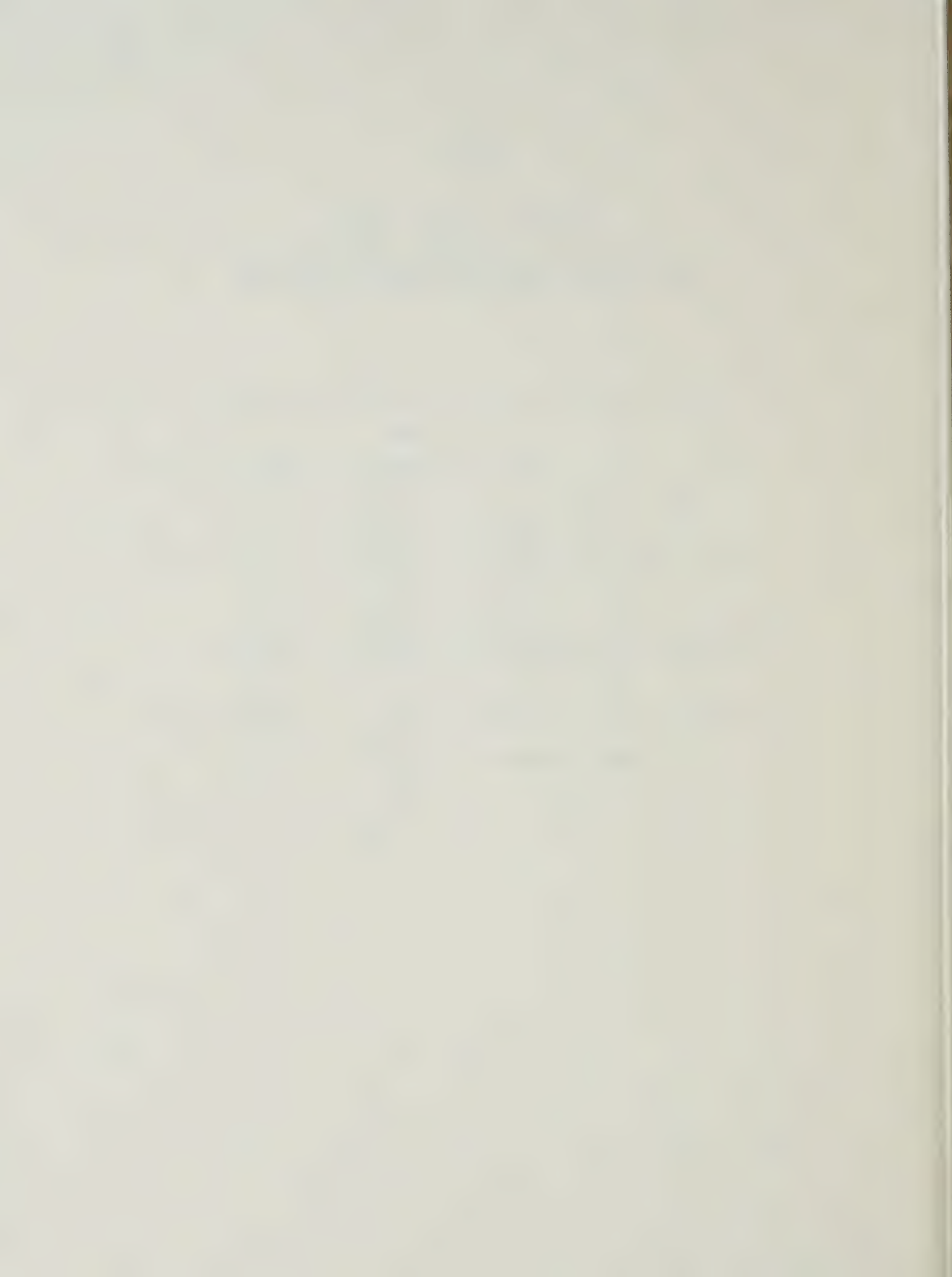
ASYMPTOTIC NUSSELT NUMBERS
FOR CONSTANT WALL TEMPERATURE AND UNIFORM WALL
HEAT FLUX BOUNDARY CONDITIONS

Pr	r	K	$(Nu)_{T_w}$	MxN	$(Nu)_{q_w}$	MxN
0.1	100	100	3.90	20x10	3.92	20x10
0.1	10	368	5.86	40x20	6.25	40x20
0.1	4	488	6.26	40x20	7.81	20x10
0.7	100	14	3.02	20x10	3.09	20x10
0.7	100	55	4.70	"	5.28	"
0.7	100	100	6.00	"	6.25	"
0.7	10	368	10.76	40x20	10.92	40x20
0.7	4	488			13.13	20x10
5	100	14	3.65	40x20	3.89	"
5	100	55	6.18	"	6.68	"
5	100	100	7.87	"	7.95	"
5	100	202			12.05	"
5	10	368	15.45	40x20	16.90	40x20
500	100	5.0	5.82	"	6.01	20x10
500	100	10.0	6.18	"	6.82	"
500	100	14.0	6.35	"	7.34	"

TABLE 6

ASYMPTOTIC NUSSELT NUMBERS
FOR UNIFORM CONVECTIVE BOUNDARY CONDITION

Pr	K	Nu_f		
		Bi=1	Bi=10	Bi= ∞
	0	3.009	2.985	2.98
0.7	100	6.051	6.023	6.000
	368	11.340	11.000	10.760
	55	7.003	6.799	6.793
10.05	100	8.323	8.127	8.018
	368	16.836	16.390	16.031



B30082